THESIS FOR THE DEGREE OF DOCTOR OF PHILOSOPHY

On the Local Filtration Properties of LignoBoost Lignin

Studies of the influence of xylan and ionic strength

JULIE DURRUTY

Department of Chemistry and Chemical Engineering

CHALMERS UNIVERSITY OF TECHNOLOGY

Gothenburg, Sweden

2017

On the Local Filtration Properties of LignoBoost Lignin

Studies of the influence of xylan and ionic strength

JULIE DURRUTY

Forest Products and Chemical Engineering

Department of Chemistry and Chemical Engineering

Chalmers University of Technology

SE-412 96 Gothenburg

Sweden

Telephone: +46 (0)31 772 1000

Cover:

[Left up: ESEM image of LignoBoost lignin. Left down: Native softwood lignin structure, adapted from Alder (1977). Middle: Orion forest in Estérençuby, France, by Andre Durruty. Right: schematic diagram of cake filtration]

On the Local Filtration Properties of LignoBoost Lignin

Studies of the influence of xylan and ionic strength

JULIE DURRUTY

Forest Products and Chemical Engineering
Department of Chemistry and Chemical Engineering
Chalmers University of Technology

ABSTRACT

Kraft pulping technology is currently the most commonly-used method for producing paper pulp from wood. A new and promising opportunity for Kraft pulp mills is to take a step towards becoming biorefineries by implementing technologies able to extract and convert the organic by-products, such as lignin, into a wide range of value-added products and chemicals. The LignoBoost process, which is a new technique that has recently been implemented on an industrial scale, is designed to extract lignin from the Kraft process with a high degree of purity, making it potentially suitable for the manufacture of e.g. carbon fibres. Following a lignin precipitation stage, filtration, performed by dead-end filtration, is one of the key steps of the LignoBoost process.

The aim of this work is to improve the efficiency of the filtration stage of the LignoBoost process further. The local and average filtration properties of the cake formed from softwood lignins extracted using the LignoBoost process were investigated through the use of model liquors and by varying the condition parameters and the preparation procedures. The influence of the hemicellulose xylan on the filtration and precipitation of LignoBoost lignin was studied. LignoBoost lignin was (i) suspended in acid water with xylan added and (ii) dissolved together with xylan and then re-precipitated. The effects of ionic strength, applied pressure, slurry concentration, pH, precipitation temperature and rate of acidification on the resulting material and its filtration properties were all investigated. Moreover, the evolution of the size of the particles agglomerates during the course of precipitation was monitored *in situ* using the Focus Beam Reflectance Measurement (FBRM) technique.

The lignin-xylan mixtures were more difficult to filter than the original LignoBoost lignin. The latter was found to be a material that was relatively easy to filter (2 to 6 ·10^{11} m/kg in filtration resistance), forming weakly compressible filter cakes over the filtration pressure range studied (2-28 bar). The slurry concentration (8.8-21.6 wt%) was not found to affect the filtration behaviour. Chemical analysis of different layers of the filter cakes formed showed that xylan was distributed evenly on the solid lignin when both solids were precipitated together. It is thus likely that xylan is sorbed onto the surface of the lignin particles-agglomerates, opening their structure and increasing the contact area between solid and liquid during filtration: the flow resistance is increased. Furthermore, it was found that increasing the ionic strength of the slurries made the solid/liquid separation process easier. A plausible explanation for this is a decrease in the electrostatic repulsive interactions between the solids and the subsequent formation of a denser solid structure. Similarly, lowering the pH below the pKa values of the carboxylic acid groups of xylan made the lignin-xylan mixtures significantly easier to filter. Finally, the onset of precipitation (particle sizes $\geq$ 1μm) was not found to be affected by either the precipitation temperature (45-77 °C) or the addition of xylan; a broader particle size distribution was obtained when acidification was rapid compared to that performed slowly and stepwise.

Keywords: LignoBoost process, softwood lignin, xylan, dead-end filtration, compressible filter cake, local filtration properties, particle interactions, constitutive relationships, acid precipitation.

List of Publications

This thesis is based on the following appended papers, referred to by Roman numerals in the text:

I. **Local and average filtration properties of Kraft softwood lignin**
J. Durruty, T. Mattsson and H. Theliander
Nordic Pulp and Paper Research Journal, 2015, 30(1), 132-140.

II. **Local filtration properties of Kraft lignin: The influence of residual xylan**
J. Durruty, T. Mattsson and H. Theliander
Separation and Purification Technology, 2017, 179, 455-466.

III. **Filtration properties of Kraft lignin: The influence of xylan and precipitation conditions**
J. Durruty, T. Sewring, H. Schneider, L. Schneider, T. Mattsson and H. Theliander
Accepted for publication in *Nordic Pulp and Paper Research Journal.*

IV. **Acid precipitation of Kraft lignin from aqueous solutions: Influence of xylan and temperature**
T. Sewring, J. Durruty, L. Schneider, H. Schneider, T. Mattsson and H. Theliander
Submitted manuscript.

V. **The influence of ionic strength on the local filtration properties of titanium dioxide**
T. Mattsson, J. Durruty, J. Wetterling and H. Theliander
Filtration, 2015, 15(1), 48-57.

Results related to this work have been presented at the following conferences:

i. **Influence of ionic strength on the local filtration properties of TiO₂**
T. Mattsson, J. Wetterling, J. Durruty and H. Theliander
(Oral presentation)
FILTECH, Weisbeden, Germany, October 22-24, 2013

ii. **Local and average filtration properties of softwood LignoBoost lignin**
J. Durruty, T. Mattsson and H. Theliander
(Poster presentation)
15th Nordic Filtration Symposium, Lund, Sweden, September 9-10, 2014

iii. **Local and average filtration properties of Kraft softwood lignin**
J. Durruty, T. Mattsson and H. Theliander
(Oral presentation)
FPS 2014, European Conference on Fluid Particle Separation, Lyon, France, October 15-17, 2014

iv. **Local filtration properties of Kraft lignin: Influence of lignin-carbohydrate complex**
J. Durruty, T. Mattsson and H. Theliander
(Poster presentation)
Nordic Wood Biorefinery Conference, Helsinki, Finland, October 20-22, 2015

v. **Local filtration properties of Kraft lignin: Influence of lignin properties**
J. Durruty, T. Mattsson and H. Theliander
(Oral presentation)
12th World Filtration Congress, Taipei, Taiwan, April 11-15, 2016

vi. **Local filtration properties of Kraft lignin: Influence of xylan**
J. Durruty, T. Mattsson and H. Theliander
(Oral presentation)
16th Nordic Filtration Symposium, Lappeenranta, Finland, August 24-26, 2016

Contribution report

The author of this thesis has made the following contributions to the appended papers:

<u>Papers I-II.</u> Main author. The experiments were planned, and the results evaluated, together with Dr. Tuve Mattsson and Prof. Hans Theliander. The author performed the experiments, the data analyses involved and the modelling work.

<u>Paper III.</u> Main author. The study is based on a preliminary experimental study performed by Helen Schneider and Lynn Schneider under the supervision of both the author and Tor Sewring. The author was active in planning, performing and analysing all the experiments in the main study and was fully responsible for the filtration and laser diffraction performed (experimental work and data analyses). The results were evaluated together with Tor Sewring, Dr. Tuve Mattsson and Prof. Hans Theliander.

<u>Paper IV.</u> Co-author. The study is based on a preliminary experimental study performed by Helen Schneider and Lynn Schneider under the supervision of both the author and Tor Sewring. The experiments in the main study were planned and performed by the author and Tor Sewring. The results were evaluated together with Tor Sewring, Dr. Tuve Mattsson and Prof. Hans Theliander.

<u>Paper V.</u> Co-author. The experiments were planned, and the results evaluated, together with Dr. Jonas Wetterling, Dr. Tuve Mattsson and Prof. Hans Theliander. The author was responsible for the experimental work in collaboration with Dr. Jonas Wetterling and contributed to the data analyses involved.

Contents

1. Introduction

1.1 The biorefinery concept

General living standards have increased drastically during the past century as a benefit of the tremendous technological advancements that have taken place in that period: these are unique in the history of human civilization, considering their relative great extent and fast rate at which they have occurred. The population of the world has also grown immensely in that same time frame as a result: from around 1.6 billion in 1900 to over 7 billion in 2017. One of the main contributors to this rapid and important increase in technological development and general living standards is the development of the petroleum-based industry. Consequently, the society today also relies, to a great extent, on a large number of products that originate mainly from fossil oil, e.g. transportation fuels, materials, energy and chemicals. However, the world's resources of natural oil are not only expected to be depleted in the coming century: their use also contributes to the emission of carbon dioxide and the subsequent changes in the climate. More sustainable alternatives to fossil oil must, therefore, be found rapidly and implemented into the society in order to maintain current standards of living and minimize damage to the environment.

Three abundant and sustainable resources are currently expected to replace fossil oil as a source of energy in the future: solar, wind and biomass energy. However, for the production of consumer material commodities, biomass is the only viable potential resource available on Earth. The concept of the biorefinery was thus developed in this context and became a focus of research of great importance in the past few decades (Ragauskas *et al.,* 2006). According to the International Energy Agency, a biorefinery is a plant where "*the sustainable processing of biomass into a spectrum of marketable products ranging from energy, food, feed, chemicals and materials applications*" takes place.

Biomass is, however, a highly heterogeneous material, so processing biomass to use as an alternative to fossil oil (which has a rather homogeneous composition) is thus challenging. Moreover, biomass has a lower carbon density than crude oil; it also consists of solid materials, making its collection and transport more complicated. One advantage of using biomass compared to crude oil is that the latter needs to be cracked, decomposed and functionalized for the production of chemicals and materials, whereas the former already consists of functionalized building blocks, such as carbohydrate, protein and aromatics. Consequently, the ability to design processes that are capable of separating biomass into its major compounds efficiently, making the best use of each respective fraction, constitutes the key to a cost-effective biorefinery industry.

The various existing biomass feedstocks can be classified into four sectors of origin (Cherubini, 2011): (i) agricultural crops and residues, (ii) wood and plants, (iii) industry (process residues and leftovers) and households (municipal solid waste and wastewater) and, finally, (iv) aquaculture (algae and seaweeds).

Wood has several advantages over the other possible feedstocks: it is the most abundant organic material found on Earth, it can be harvested during the all year and, furthermore, it does not compete directly with the food industry.

1.2 Pulp mills as biorefineries

Technologies focusing on separating the components of wood have been well established since the 19th century with the massive development of the pulp and paper industry. Among the various pulping techniques currently employed, the Kraft pulping process is the one most commonly used. It produces paper pulp with stronger cellulosic fibres than those obtained using the alternatives: mechanical, sulphite and soda pulping processes. Another advantage of the Kraft process is that it allows for an efficient and economical recovery of the cooking chemicals employed, i.e. hydroxide and hydrosulphide ions. It does, however, have the drawback of a low material yield. Wood is composed mainly of cellulose (40-50 %), hemicelluloses (15-25 %) and lignin (20-35 %). Lignin and part of the hemicelluloses are dissolved in the cooking liquor during the Kraft pulping operation: the undissolved cellulose and hemicelluloses of the original wood chips are what constitute the paper pulp. Only about half of the original wood material is therefore used in the production of paper pulp. Moreover, lignin is the main organic by-product of the Kraft pulp industry.

The spent cooking liquor, which contains the dissolved lignin, the cooking chemicals and some other wood constituents (mainly residues from hemicelluloses), is known as "black liquor" after the cook. To date, the lignin dissolved in black liquor has been used almost exclusively as an internal fuel in the mill's recovery boiler. The amount of lignin generated in a modern Kraft pulp mill is, however, greater than what is required to run the pulping process: although it varies, this excess represents more than 20-30 % of the total amount of dissolved lignin. Considering that about 50-60 Mt of Kraft lignin is generated worldwide every year, a minimum of 10-18 Mt of lignin could be made available each year without disturbing the operation of either the recovery boiler or the heat balance of the pulp mills.

Additionally, it is the capacity of the recovery boiler that usually limits the quantity of pulp that can be produced in a modern pulp mill. Extracting the excess amount of lignin from the black liquor can thus be beneficial, allowing more pulp to be produced. Finally, incorporating a lignin extraction process into the pulping process may also act as a "kidney" by removing certain undesirable non-process elements, such as aluminium and silica, in the Kraft process and thus being beneficial (Öhman *et al.,* 2007a).

After extraction, the lignin excess can be used directly in the mill as a solid biofuel (i.e. replacing fossil oil), or sold and exported elsewhere. Lignin is actually a particularly interesting potential raw material for the production of a large number value-added chemicals: it is the only biomaterial based on aromatic units (i.e. has a relatively high carbon content) that is available on a large scale. Among potential applications of lignin, the production of carbon fibres can, for example, be cited as being a very lucrative prospect (Kadla *et al.,* 2002; Brodin *et al.,* 2012). Furthermore, the demand for lignin and, consequently, also the profits it and other lignocellulosic raw materials generate are expected to increase drastically in coming years because of the inevitable depletion of fossil oil coupled with growing environmental concerns. Therefore, a promising opportunity for Kraft pulp mills would be to take a step towards becoming biorefineries, i.e. implementing processes designed to extract and convert efficiently the available excess of lignin (and other organic by-products) into valuable products and chemicals. A good example of a well-established industrial biorefinery is the Borregaard pulp mill in Norway (sulphite pulping): more than 90 % of the wood input is converted into valuable products and chemicals.

The LignoBoost process is a new technique designed to extract lignin from black liquor efficiently and with a high degree of purity (Öhman *et al.,* 2007a): this was not achievable with the previous method used to extract lignin. Two commercial LignoBoost units have already been successfully brought on line: Domtar's pulp mill in Plymouth, USA and Stora Enso's pulp mill in Sunila, Finland[1].

During the LignoBoost process, the lignin dissolved in the black liquor is first re-precipitated by the addition of acid, which is performed at controlled pH and temperature. One of the main unit operations of the LignoBoost process is the following filtration step, used to separate the precipitated lignin from the black liquor.

1.3 The filtration unit operation

Filtration is a common energy efficient unit operation used to separate solids from liquids: it is essential in the emerging biorefinery industry in which raw materials and products often consist of solid materials. Filtration is already employed widely in e.g. food, mineral and pulp and paper industries. The principle of filtration for solid-liquid separation is the use of a porous medium that allows the fluid to pass through it while it retains the solid particles (King, 1980). There are three existing techniques of filtration: dead-end, deep-bed and cross-flow. This work focuses on dead-end filtration because it is the one used in the LignoBoost process.

In dead-end filtration, the solid particles accumulate on the top of the filter medium and form a filter cake. The pressure difference across the filter medium and the filter cake is the driving force of the operation, and may be obtained in several ways: either by having a higher pressure at the solid suspension (using e.g. gravity, centrifugal force or a piston press in a sealed environment), or by decreasing the pressure at the filtrate side (i.e. vacuum filtration).

Once the filtration is terminated, the cake may be subjected to expression and washing in order to increase its dry content and purity; sometimes, this is followed by blowing gas through the cake to displace any remaining liquor. The term "dead-end filtration" usually embraces the four steps mentioned above: cake build-up, expression, washing and gas blowing.

Two main filtration properties are usually considered when evaluating the filterability of a material: the solid content (known as the "cake solidosity") and the flow resistance (known as the "filtration resistance") of the filter cake that is formed. The higher the solidosity and the lower the filtration resistance of the cake, the better the efficiency of the filtration process. These properties depend mainly on the shape and size of the particles, the solid structure of the filter cake, the viscosity of the liquid and, finally, the maximum pressure difference possible across the filter cake and the filter medium. Another important aspect is the various particle-particle/slurry interaction mechanisms that act during the cake build-up stage (e.g. friction and/or electrostatic forces): these influence the structure of the cake and, thereby, also the filtration properties.

Furthermore, all materials form more or less compressible filter cakes in which the local solidosity increases as the local solid compressive pressure increases. A more compact solid structure is therefore found towards the bottom of compressible filter cakes, which also leads to an increase in the local filtration resistance. Thus, in the case of compressible filter cakes, the local filtration properties vary in the direction of the flow. This effect may have an important impact on the filtration behaviour of the material and, consequently, on the design of the filtration unit, depending on the degree of compressibility. In the case of compressible filter

---

[1] A LignoBoost demonstration pilot plant was also started at the Bäckhammar mill in Sweden.

cakes, determination of the local filtration properties is therefore one important step that must be taken in order to achieve accurate modelling of the filtration behaviour (which is still a challenge).

1.4 Objectives

The LignoBoost process is a new technology recently implemented on an industrial scale, designed specifically to extract and purify the excess of lignin generated during the Kraft pulping process. The long-term aim of this work is to optimize the efficiency of the filtration stages of the LignoBoost process further.

Achieving this aim requires deepening current knowledge of both the physical properties of the lignin particles obtained using the LignoBoost process and the filtration properties of the cake it forms. The first objective of this work was therefore to investigate the local and average filtration properties of softwood lignin extracted using the LignoBoost process. The use of model liquors was preferred over that of black liquor in order to isolate the influence of the parameters of interest better. LignoBoost lignins that originate from two different Nordic pulp mills were thereby considered and characterized using a number of different methods. The influence of several parameters on the filtration of lignin were studied, and included the slurry concentration, its ionic strength and the applied filtration pressure for three types of filter media. To the author's knowledge, no local filtration data of industrial LignoBoost lignin has been published previously. This is probably due to two factors: industrial LignoBoost lignin material has only very recently become available, and the experimental measurements involved in collecting local filtration data are complicated compared to that of average filtration data. However, local filtration data may be very relevant for optimizing the filtration efficiency of a material, for instance in investigating the compressibility behaviour of the filter cake formed during its build-up stage.

An important aspect that should be considered in order to achieve the objective pursued is the origin of the wood species used in the Kraft process. These are generally categorized into two groups: softwood and hardwood. Softwood Kraft lignin is known to be usually easier to filter than hardwood Kraft lignin. Although the reasons behind this are not fully understood, one is related to the content and nature of the residual lignin-hemicelluloses complex present in the extracted lignin. Xylan is known to be the main hemicellulose found in hardwood, and previous studies have indicated that a high content of xylan has a negative impact on the filtration of Kraft lignin (Wallmo *et al.*, 2009). Thus, the second objective of this thesis was to extend understanding of the influence of the hemicellulose xylan on the local and average filtration properties of lignin. Model liquors were prepared using different procedures, based on hardwood xylan added to softwood LignoBoost lignin with a very low original content of xylan. The effects of ionic strength, applied filtration pressure, pH and preparation procedure on the filtration of the lignin suspensions containing xylan were then investigated. Additionally, the localization of xylan throughout the cake formed by the agglomerates of lignin particles was conducted, using both high performance anion exchange chromatography and fluorescent microscopy analysis.

Another important aspect to consider for improving the efficiency of the filtration of lignin during the LignoBoost process is the conditions used during the acid precipitation stage (which precedes the filtration stages). These influence directly the solid particles formed and have thereby a great impact on the filtration of lignin. The third objective of this work was therefore to gain more knowledge of the ways in which the precipitation temperature, ionic strength and

addition of xylan influence the precipitation of LignoBoost lignin. Precipitation of lignin was moreover evaluated *in-situ* by acidification of the model liquors over the whole range of pH that is of industrial relevance (pH 13.6 to pH 4). To the author's knowledge, such data that considers non-diluted conditions is still lacking. Investigation at the concentrations of interest was made possible in this work thanks to the Focus Beam Reflectance Measurement (FBRM) technique. Moreover, filtering the various suspensions obtained allowed the impact of the precipitation conditions used on the filtration of lignin to be investigated thereafter.

Finally, a better general understanding of the mechanisms of the inter-particle interactions that occur during the filtration process is of great interest in order to achieve the long-term aim being pursued. The fourth part of this work focuses therefore on the influence of the electrostatic inter-particle interactions on the local filtration properties. Here, a general perspective was considered, with titanium dioxide being chosen as the model material. The ionic strength of the titanium dioxide suspension, which influences the electrostatic interactions, was altered through the addition of sodium chloride; the corresponding local and average filtration properties were determined at varying applied filtration pressures. The data obtained in the case of titanium dioxide was thereafter compared briefly to those determined for LignoBoost lignin. Finally, the local data was used to evaluate the performance of several constitutive relationships in the modelling of the filtration process.

1.5   Outline of the thesis

This thesis is based on five research papers, all of which are appended. Following the introduction in Chapter 1, Chapter 2 provides a short overview of lignin, its potential applications and its separation from black liquor using the LignoBoost process. Chapter 3 discusses, in general terms, the theory and mathematical models that apply to the filtration process. The equipment and procedure used to determine the local data are presented in Chapter 4, while the materials and experimental conditions are described in Chapter 5. The methods applied for characterization are summarized in Chapter 6, and the main results obtained are presented and discussed in Chapter 7. The most important conclusions that can be drawn from this work are reported in Chapter 8, along with possible industrial applications; suggestions for future work are made in Chapter 9.

2. Overview of Lignin in the Context of Pulping

2.1 Content and function of lignin in wood

The word "lignin" was introduced in 1813 by M.A.P. de Candolle, a Swiss botanist, in order to name the product obtained after treating wood with alkaline solvent and mild acid. It is actually derived from *lignum,* the Latin for wood. Lignin is indeed one of the main components of wood, along with cellulose and hemicelluloses. Besides being the second most abundant biopolymer found on Earth after cellulose, lignin[2] is the only biomaterial based on aromatic units that is available on a large scale.

Wood is usually categorized into two groups: softwood (gymnosperm, i.e. conifers) and hardwood (angiosperm, i.e. deciduous or broad-leaved). These categories differ mainly in the respective types of wood cells: a more elaborated microscopic structure is found in hardwood, with a larger number of different types of cells, than in softwood. The amount of lignin present in these two types of wood differs: for trees that grow in the temperate climate zone, it varies between 26 and 32 % in softwood and between 20 and 26 % in hardwood (Sjöström, 1993).

The principal function of lignin in wood is to act as "glue" in the cell wall matrix of constituents: it not only glues the cells to each other but also keeps them from collapsing. Thus, lignin provides the wood material with its unique structural strength, rigidity and resistance to environmental stresses (Sjöström, 1993). Lignin also plays an important role in the transport of water into the vascular tissues: because of the hydrophobic nature of lignin, water is prevented from entering the cell wall. Finally, lignin provides a resistant protection against microorganisms, which is why wood is degraded much more slowly than other non-lignified plant materials: only a few specialized fungi and bacteria are able to degrade lignin.

2.2 Structure and properties of lignin

The structure of lignin is one of the most complex among naturally occurring polymers. It is generally described as a three dimensional, randomly cross-linked matrix of phenyl propane units. The structure of lignin is thus singular compared to the more ordered repeating units usually found in biopolymers, e.g. proteins and carbohydrates. Lignin also differs from other biomolecules by being optically inactive, i.e. its asymmetrical carbons are racemic.
The structure of the lignin macromolecules has not been defined yet, because its chemistry and biosynthesis are still not fully understood: these are currently the object of extensive investigation. Nevertheless, what is known is that the building blocks of native lignin consist of three different phenyl propane units: coniferyl alcohol, sinapyl alcohol and p-coumaryl alcohol, Figure 1.

---

[2] Lignin is found not only in woody plants but also in all vascular plants. It is actually believed to be the key in evolution that enabled vascular plants to develop at all.

The relative occurrence of the building blocks differs between the wood species: the coniferyl alcohol unit is almost exclusive in native softwood lignin, while 45-75 % of native hardwood lignin consist in sinapyl alcohol (Henriksson, 2009), Table 1[3].
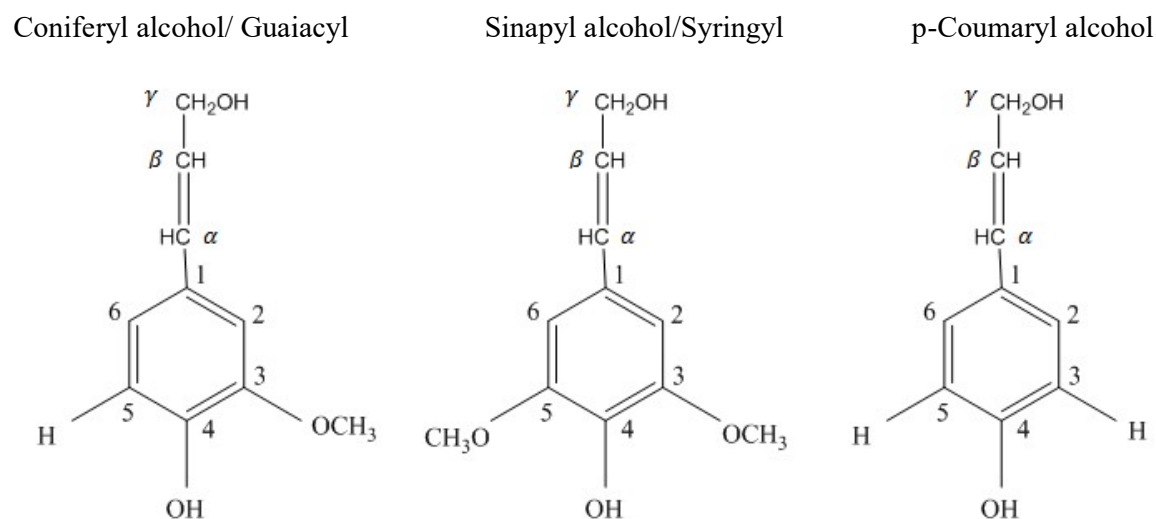
Coniferyl alcohol/ Guaiacyl   Sinapyl alcohol/Syringyl   p-Coumaryl alcohol

Figure 1. The building blocks of native lignin.

Table 1. Composition of monolignols in softwood and hardwood (Henriksson, 2009).

Wood specie	p-Coumaryl alcohol (%)	Coniferyl alcohol (%)	Sinapyl alcohol (%)
Softwood	< 5	> 95	0
Hardwood	0-8	25-50	45-75

No linkages that are ordered systematically have been determined so far between the different lignin building blocks: these are therefore currently considered to be random. It has been nevertheless found that, on average, approximately two-thirds of the chemical bonds are ether linkages (C-O-C), with the β-O-4 bond being the most common type of linkage found in native lignin (Henriksson *et al.,* 2010). The remaining one third of the chemical bonds are carbon-carbon linkages (C-C). The specific types of bonds and their relative occurrence vary between the wood species, as summarized in Table 2.

The main functional groups found in native lignin are hydroxyl (i.e. aliphatic & phenolic), methoxyl and carbonyl groups. Their relative amounts also depend on the wood specie, as presented in Table 3. The reactivity of lignin is affected by the proportion of these functional groups. A hypothetical representation of native softwood lignin, showing its main functional groups and the different linkages between its building blocks, was proposed by Alder (1977), see Figure 2.

Finally, the structure and functional groups of lignin are affected substantially by chemical reactions when it is extracted from the other wood constituents: extracted lignin is therefore referred to as "technical lignin" to distinguish it from native lignin.

---

[3] The structure and composition of lignin vary between the different wood species as well as within the tree itself in the different types of plant tissues and cells, and in the layers of the cell walls.

Table 2. Frequencies of the different types of linkage found in native softwood and hardwood lignins per 100 C_6C_3 units (Henriksson *et al.,* 2010).

Type of bond	Structure	Softwood	Hardwood
β-O-4		40-50	50-60
β-5		10-12	3
5-5		13	3
4-O-5		3	3
β-*β*		3	3
Bonds to 1-position		1-3	3
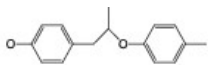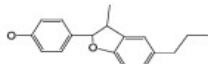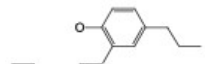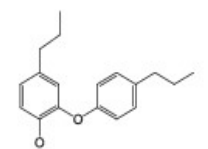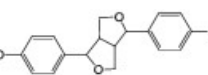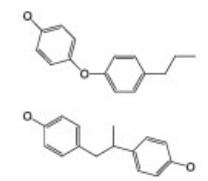
Table 3. Functional groups in native lignins (per 100 C_6C_3 units) (Sjöström, 1993).

Functional group	Softwood lignin	Hardwood lignin
Methoxyl	92-97	139-158
Benzyl alcohol (Aliphatic)	30-40	40-50
Phenolic hydroxyl	15-30	10-15
Carbonyl	10-15	
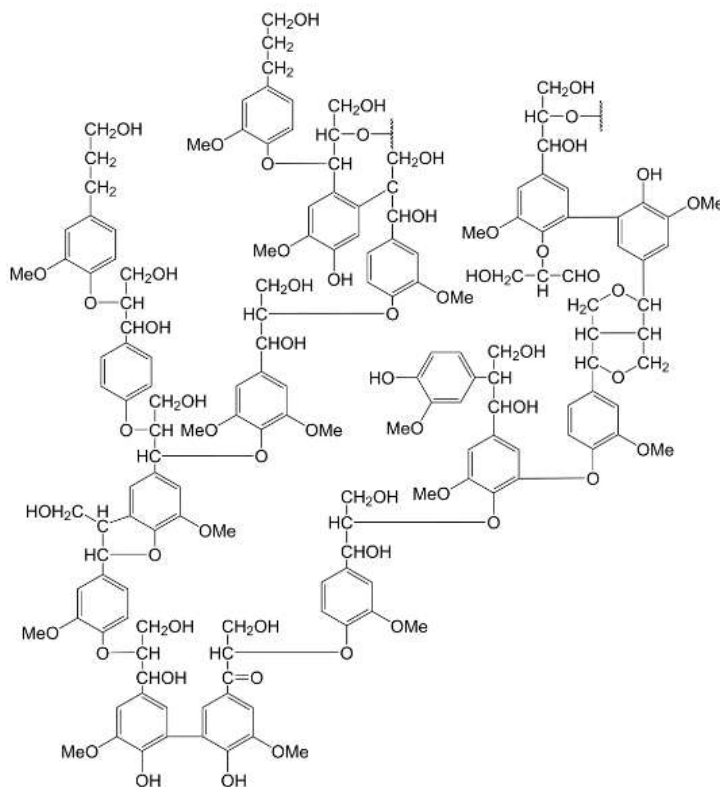
Figure 2. Hypothetical representation of the main functional groups and possible linkages found in native softwood lignin. Adapted from Alder (1977), (Zhu, 2015b).

2.3 Lignin-carbohydrate complexes

Beside lignin, the cell walls of wood are mainly composed of cellulose (i.e. linear D-glucose homo-polysaccharides) and hemicelluloses (i.e. hetero-polysaccharides). The latter differ from cellulose in that they are significantly smaller[4], relatively easy to hydrolyse, heterogeneous and are substituted by short branches.

It has been proposed that hemicelluloses act as an interface between the cellulose fibrils and lignin in the cell wall matrix of the constituents (Ljungberg, 2008). Chemical covalent linkages have been observed between lignin and the carbohydrate components, which include benzyl ether, benzyl ester, phenyl glycoside and acetal types of bonds (Watanabe, 2003). These chemically-linked complexes are often referred to as "lignin-carbohydrate complexes" (LCC). During Kraft pulping, LCC bonds are cleaved and smaller complexes, with a lower molecular weight, are formed: some LCC thus become soluble in black liquor (Gellerstedt and Lindfors, 1984).

The two main types of hemicellulose found in wood are xylans and glucomannans. While the main hemicellulose found in softwood is (galacto)glucomannan (about 20 wt% of wood and 60 wt% of total hemicelluloses), xylan is the most abundant hemicellulose found in hardwood (about 15-30 wt% of wood and 75-85% of total hemicelluloses). Furthermore, on molecular

---

[4] The degree of polymerization (DP) of hemicelluloses in native wood is about 100-200 while that of cellulose is around 10 000.

level, lignin seems to be associated more closely with xylan than with glucomannan or cellulose (Ljungberg, 2008).

The focus of this thesis is the hemicellulose xylan: a previous study has indicated that xylan might have a significant influence on the filtration of Kraft lignin when extracted from black liquor (Wallmo *et al.*, 2009). Xylan is composed of monomers of the pentose sugar xylose, which are linked to each other by glycosidic bonds as shown in Figure 3. Hardwood xylan is substituted mainly by acetyl ester groups: these are usually absent from softwood xylan[5], which contains arabinose units instead. One of the side groups of xylan that is present in both softwood and hardwood xylans is a specific uronic acid, namely 4-O-methylglucuronic acid (MeGlcA). On average, one MeGlcA is found for 8-20 (hardwood) and 5-6 (softwood) xylose residues (Ljungberg, 2008).
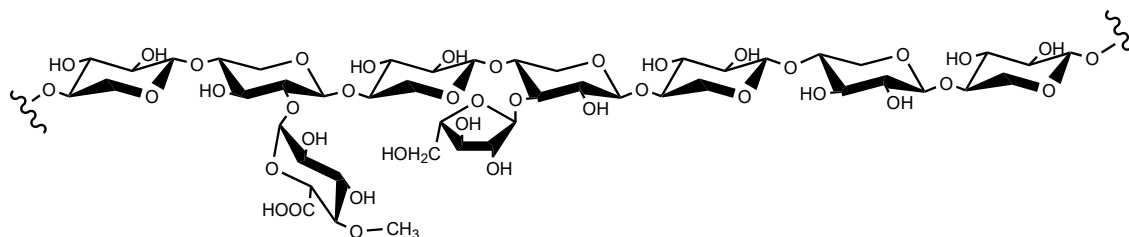

Figure 3. Representative structure of xylan. Adapted from Gellerstedt and Henriksson (2009).

2.4 Reactions during Kraft pulping

2.4.1 Lignin reactions

The principal reaction that occurs during Kraft pulping is the cleavage of the β-O-4 bonds of lignin, which is performed at controlled temperature (i.e. 150-170 °C) and using hydroxide and hydrosulphide ions as active cooking chemicals. The resulting degraded lignin has a significantly lower molecular weight than when non-degraded, and is substituted by a much larger amount of free phenolic groups; some carboxyl and aliphatic hydroxyl groups are also formed during the process (Froass *et al.,* 1998; Gellerstedt, 2009). Lignin thus becomes more hydrophilic and soluble in the cooking liquor, which is highly alkaline, due to deprotonation of the phenolic groups: this enables its separation from the cellulosic material of wood.

Furthermore, the polydispersity of the soluble lignin in black liquor is high (McNaughton *et al.,* 1967; Conors *et al.,* 1980) due partly to its variable degradation during cooking and partly to possible condensation reactions (Gierer, 1970; Gellerstedt, 2009).

It has been shown that, towards the final stage of delignification, dissolved lignin with a larger molecular weight and higher content of carbohydrates (most likely as LCC) is removed (Gellerstedt and Lindfors, 1984).

2.4.2 Xylan reactions

Xylan also undergoes several reactions during Kraft pulping that affect its structure and solubility. The so-called "peeling reaction" causes degradation of the hemicelluloses by splitting off the reducing end groups of the carbohydrate chain (Green *et al.,* 1977, Gellerstedt, 2004). This reaction is, however, limited in the case of xylan[6] due to the possible formation of stable metasaccharinic acid, which stops the peeling reaction; the uronic acid and arabinose side

---

[5] About 5-10 wt% of (arabinoglucorono) xylan is found in softwood (15-35 wt% of total hemicelluloses).

[6] In the case of glucomannan, the peeling reaction is very extensive during the Kraft process and it becomes heavily degraded.

groups also slow down the reaction. Xylan also undergoes alkaline hydrolysis during cooking which leads to the cleavage of some of its glucosidic bonds.

Furthermore, the acetyl groups of hardwood xylan are cleaved by hydrolysis, resulting in the formation of acetate (Ek *et al.*, 2009). Moreover, the main part of the glucoronic acid groups (MeGlcA) of xylan are converted into hexenuronic acid by elimination of their methoxyl groups; some hexenuronic acids are also cleaved off during cooking (Buchert *et al.,* 1995).

Even though the solubility of xylan in black liquor is high due to its remaining uronic acid side groups, pKa around 3.4 (Laine *et al.,* 1994), it has also been found that part of the dissolved xylan in black liquor redeposits onto the cellulose fibre surface (Yllner & Enström, 1956).

2.5 Potential applications of lignin

A classification of the potential applications of lignin has been made by considering the respective time needed to reach the market economy (Gosselink, 2011; Holladay et al., 2007; Higson 2011), as reported in Table 4. The first group includes near-term applications: lignin is seen as a feedstock for the production of energy and power, such as fuel and syngas. The second corresponds to medium-term applications: lignin is used as a macromolecule for the production of e.g. wood adhesives, carbon fibres and polyurethane foams. The final group consists mainly of long-term applications: lignin is degraded into its monomers to obtain aromatic building blocks, such as benzene, toluene, phenol and aromatic acids.

An important, and increasing, number of studies are currently being undertaken to develop technologies able to convert lignin efficiently into valuable products, e.g. carbon fibres (Kadla *et al.,* 2002; Baker *et al.,* 2011; Brodin *et al.,* 2012). When such new technologies become available, the popular, old and caustic maxim "you can do anything with lignin except make money" (which is already misleading) will definitely belong to the past. The first step in realising this is the ability to obtain an original lignin feedstock with a high degree of purity: this is what the LignoBoost process, which extracts lignin from Kraft black liquor, allows.

Table 4. Potential applications of lignin (Gosselink, 2011; Holladay *et al.,* 2007; Higson 2011).

		Lignin		
Fuel and syngas products	Macromolecule-derived products	Monomer-derived products		
		Hydrocarbons	Phenols	Oxidized products
Methanol	Carbon fibres	Benzene	Phenol	Vanillin
DME	Polymer	Toluene	Substituted	Vanillic acid
Ethanol	extenders	Xylene	phenols	DMSO
Mixed alcohols	Thermoset resins	Cyclohexane	Catechols	Aromatic acids
Fisher-Tropsch	Composites	Styrene	Cresols	Aliphatic acids
liquids	Adhesives	Biphenyls	Resorcinols	Syringaldehyde
C1-C7 gases	Binders		Eugenol	Aldehydes
	Preservatives		Syringols	Quinones
	Pharmaceuticals		Coniferols	Cyclohexanol
	Polyols		Guaiacols	B-keto adipate

2.6 The extraction of lignin from black liquor

2.6.1 Background

The following requirements should be fulfilled before the extraction of lignin from black liquor can be considered as being effective:

- High yield of the extracted lignin.
- Low amount of impurities in the extracted lignin.
- Relatively simple and robust procedure, with small energy demands and consumption of chemicals and water (i.e. low costs).

The two main methods that currently exist for extracting lignin are acid precipitation, followed by filtration and displacement washing, and ultrafiltration. Although the production of Kraft lignin by ultrafiltration can be considered as being technically feasible (Jönsson and Wallberg, 2009; Arkell *et al.,* 2014), the use of acid to precipitate lignin has been shown to provide a higher lignin yield at a lower estimated cost (Uloth and Wearing, 1989a & b), making this the method usually preferred. Furthermore, the lignin separated by the ultrafiltration method remains in a dissolved form. Performing ultrafiltration prior to precipitation can nevertheless be beneficial in some cases, e.g. in lowering the filtration resistance of difficult-to-filter lignin that originates from hardwood (Wallmo *et al.,* 2009) or for separating the lignin fraction into defined molecular weight distributions (Toledano *et al.,* 2010).

The acid precipitation of lignin, followed by filtration and washing, is a relatively old technique that was commercialized in 1942 by the Westvaco Company, in USA (now MeadWestvaco Corporation) (Pye, 2008). Three main parameters affect the efficiency of this procedure: pH, temperature and ionic strength. A pH between 9.5-10.5 and a temperature range of 60-80 °C were found to be the operational ranges that ensured a relatively high precipitation yield of lignin from black liquor and a lignin that was also relatively easy to filter (Öhman and Theliander, 2007b; Zhu *et al.,* 2014). Furthermore, the precipitation yield was found to increase when the ionic strength of the initial black liquor was increased (Zhu *et al.,* 2015a).

The use of carbon dioxide as the acidifying agent is preferable to sulphuric acid, which is the other main acidifying candidate, since carbon dioxide does not disturb the sulphur balance of the Kraft process (Wallmo *et al.,* 2007).

Subjecting the black liquor to heat treatment prior to precipitation was also found to improve the filtration properties (Öhman *et al.,* 2007c). Additionally, the efficiency of the lignin extraction process was shown to be affected significantly by the dry solid content of the initial black liquor (Loufti *et al.,* 1991). Consequently, the intake of black liquor is placed after the liquor has passed through part of the evaporation train in the Kraft pulping process line (dry content about 30-45 %).

The traditional acid precipitation technique could not, however, provide a lignin feedstock with a high degree of purity: a residual content of sodium[7] after washing was found, in some cases, to exceed 4 w % (Öhman and Theliander, 2006). Yet, high level of purity may be required if the lignin is to be used further as a raw material.

---

[7] Sodium ions constitute the main metal ion impurity found Kraft lignin followed by potassium: concentrations of about 85-94 wt% and 5-10 wt%, respectively, of the total residual metal ions, were found in Nordic softwood and Eucalyptus black liquors (Öhman and Theliander, 2006; Ziesig *et al.,* 2014b).

2.6.2   The LignoBoost process

The LignoBoost process is an improved version of the acid precipitation extraction technique. Performed at controlled pH and temperature, its main difference is the addition of an extra filtration stage (without washing) followed by a re-slurring step wherein the pH is decreased prior to the final filtration and washing stage (Öhman *et al.,* 2007a). This allows for the extraction of lignin with a much higher degree of purity, as explained below.

The principal issue with the old process is that part of the precipitated lignin is re-dissolved during the washing stage. This, in turn, can lead to clogging of the filter medium and/or of the filter cake if some of the lignin precipitates again, with severe consequences for the efficiency of the washing stage. Complete clogging results in virtually no washing flow, while partial clogging favours the existence of a preferred flow path within the filter cake, thereby causing a very uneven washing of the cake (Öhman *et al.,* 2006). Additionally, this partial re-dissolution of lignin leads to a lower yield of lignin extracted: a loss in solid lignin of around 13-23% has been recorded during washing (Öhman *et al.,* 2006).

The re-dissolution of lignin was found to be the consequence of the large pH and ionic strength gradients existing in the displaced liquor, throughout the lignin filter cake, during washing. Hence, lignin is extracted at a pH value of about 10, while the acid wash water has a pH of about 2-3. Furthermore, a relatively high amount of ions (mainly sodium) is trapped in the precipitated lignin, yet they have also been found to be displaced easily by the wash liquor (Öhman *et al.,* 2006). So, while the ionic strength decreases rapidly during washing, the pH value remains rather high because of the high buffering capacity of the system (phenolic groups on lignin and carbonate ions). The resulting wash water conditions, i.e. low ionic strength coupled with a relatively high pH, favour the re-dissolution of lignin in the wash water. Yet, a further small decrease in the pH when washing is continued, results in the re-precipitation of the lignin dissolved, which can lead to the pores in the filter cake or the medium being blinded.

With its two-stage separation process, the LignoBoost process minimises the dissolution of lignin during the washing stage, thereby avoiding possible plugging of the filter cake and/or the filter medium; a schematic diagram of the process is presented in Figure 4. Prior to the washing stage, the filter cake is re-dispersed in acid water the pH of which is adjusted to that of the final wash water using sulphuric acid. Consequently, the main changes in pH and ionic strength take place simultaneously in the re-slurring tank. The pH gradient in the final washing stage is, in turn, very small; the ionic strength gradient is also reduced considerably due to dilution in the re-slurring tank's water. Consequently, plugging problems no longer occur during washing and a good degree of efficiency is reached. Furthermore, the consumption of both water and sulphuric acid is minimised by taking the re-slurring water from the spent wash water stream, Figure 4.

Moreover, the low pH of the re-slurring water causes additional precipitation to take place during the re-slurring stage. This leads to a higher yield of lignin being extracted which, along with the improved washing efficiency of the LignoBoost process, means that investments costs can be reduced. The size of the filter area and the volume of the acid wash water can also be reduced. Also, since part of the spent wash water is recirculated back to the black liquor stream, the reduction in the amount of wash water required thanks to the greater efficiency of the new technique is also beneficial in terms of the energy demand of the evaporator. Using the LignoBoost process allows a wash ratio as low as 2 to yield a lignin with a very low content of residual sodium: 0.1-0.4 wt% (Öhman *et al.,* 2007a). The purity can be enhanced even further by additional washing, decreasing the pH of the re-suspension and/or wash water and increasing

the residence time in the re-suspension stage (Öhman *et al.,* 2007c; Ziesig *et al.,* 2014a; Ziesig *et al.,* 2015).
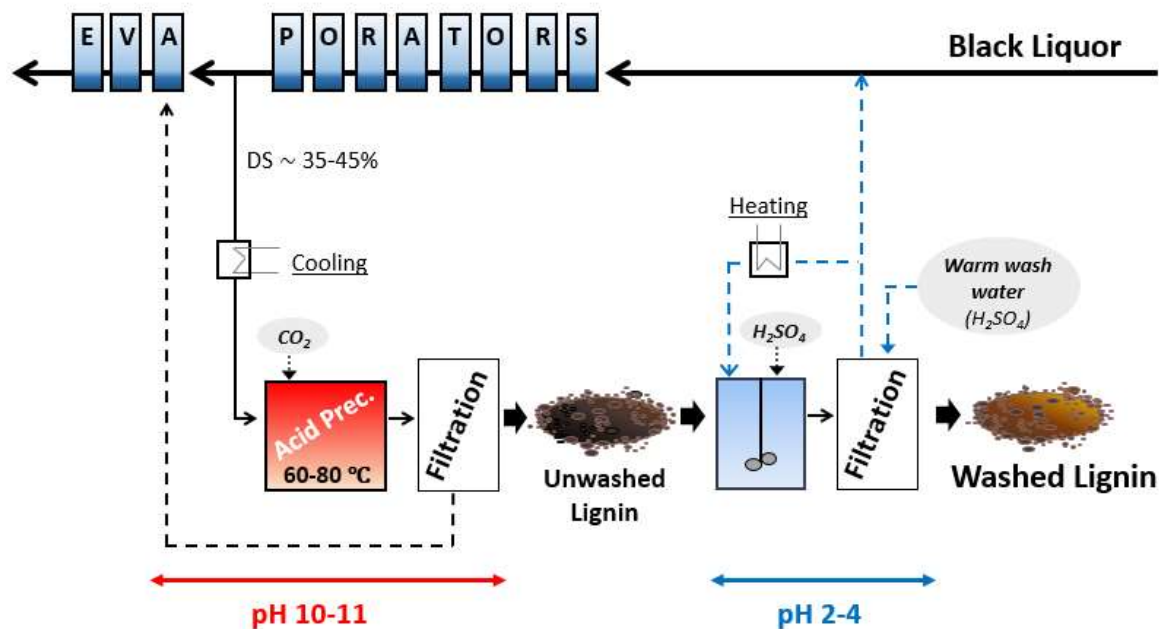

Figure 4. Schematic diagram of the LignoBoost process. DS: dry solid content. Prec.: precipitation.

2.6.3 Mechanisms of lignin precipitation during the LignoBoost process

Kraft lignin macromolecules, as mentioned previously, contain weakly acidic groups (i.e. mainly phenolic groups together with a few carboxylic acid groups) that are de-protonated in alkaline conditions and make the lignin charged and soluble in black liquor. Kraft lignin macromolecules can thus be considered as being polyelectrolytes in the aqueous black liquor solution. Furthermore, the negatively charged groups are likely to be concentrated on the surface of individual macromolecules; the shape of dissolved lignin being a spherical macromolecule is a commonly-used first approximation. Surrounding the negatively charged surface layer are the cations, which form a second layer of charges (mainly Na^+ and K^+) distributed according to the Boltzmann distribution (Goring, 1962; Lindström and Westman, 1980).

When the pH of the solution is decreased by the addition of carbon dioxide during the LignoBoost process (Figure 4), the protons that are formed neutralise the surface charge of the lignin macromolecules by protonating the phenolic groups. This starts to occur at a pH near/below the pKa of the phenolic groups of Kraft lignin, i.e. around pH 10.5 (Norgren *et al.,* 2000). As a result, the repulsive electrostatic interactions between the lignin macromolecules are reduced and the attractive forces[8] (i.e. van der Waals and hydrophobic forces) become dominant. This, in turn, causes the macromolecule to aggregate and, eventually, coagulate and precipitate. Although this interplay between attractive and repulsive forces is mainly dependent on the pH, it is also influenced by the ionic strength of the initial black liquor and temperature, together with the structure of the Kraft lignin, i.e. its molecular weight and functional groups

---

[8] The attractive forces were found to be generally independent from the conditions of the solution/suspension (i.e. pH and ionic strength) (Norgren *et al.,* 2001).

(Rudatin *et al.,* 1989; Norgren *et al.,* 2001; Norgren *et al.,* 2002). Increased ionic strength and lignin molecular weight were thus found to favour the aggregation and precipitation of lignin (Norgren and Lindström, 2000; Norgren *et al.,* 2001). The influence of temperature on lignin precipitation is, however, ambiguous: both an increase (Norgren *et al.,* 2001) and decrease (Zhu *et al.,* 2014; Öhman and Theliander, 2007b) in the amounts of lignin precipitated have been reported at increased temperatures, so this requires further investigation.

It has also been proposed that lignin behaves as a colloid in aqueous solutions, in case of high molecular weight macromolecules, (Marton, 1964; Lindström, 1979). Kraft lignin precipitation may thus be divided into different phases (as it is for the precipitation of colloids) (Norgren *et al.,* 2002). When the solution conditions become favourable for precipitation, the macromolecules first self-associate to form nuclei; high molecular weight macromolecules may also act as natural nuclei (Leubner, 2000). The formed nuclei then start to grow into colloidal seed points, onto which lower molecular weight macromolecules progressively sorb. The colloidal lignin particles also aggregate further to form clusters that, in turn, precipitate.
Besides nucleation and particle growth, the dynamics of particle formation also include particle breakage due to shear forces generated by mixing.

Typical yields of lignin precipitation during the LignoBoost process (performed at a pH of 9-10 and a temperature of 80 °C) are 50-70 wt% when using black liquors with a dry solid content of 29-30 wt% (Öhman and Theliander, 2007b).

2.6.4 Xylan reactions during the LignoBoost process

The xylan dissolved in black liquor is exposed to acidic conditions during the LignoBoost process, so the acid hydrolysis of the glycosidic linkages of xylan should be considered. The rate of hydrolysis decreases in the following order: hexenuronic acid > xylan backbone > glucoronic acid (MeGlcA), with the MeGlcA linkage being rather acid resistant (Ek *et al.*, 2009). The degradation of the xylan backbone also requires relatively severe conditions: in the case of birch xylan, for example, using a temperature of 90 °C or higher and a pH of 1 for 6 h has been shown to give a 60% degradation yield into xylose (Hilpmann *et al.,* 2016). The hexenuronic acid linkage can be hydrolysed selectively under slightly milder acidic conditions, such as pH 3.0-3.5 at a temperature of 90-95°C for 2-4h (Clavijo *et al.,* 2012).
Acid hydrolysis of the glycosidic linkages of xylan is therefore not likely to occur at the acid conditions used during the LignoBoost process, which are pH 2-4, temperature ≤ 60 °C and relatively short residence time.

3. Theoretical Aspects of Dead-End Filtration

3.1 Cake build-up during dead-end filtration

A schematic representation of cake formation during dead-end filtration (i.e. cake filtration), showing the case of an incompressible and a compressible filter cake, is presented in Figure 5. The applied piston pressure forces the liquid to flow through the filter medium. The solid particles do not, however, pass through the filter but accumulate on top of it. This results in the formation of a cake with a more or less homogeneous solid density in the direction of the flow, depending on the degree of compressibility, as illustrated in the Figure 5. All filter cakes form more or less compressible structures in reality.
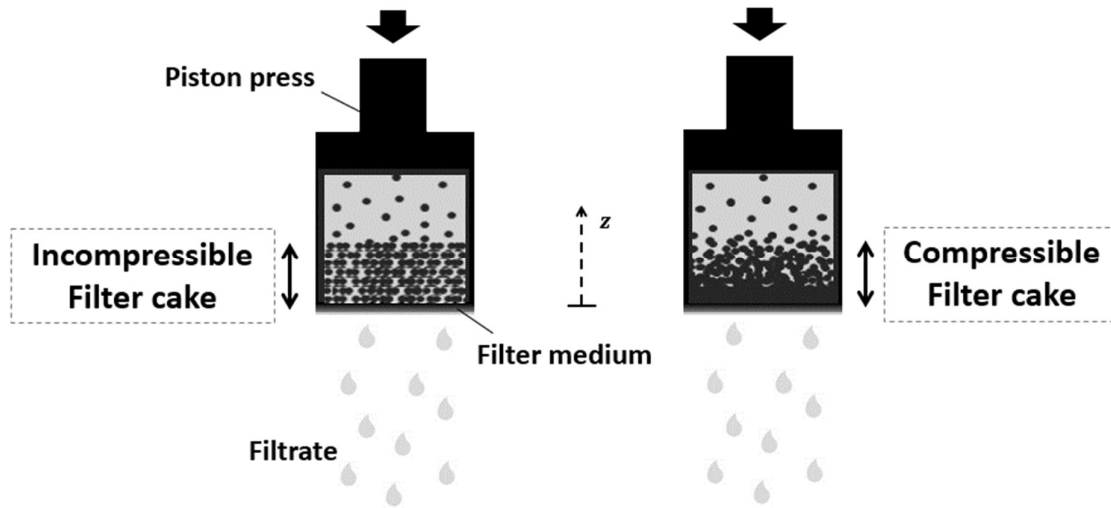
Figure 5. Schematic diagram of cake formation during dead-end filtration. Left: an incompressible filter cake. Right: a compressible filter cake.

3.1.1 Definition of the cake properties

The solid content of a filter cake is often described as its "solidosity", i.e. the volume-based fraction of solids within it. The expression of the average solidosity, $\emptyset_{av}$, of the filter cake is defined by Eq. 1 and 2; the solidosity can also be related to the porosity of the cake according to Eq. 3.

$$\emptyset_{av} = \frac{V_{solid}}{V_{total}} \qquad\qquad \text{Eq. 1}$$

$$\emptyset_{av} = \frac{1}{L} \int_0^L \phi\, dz \qquad\qquad \text{Eq. 2}$$

$$\emptyset_{av} + \varepsilon_{av} = 1 \quad (\text{also: } \phi + \varepsilon = 1) \qquad\qquad \text{Eq. 3}$$

In the equations, V_{solid} and V_{total} are the volume of non-dissolved solids and the total volume of the cake (i.e. volumes of non-dissolved solids and of liquid including dissolved solids such as salt), respectively, L the cake thickness, ϕ the local solidosity at a height z from the filter medium and ε_{av} and ε the average and local porosity of the cake, respectively.

When flowing through the cake, the liquid acts on the solid through skin friction: a drag force is exerted on the particles. A one-dimensional force balance performed at time t of the filtration experiment, and on a small element dz of the filter cake, can be written as Eq. 4. The atmospheric pressure appears on both sides of this equation and is therefore cancelled out in the force balance; the gravitational and inertial forces are neglected and not included in Eq. 4:

$$P_{piston}(t) = \Delta P(t) = \frac{f_s(z,t)}{A} + p_l(z,t)$$

Eq. 4

where $P_{piston}(t)$ is the piston pressure applied (which is also equal to the pressure drop over the filter cell ΔP), f_s the sum of the liquid drag on the solid particles, A the cross-sectional area of the filter cell and p_l the local liquid pressure or hydrostatic pressure.

The solid stress ratio $\frac{f_s(z,t)}{A}$ is usually interpreted as a pressure: the local compressive pressure of the solid during filtration, i.e. $p_s(z,t) = \frac{f_s(z,t)}{A}$, with the assumption of point contact between the particles.

Another way of interpreting the drag force exerted by the flowing liquid on the solid particles is to consider that the filter cake being formed induces a resistance towards the flow of liquid passing through it, known as the "cake filtration resistance". This gives a measure of how easy or difficult a material is to filter. The average filtration resistance of a filter cake can be defined by Eq. 5 thus:

$$\frac{1}{\alpha_{av}} \equiv \frac{1}{P_c} \int_0^{P_c} \frac{dp_s}{\alpha}$$

Eq. 5

where α_{av} is the average filtration resistance of the filter cake, P_c the pressure drop over the filter cake and α the local specific filtration resistance.

Finally, the permeability, K, is a characteristic of a solid bed that describes its ability to allow a fluid to pass through it. It is usually considered as being related only to the properties of the bed. Yet, in the case of filtration, it is common for this characteristic of a solid bed to be presented in term of resistance to flow. The relation between the local permeability, K, of a cake and its local filtration resistance is defined by Eq. 6:

$$\alpha = \frac{1}{K\rho_s\phi}$$

Eq. 6

where ρ_s is the solid density of the particles.

3.1.2 Spatial and time dependence of the cake properties

The same total pressure is applied to any cross-section of height z of the filter cell, i.e. the applied piston pressure in addition to the atmospheric pressure. Therefore, the total applied pressure may only vary with time, depending of the filtration mode. There are three filtration modes possible during cake build-up: constant applied pressure, constant flow rate and variable

pressure and flow rates. In this work, all filtration experiments were performed at constant applied pressure over time.

Even if the total applied pressure is constant, however, both the solid compressive pressure and the hydrostatic pressure vary not only with time but also spatially in the direction of the flow. At constant applied pressure, the local hydrostatic pressure decreases with time and in the direction of the flow, while a corresponding increase in solid compressive pressure is observed as the liquid transmits its pressure load to the solid forming the filter cake via skin friction.

In the general case of a compressible filter cake, the solid structure cannot sustain this increase in drag on the solid particles over time and in the direction of the flow. Therefore, a new, more compact, structure is gradually formed over time and the closer from the filter medium by the rearrangement and/or deformation of the particles/agglomerates. A stable and compact structure eventually forms when the solid compressive pressure is sufficiently high, and the compressibility of the filter cake levels out.
Because of the more compact structure that is formed over time and in the direction of the flow, the filtration resistance is also increased over time and in the direction of the flow.
Furthermore, in the case of a compressible structure, the solid particles move within the filter cake during filtration: the velocities of both the solid and the liquid are thus time and spatially dependant. Yet, the mobility of the solid particles within the filter cake becomes gradually more limited as the structure of the cake becomes more compact, and it therefore decreases with time and in the direction of the flow. On the other hand, the liquid velocity increases in the direction of the flow even though the liquid hydrostatic pressure decreases in the direction of the flow, because the flow channels are smaller in size where the structure of the cake is being compressed.

The extent to which a filter cake is compressible can be evaluated by investigating the influence of the solid compressive pressure on its solidosity and filtration resistance. This can be determined during cake build-up by making local measurements during the filtration experiment (see Section 3.5). Furthermore, the study of the local influence of the solid compressive pressure on the filtration properties can be performed at one single height within the filter cake because a range of solid compressive pressures is covered over time at one given position in it.

3.2 Modelling cake build-up

3.2.1 The case of incompressible cakes

3.2.1.1 Spatial description: the Darcy equation
In 1856, Darcy proposed a correlation for an incompressible structure that described the flow of liquid through a porous solid bed as a function of the pressure drop (Darcy, 1856). The Darcy equation[9] can be applied locally to describe the flow of liquid passing through a differential element of a filter cake being formed during filtration, Eq. 7:

$$v = -\frac{K}{\mu}\frac{dp_l}{dz} \qquad\qquad \text{Eq. 7}$$

---

[9] Even though the influence of the fluid viscosity was not included in the original relation proposed by Darcy, Eq. 7 is still referred to as Darcy's equation.

where v is the z coordinate of the superficial fluid velocity and μ the fluid viscosity.

Eq. 7 can then be expressed in terms of flow resistance using Eq. 6, which gives Eq. 8:

$$v = -\frac{1}{\alpha \rho_s \phi \mu} \frac{dp_l}{dz}$$

Eq. 8

In order to solve the above equation, two constitutive relationships are needed that relate α and ϕ, respectively, to p_l (cf. Section 3.3.1). In practice, correlations relating α and ϕ to p_s are preferred because they have a more direct physical meaning. Eq. 8 is thus also rewritten in terms of p_s (Eq. 9 below) using the spatial derivative of Eq. 4, which gives $\frac{dp_l}{dz} = -\frac{dp_s}{dz}$.

$$v = \frac{1}{\alpha \rho_s \phi \mu} \frac{dp_s}{dz}$$

Eq. 9

3.2.1.2 Cake formation over time: the classical filtration equation

The classical filtration equation is used to describe the formation of a cake over time and allows for the determination of its average filtration resistance, as defined by Eq. 5. This equation was proposed by Ruth in 1935, and was obtained by integrating the Darcy equation over the entire filter cake. Using Eq. 6, the equation can be expressed in terms of filtration resistance as Eq. 10. The relation is based on the assumption that the filter cake is incompressible, which implies that:

- the velocity of the solid particles is zero
- the superficial velocity of the fluid is constant over the entire filter cake and can be considered equal to the filtrate velocity, i.e. $\frac{1}{A}\frac{dV}{dt}$, where V is the volume of the filtrate
- the solidosity is constant over the entire filter cake and is equal to its average solidosity
- the filtration resistance is constant over the entire filter cake and is equal to its average filtration resistance

$$\frac{P_c}{\alpha_{av}} = \mu L \rho_s \phi_{av} v = \mu L \rho_s \phi_{av} \frac{1}{A}\frac{dV}{dt}$$

Eq. 10

The pressure drop over the filter cake is often difficult to measure experimentally, so it is usually more convenient to use the pressure drop over the entire filter cell, i.e. the filter cake and the filter medium, which equals the filtration pressure, Eq. 11. In order to express the pressure drop over the filter medium, P_m, a filter medium resistance, R_m, is introduced, Eq. 11. This is done based on analogy with Ohm's law: the resistances of the medium and the filter cake (towards the flow of liquid), respectively, are regarded as two resistances in series.

$$P_{piston} = \Delta P = P_c + P_m = P_c + \mu R_m v$$

Eq. 11

The classical filtration equation is obtained by combining Eqs. 10 and 11, and is often written as Eq. 12:

$$\frac{dt}{dV} = \frac{\mu(\alpha_{av} c V + R_m A)}{A^2 \Delta P}$$

Eq. 12

where c is the mass of solids per unit filtrate volume, which can be considered constant for incompressible filter cakes.

Plotting $\frac{dt}{dV}$ against V gives a straight line during cake formation at constant applied pressure: the average filtration resistance can then be determined from the slope of the line obtained. The resistance of the filter medium can also be deduced from its interception with the ordinate axis.

Yet, the pressure drop over the filter cake, and therefore its average filtration resistance, might not be stabilized at the early stage of the filtration process due to the relatively high flow velocity when the filter cake is very thin (Hermia, 1988). Consequently, a straight line is not usually obtained from the start: the calculated average filtration resistance does not therefore describe the very early stage of filtration.

Eq. 12 is also used at times in its integrated form to determine α_{av} by measuring the volumes of filtrate obtained at some chosen experimental times. However, the differential expression is more accurate since it considers instant values: this makes possible variations in flow easier to detect (especially at the beginning of the filtration process).

3.2.2 The case of compressible filter cakes

When the solid structure is compressible, the solids particles are also in motion within the cake, so the liquid velocity in Eq. 7 should be replaced by the liquid velocity relative to the velocity of the solid particles. The Darcy equation was therefore modified by Shirato *et al.* (1969): the velocity of the solid particles is taken into account in order to extend the use of the equation to compressible solid packing, Eq. 13:

$$v - \frac{1 - \phi}{\phi} v_s = -\frac{K}{\mu} \frac{dp_l}{dz} \qquad\qquad \text{Eq. 13}$$

where v_s is the superficial velocity of the solid material in the z direction.

Furthermore, when experiments are performed at constant applied filtration pressure, Eq. 12 also works well for weakly compressible filter cakes in the determination of α_{av} by plotting $\frac{dt}{dV}$ against V. This is because the filter media often has a very low flow resistance compared to the cake (apart from a few seconds at the beginning of the experiment), so the pressure drop across the filter cake is virtually constant when performing experiments at constant applied pressure. Yet, in the case of weakly and even moderately compressible filter, the average filtration resistance is often virtually constant, regardless of the height of the filter cake when subjected to a constant pressure drop over the filter cake. This last statement can be verified by plotting the dimensionless height of the filter cake versus the filtration pressure to investigate whether or not the same profile is obtained regardless of its true height. It can also be confirmed by the fact that the plot of $\frac{dt}{dV}$ versus V gives a straight line for Eq. 12. If the plot that is obtained is not linear, it is then clear that the cake is highly compressible and/or there are severe blinding effects.

Finally, for highly compressible filter cakes, Tiller and Shirato (1964) introduced a correction factor scaling the product $\alpha_{av}cV$ in Eq. 12 in order to consider the variations in α_{av} and c over such compressible cakes. The "J_R factor" accounts for the variations in the velocities of both the liquid and the solid within the filter cake during filtration. It is a function of both the initial concentration of the slurry and the pressure applied; it was also found to approach unity for a highly diluted slurry.

3.3 Constitutive relationships

3.3.1 Empirical constitutive relationships

A number of empirical relationships have been proposed that relate the local filtration resistance and the local solidosity to the local compressive solid pressure in order to solve Eqs. 8, 9 and 13. These constitutive relationships can be used to evaluate the degree of compressibility of a filter cake. The solid compressive pressure is considered as being the only independent variable: the filtration resistance and the solidosity are thus often modelled as power law functions of the solid compressive pressure. The following relationships, Eqs. 14 and 15, proposed by Tiller and Leu (1980), are examples of such correlations:

$$\alpha = \alpha_0 \left(1 + \frac{p_s}{P_a}\right)^n \qquad\qquad \text{Eq. 14}$$

$$\phi = \phi_0 \left(1 + \frac{p_s}{P_a}\right)^\beta \qquad\qquad \text{Eq. 15}$$

where n, β, α_0, ϕ_0 and P_a are parameters.

The parameters β and n give an indication of the degree of compressibility of the filter cake being investigated: high values of β and n correspond to a high degree of compressibility. The additional parameters α_0 and ϕ_0 may be interpreted as the respective values of α and ϕ obtained at zero solid compressive pressure, i.e. at the very top of the filter cake.

Local data obtained experimentally is used in order to determine the value of the parameters of these empirical constitutive relationships, and is necessary for every particles system investigated. As it is often simpler to determine average filtration data experimentally, expressions of the average filtration properties as a function of the parameters of the empirical correlations are also used.

The average filtration resistance and average solidosity during cake build-up can be defined by Eqs. 5 and 2, respectively. Integration of Eqs. 5 and 2 using the Tiller and Leu relationships expressing the local properties, Eqs. 14 and 15, gives the relations of the average filtration properties as functions of the parameters of the empirical relationships, Eqs. 16 and 17. Eq. 9 was also used to develop Eq. 17 using a quasi-steady state approximation of a constant v over the entire filter cake.

$$\alpha_{av} = \alpha_0 \frac{(1-n)(P_c/P_a)}{(1 + P_c/P_a)^{1-n} - 1} \qquad\qquad \text{Eq. 16}$$

$$\phi_{av} = \phi_0 \frac{1 - n - \beta}{1 - n} \frac{(1 + P_c/P_a)^{1-n} - 1}{(1 + P_c/P_a)^{1-n-\beta} - 1} \qquad\qquad \text{Eq. 17}$$

Once the fitted parameters obtained for the filtration of several materials known to be more or less compressible were determined, a material classification was constructed (Leu, 1981), Table 5. This classification is based on the values of the Tiller and Leu parameters, Eqs. 14 and 15, and characterises a material filter cake with respect to its degree of compressibility.

Table 5. Material classification based on the parameters of the empirical constitutive relationships proposed by Tiller and Leu, (Leu, 1981).

Parameter	Pressure dependency of the filter cake		
	weak	moderate	high
n [-]	0.20	0.60	1.20
α_0 [m/kg]	10^9	10^{10}	10^{11}
β [-]	0.05	0.15	0.30
ϕ_0 [-]	0.30	0.20	0.10

3.3.2 Permeability relationships

3.3.2.1 The Kozeny-Carman equation

The Kozeny-Carman equation (Kozeny, 1927) is used to describe the flow of liquid through a porous bed at laminar conditions as a function of the pressure drop over the bed, the structure of the bed and the liquid viscosity, Eq. 18. It considers a bed structure composed of an assemblage of tortuous capillaries and is based on the Hagen-Poiseuilles equation that describes the laminar flow of a Newtonian fluid in a cylinder. A good accuracy of the Kozeny-Carman equation was obtained in the case of rigid particles with a narrow size distribution that were relatively large in size.

$$v = -\frac{1}{kS_p^{\,2}\mu}\frac{\varepsilon^3}{(1-\varepsilon)^2}\frac{dp_l}{dz} \qquad \text{Eq. 18}$$

In Eq. 18, k is the Kozeny-Carman constant, which depends on the geometry of the particles and the porosity of the bed, and S_p is the specific surface area of the particles.

By comparing Eq. 18 to Darcy's equation, Eq. 7 (and given the relation between solidosity and porosity, Eq. 3), an expression of the permeability as a function of the cake structure can be obtained, Eq. 19:

$$K = \frac{(1-\phi)^3}{kS_p^2\phi^2} \qquad \text{Eq. 19}$$

Assuming that the solid is composed of perfect spheres, the specific surface area of the particle can be replaced by its diameter according to $d_p = 6/S_p$. A k value of 4.8 is also often used in the case of solid spheres. The permeability in Eq. 19 can be replaced by the filtration resistance using Eq. 6. Consequently, Eq. 19 can be rewritten as Eq. 20:

$$\alpha = \frac{172.8\times\phi^2}{d_p^{\,2}(1-\phi)^3}\times\frac{1}{\rho_s\emptyset} \qquad \text{Eq. 20}$$

3.3.2.2 Cell models

Cell models assume that the bed is comprised of an assemblage of cells: one cell consists of a solid and a liquid phase that can vary in shape. The solid phase is surrounded by the liquid phase and the volumes of the two satisfy the solidosity of the system. Solving the simplified Navier-Stokes equation with the assumption of creeping flow on a cell-structured bed, gives an expression of the permeability as a function of the geometry of the system.

3.3.2.2.1 Happel's cell model

The cell model developed by Happel (1958) considers two concentric spheres, with the inner sphere being solid. The simplified Navier-Stokes equation is solved by assuming a non-slip condition at the solid-liquid interface, zero tangential stress and uniform velocity at the outer liquid surface. The following expressions, Eqs. 21 and 22, are then obtained:

$$K = \frac{2 - 3\gamma + 3\gamma^5 - 2\gamma^6}{3 + 2\gamma^5} \frac{a^2}{3\gamma^3} \qquad \text{Eq. 21}$$

$$\gamma^3 = (a/b)^3 = \phi \qquad \text{Eq. 22}$$

where a is the radius of the inner solid sphere and b is the radius of the whole cell.

Eq. 6 can be used to rewrite Eq. 21 in terms of filtration resistance, giving Eq. 23 below:

$$\alpha = \left[\frac{2 - 3\gamma + 3\gamma^5 - 2\gamma^6}{3 + 2\gamma^5} \frac{a^2}{3\gamma^3} \right]^{-1} \times \frac{1}{\rho_s \gamma^3} \qquad \text{Eq. 23}$$

3.3.2.2.2 Cell model with a porous spherical core

An extension of Happel's cell model was developed by Deo (2009), which considers that the inner solid sphere is porous rather than compact: the Brinkman equation (Brinkman, 1947) is then used to describe flow through it. The simplified Navier Stokes equation is still used to describe the flow outside the solid core, with the same outer boundary conditions as in Happel's model, i.e. no tangential stress and a uniform flow velocity. The following expressions are obtained, Eqs. 24-27:

$$K = \frac{2a^2 \left(1 + \frac{3}{2} \{ k_1 - \gamma + (1 + 14k_1 + 30k_1^2)\gamma^5 \} \right)}{9\gamma^3 \left(1 + \frac{2}{3}\gamma^5 + 10\gamma^5 \left(k_1 - \frac{1}{3}\lambda \right) \right)}$$
$$+ \frac{2a^2 (\lambda\{1 - 3(2 + 5k_1)\gamma^5 + 5\gamma^6\} - (1 + 15k_1)\gamma^6)}{9\gamma^3 \left(1 + \frac{2}{3}\gamma^5 + 10\gamma^5 \left(k_1 - \frac{1}{3}\lambda \right) \right)} \qquad \text{Eq. 24}$$

$$\lambda = \frac{\sinh\left(\frac{1}{\sqrt{k_1}} \right)}{\frac{1}{\sqrt{k_1}} \cosh\left(\frac{1}{\sqrt{k_1}} \right) - \sinh\left(\frac{1}{\sqrt{k_1}} \right)} \qquad \text{Eq. 25}$$

$$k_1 = k_i/a^2 \qquad \text{Eq. 26}$$

$$\gamma^3 = (a/b)^3 = \phi/\phi_i \qquad \text{Eq. 27}$$

where k_i and ϕ_i are the permeability and solidosity of the inner sphere, respectively.

Eq. 6 can be used to rewrite Eq. 24 in terms of filtration resistance, giving Eq. 28:

$$\alpha = \left[\frac{2a^2\left(1+\frac{3}{2}\{k_1-\gamma+(1+14k_1+30k_1^2)\gamma^5\}\right)}{9\gamma^3\left(1+\frac{2}{3}\gamma^5+10\gamma^5\left(k_1-\frac{1}{3}\lambda\right)\right)} + \frac{2a^2\left(\lambda\{1-3(2+5k_1)\gamma^5+5\gamma^6\}-(1+15k_1)\gamma^6\right)}{9\gamma^3\left(1+\frac{2}{3}\gamma^5+10\gamma^5\left(k_1-\frac{1}{3}\lambda\right)\right)} \right]^{-1} \times \frac{1}{\rho_s\phi_i\gamma^3} \qquad \text{Eq. 28}$$

3.4 Electrostatic and other particle interactions during filtration

3.4.1 General aspects

Friction, interlocking between particles (steric interactions) and forces such as van der Waals and electrostatic interactions are among the main inter-particle interactions that occur during cake build-up. Although all these interactions may be of importance during filtration, this thesis focuses on the latter, i.e. electrostatic interactions. These are governed by the structure, shape and the surface charge of the solid particles, and have been shown to be highly significant for particles on a micrometer scale or smaller (Fu and Dempsey, 1998; Wakeman *et al.,* 1989).

Modifying either the pH or the ionic strength of the surrounding liquid are two possible ways of reducing the electrostatic repulsive interactions between particles which, in turn, favours agglomeration. Studies have shown that modification of the ζ-potentials or the particle surface charge by varying the pH of the slurry had a significant effect on the resulting flow rate, porosity and filtration resistance of the cake (Wakeman *et al.,* 1989; Koenders and Wakeman, 1996; Larue *et al.*, 2003; Mattsson *et al.,* 2011). For example, when the pH of the filtration slurry was lowered, a decrease in the surface charge of particles was obtained for titanium dioxide suspensions: the result was a cake with a more porous structure and reduced filtration resistance (Mattsson *et al.,* 2011). In the case of charged colloidal particles, an electric field might also be used to influence the filtration behaviours and give and additional driving force for separation (Kobayashi *et al.,* 1979).

3.4.2 Filtration models accounting for inter-particle interactions

Inter-particle interactions influence the filtration properties of the filter cake greatly by governing the solid structure being formed. Several models have therefore been proposed that aim at relating the filtration properties to inter-particle interactions. In addition to the Darcy equation commonly used to relate the liquid velocity to the solid compressive pressure, the continuum and momentum equations of the solids and the fluids, respectively, constitute the starting point of these models. The way in which the particle interactions are modelled differ between them: they may be based, for example, on micromechanics (Koenders and Wakeman, 1997; Koenders *et al.,* 2000) or compressional rheology (Landman *et al.,* 1995; Stickland and Buscall, 2009). The models are also expressed using different coordinate systems, i.e. spatial (Wakeman 1978; Tien and Bai, 2003) or material (Sorensen *et al.,* 1996), and differ in the boundary conditions considered.

3.5 Overview of techniques for measuring local filtration properties

3.5.1 Local pressure

A direct way of estimating the local solid compressive pressure during filtration is to measure the local hydrostatic pressure and, given the known total applied pressure, using the relation between them, i.e. Eq. 4. Pressure probes have therefore been mounted inside the filter cell in various studies. Several configurations have been proposed for the location of such probes:

attached to the cell wall (Chase and Willis, 1992; Fathi-Najafi and Theliander, 1995), mounted downwards from the top of the cell (Okamura and Shirato, 1955; Shirato *et al.,* 1971) or at the bottom of the filter cell and through the filter medium (Johansson and Theliander, 2003). The actual flow of filtrate and the build-up of the cake may, however, be affected by proximity to the cell wall (Tiller *et al.,* 1972), so the probes are often placed a few millimetres away from the cell wall. Also, it is possible that free flow paths may form around the probes when they are mounted downwards from the top of the cell: this does not occur when the probes are mounted at the bottom of the filter cell.

3.5.2   Local solid content

Several techniques can be used to measure the local solid content of a filter cake. One traditional method, which is relatively simple and inexpensive, is cake dissection: the cake is physically separated into several layers when filtration is complete (Dell and Sinha, 1964; Meeten, 1993; Yim and Song 2008). This method, however, is not only tedious and destructive but also does not allow the local solid content to be determined continuously during a filtration experiment.

A non-destructive and continuous method for measuring solidosity is the use of nuclear magnetic resonance (NMR) measurements (Horsfield *et al.,* 1989; Dirckx *et al.,* 2000; Saveyn *et al.*, 2006), which allows a high level of accuracy to be reached (e.g. error of less than 1% was found by La Heij *et al.,* 1996). Another advantage of the NMR technique is that the water which is bound physically or chemically can be distinguished from the free water (Kopinga and Pel, 1994; La Heij *et al.,* 1996).

Alternative non-destructive and continuous methods include measuring the attenuation of γ-rays (Bergström, 1992; Johansson and Theliander, 2003; Mattsson *et al.,* 2011) and x-rays (Shen *et al.,* 1994; Tiller *et al.,* 1995). In this case, the use of a strong radiation source may improve the time resolution considerably and reduce the measurement error: an estimated error of less than 2 % may be achieved (Mattsson *et al.,* 2011). Measuring conductivity is another non-destructive and continuous technique, although it requires either conductive material or the addition of an electrolyte (Shirato *et al.,* 1971; Wakeman, 1981). Errors of about 5% have been reported using this method (Chase and Willis, 1992). Cake coloration, performed stepwise during filtration, has also been used to measure its local solid content, as the height of each slice can be monitored based on its colour. This technique is, however, limited partly by the height of the individual coloured layers and partly due to the procedure involved in forming the cake being complex (Hutto, 1957).

3.5.3   Compression – Permeability cell

An indirect and traditional way of measuring local filtration data in the case of compressible filter cakes is the use of the Compression-Permeability (C-P) cell introduced by Ruth in 1946 (Ruth, 1946). After the formation and expression of the filer cake at a known applied pressure, new fluid is introduced into the cell and allowed to flow through the cake. Thus, the permeability of the cake can be calculated (using the Darcy equation), along with the solidosity of the cake, at the known applied pressure.

Based on the assumption that a homogeneous filter cake is formed after expression, the average data obtained can be considered to equal the local data. The pressure dependency of the local data may therefore be evaluated either by forming a new cake at each new applied pressure or by subjecting the cake formed to a higher pressure, prior to repeating the procedure with the addition of more fluid, in order to determine the new permeability and solidosity values at the new higher applied pressure.

This procedure may, however, be criticized since the formation of a homogeneous filter cake is difficult due to e.g. friction at the cell walls. A ratio with a maximum upper limit has to be

considered between the filter cake thickness and its diameter in order to reduce the negative impact of the cell walls (Tiller et *al.,* 1972). Furthermore, such measurements do not take into account the dynamics of the cake build-up and expression phases (e.g. flow stabilization during cake build-up) that may also influence the actual local properties.

Nevertheless, this technique is still widely employed because of its relative simplicity, and new types of C-P cells and methods are being developed. For example, equipments based on centrifugal filtration such as the analytical photocentrifuge, make the continuous measurement of consolidation kinetics easier (Lerche and Sobisch, 2007; Loginov *et al.,* 2014). Furthermore, a device that enables a direct correlation between C-P cells and actual filtration test was developed (Teoh *et al.,* 2002). Simulations of the effect of the cell walls are also being conducted with the aim of correcting local measurements (e.g. Zhao *et al.,* 2003).

4. Equipment and Determination of Filtration Data

4.1 The filtration unit

The test filtration equipment used in this work was designed for filtration, expression and washing. A schematic diagram of the unit is shown in Figure 6.

A filtration pressure of maximum 6 MPa can be delivered by the pneumatic cylindrical piston. The filtration cell measures 0.175 m in height and 0.06 m in inner diameter. Visual observation is permitted during filtration experiments via the lower section of the cell, which is a Plexiglas cylinder 0.115 m in height. The base of the filter cell consists of a perforated plate that supports the filter medium and allows the filtrate to flow through the cell during the experiments.
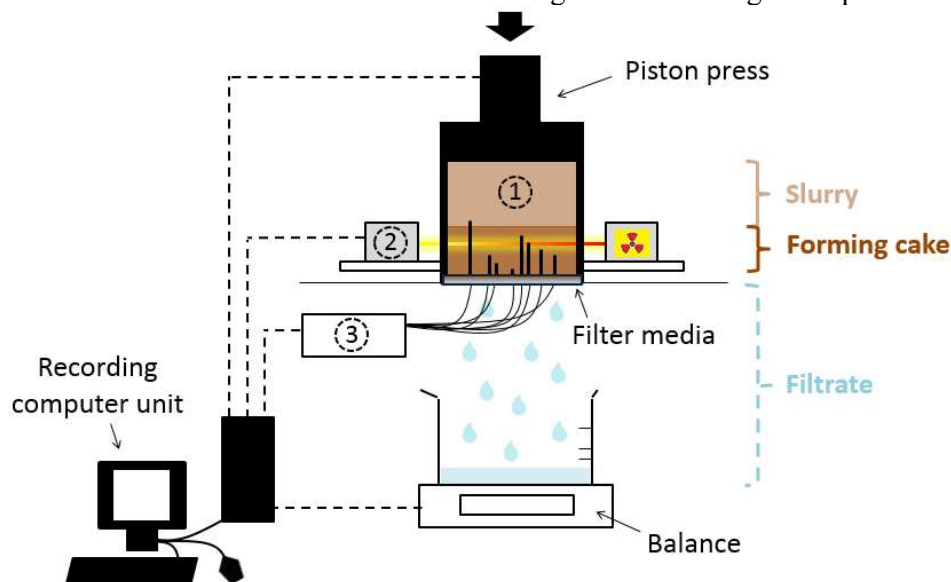

Figure 6. Schematic diagram of the filtration equipment. 1) Filtration cell, with water-filled capillaries of different heights mounted at the bottom; 2) Scintillator detector facing the ^{241}Am γ-source at the other side of the filtration cell, placed on a movable rack; 3) Pressure transducers.

The local hydrostatic pressure is measured at different heights from the filter medium using eight water-filled capillary tubes mounted at the bottom of the filter cell and connected to pressure transducers, Figure 6. The pressure transducers (Kristal Instrument AG) have a maximum measurement error of 10 kPa. Each capillary tube has an opening of 0.6 mm in diameter just below its top, which is parallel to the direction of the flow, Figure 7 (a). The openings are located between 0.5 and 12 mm above the filter medium, depending on the height of the corresponding tube. Each capillary has a sharp conical top to minimize flow disturbances, Figure 7 (a). Calibration to atmospheric pressure is performed before a filtration experiment is started; examples of hydrostatic pressure profiles obtained can be found in Section 4.2.1.

The local solid concentration of the forming cake is determined during a filtration experiment using a ^{241}Am γ-source (10^9 Bq) along with a NaI (T1) scintillation detector placed on a

movable rack, and located at each side of the filtration cell, Figure 6. The ^{241}Am γ-source and detector are fully shielded in lead, apart from a thin uncovered slit centred on each item and facing towards each other, Figure 7 (b). The openings are 24 mm wide, 3 mm high for the source and 1 mm high for the detector; both are 20 mm deep to assure a well-collimated beam. Thus the γ-radiations that pass through a precise slice of the filter cell can be recorded at a chosen height, adjusted using the movable rack. The attenuation of the γ-radiations measured allows for the calculation of the local solidosity, see Section 4.2.3.1. The energy interval investigated is 36 to 91 keV, so the attenuation of γ rays measured is mainly the result of the photoelectric effect and Compton scattering (Bertin, 1975).
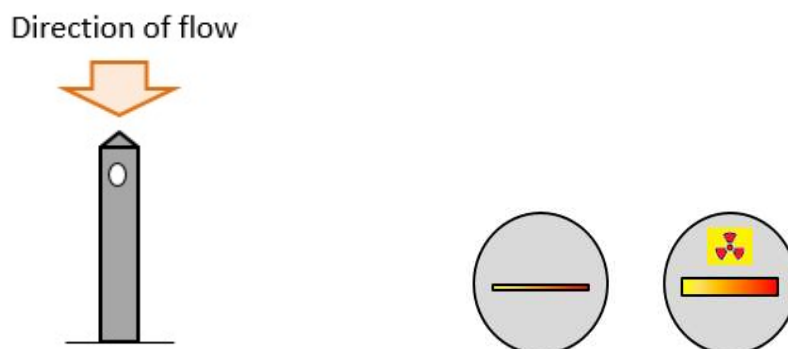

Figure 7: a (left) and b (right). (**a**): Schematic representation of a water-filled capillary tube with an opening parallel to the direction of flow and a sharp conical top. (**b**): Frontal representation of the cylindrical lead-shielded ^{241}Am γ-source and detector showing the thin, central, unshielded openings.

Several data is measured and recorded during each filtration experiment using a computer connected to the filtration unit, see Table 6.

Table 6. Experimental data measured during each filtration experiment.

Data measured	Time interval of measurement	
Position of piston (Temposonic EP-V-0200M-D06-1-V0)		
Mass of filtrate, collected in a vessel placed on a mass balance (Mettler Toledo SB 32000, repeatability of 0.5 g)	2 s	
Local hydrostatic pressure at eight different heights		
Total γ-radiation counts that pass through a local slice of the filter cell	*LignoBoost lignin*	*Titanium dioxide*
	1 or 2 min.	5 min.

4.2 Determination of the filtration data

4.2.1 Hydrostatic pressure profile

The local hydrostatic pressure that was measured continuously at various heights made it possible to plot the hydrostatic pressure profile throughout the filter cake as it continued to form throughout the filtration experiments. Large oscillations in local pressures can be observed during these experiments when cracks form in the filter cake or when air is trapped in the slurry and, subsequently, in the filter cake. Improved quality and reliability of the data was therefore

ensured by excluding data corresponding to experiments that "failed" (i.e. affected by avoidable disturbances). Examples of the absolute hydrostatic pressure profiles obtained for a successful and a non-successful filtration experiment are shown in Figure 8 (a) and (b), respectively. Another important piece of information that can be detected by this method of measuring local pressure is the potential formation of a skin layer and/or clogging of the filter medium. In such cases, the local pressure remains high and constant over the filtration process at all of the capillary heights investigated: the whole pressure drop is located very close to/at the filter medium. Examples of skin formation detected can be found in the literature (Mattsson *et al.,* 2012).
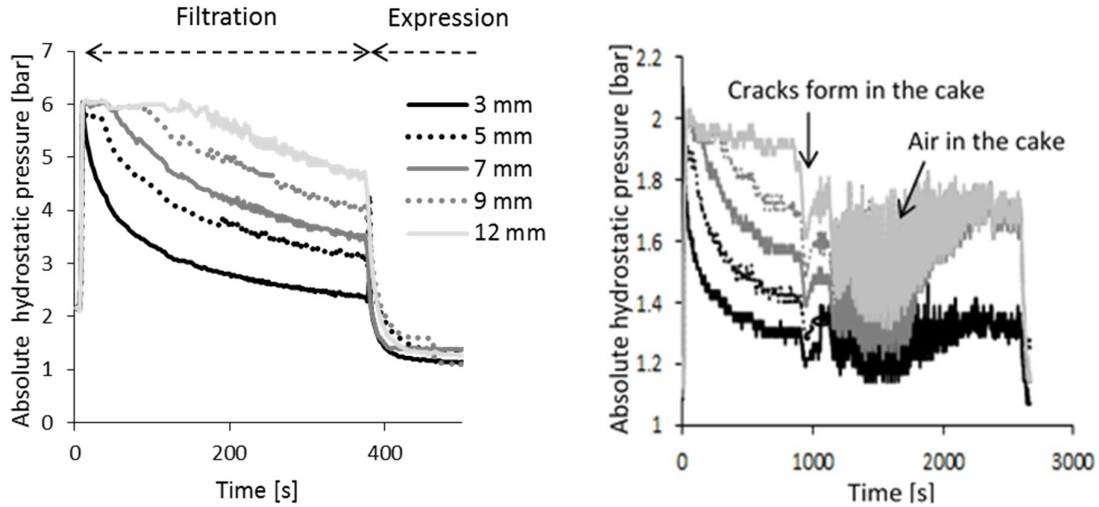

Figure 8: a (left) and b (right). Absolute local hydrostatic pressure versus time at different heights from the filter medium, obtained for: (**a**) a successful experiment (5 bar in applied piston pressure) and (**b**) a non-successful experiment (1 bar in applied piston pressure). The curves correspond to the height of the holes in the capillary tubes.

At the beginning of a filtration experiment (i.e. no filter cake has yet formed), all the local hydrostatic pressures measured are equal to the absolute applied pressure, i.e. the applied piston pressure plus atmospheric pressure, Figure 8 (a) and (b). The initial absolute hydrostatic pressure that was measured was therefore used to determine the actual applied piston pressures in the filtration cell for each experiment. Potential inaccuracies due to, for example, uncertainty related to the pressure regulator or pressure losses caused by friction of the piston on the cell walls are thereby excluded.

As the cake is being formed, friction between the liquid and the solid causes a decrease in the local hydrostatic pressure at a given position in the filter cake, see Section 3.1.2. Therefore, when the height of the forming cake reaches that of a capillary hole, a decrease in hydrostatic pressure is observed at the corresponding height, Figure 8 (a) and (b). When there is no slurry left above the filter cake, the piston reaches the surface of the cake: expression starts and the applied pressure is directly transmitted to the solid (i.e. $p_l(z, t) = 0$ and $p_s(z, t) = P_{piston}(t)$ in Eq. 4).

4.2.2 Average filtration properties

4.2.2.1 Average solidosity

The average solidosity of the filter cake was calculated after an extended time of expression according to Eq. 1, using the dry and wet weights of the cake that were measured and the known

densities of both the liquid and the solid. In the case of LignoBoost lignin, the dry content of the filtrate (measured using the moisture analyser Sartorius MA30) was also taken into consideration when determining the volume of non-dissolved solids V_{solid}.

4.2.2.2 Average filtration resistance

The classical filtration theory (Eq. 12) was used to calculate the average filtration resistance. c was assumed to be constant, and was taken as the ratio of the weighed, dry, undissolved, solid mass of filter cake over the total filtrate volume collected during each filtration experiment. A straight line was obtained for all the filtration experiments performed when $\frac{dt}{dV}$ was plotted against V. This implies that the assumption that was made in order to apply the classical filtration theory (i.e. moderately compressible filter cake, see Sections 3.2.1.2 and 3.2.2) can be considered valid. Furthermore, the resistance of the filter media R_m was found to be negligible compared to that of the filter cake in all of the cases investigated.

4.2.3 Local filtration properties

4.2.3.1 Local solidosity

The local solidosity was calculated from the γ-attenuation data (recorded during the filtration experiments) according to the Beer-Lambert law of absorption, Eq. 29:

$$-ln\frac{\eta_\gamma}{\eta_{\gamma,0}} = \mu_{\gamma,l}d_\gamma + \left(\mu_{\gamma,s} - \mu_{\gamma.l}\right)d_\gamma\phi \quad \leftrightarrow \quad \phi = \frac{ln\frac{n_{\gamma,0}}{n_\gamma} - \mu_{\gamma,l}d_\gamma}{\left(\mu_{\gamma,s} - \mu_{\gamma,l}\right)d_\gamma} \qquad \text{Eq.29}$$

where η_γ is the number of counts recorded, $\eta_{\gamma,0}$ the number of counts recorded for the empty filter cell, $\mu_{\gamma,l}$ and $\mu_{\gamma,s}$ the attenuation coefficients of the liquid and solid phases, respectively, and d_γ the average path of the γ-radiation taken as the inner diameter of the filter cell (i.e. 0.06 m).

Measurements were performed at a height of either 12 or 9 mm above the filter medium (see Sections 5.1.3 and 5.2.2). The attenuation coefficient of the liquid phase was determined by using the γ-attenuation measurements performed on a cell filled with filtrate in the LignoBoost lignin experiments, and pure water in the titanium dioxide experiments. The attenuation coefficient of the solid phase was determined after expression of the cakes, by calibrating the coefficient using Eq. 29, to match the known average solidosity of the expressed filter cakes. Furthermore, a statistical method was used to evaluate the repeatability of the γ-attenuation measurements (Nelson, 1970) which takes into consideration the fact that the radiation intensity describes a Poisson distribution.

The attenuation coefficients of the solid and liquid phases obtained for the different slurries investigated in the LignoBoost lignin experiments are presented in Table 8 (Section 5.1.3), together with the calculated absolute deviations in local solidosity, $|\Delta\phi|$, based on a 95 % confidence interval. The attenuation coefficients of the solid and the liquid phases were found to be relatively close to each other for the LignoBoost lignin experiments, Table 8 (Section 5.1.3), i.e. around 20 m^{-1} for the filtrate and 23-24 m^{-1} for the solid phase. Rather long measurement times are thus needed to obtain very accurate results. However, since the materials were also found to be relatively fast to filter, a time interval not longer than 1 or 2 min was chosen (see Section 5.1.3). Some deviation of the local solidosity (and, consequently, the local filtration resistance data) must therefore be expected for the systems investigated: absolute

deviations between 0.028 and 0.062 m³/m³ in local solidosity were determined based on a 95 % confidence interval, and are given in Table 8 for the presented data (Section 5.1.3).

Attenuation coefficients of $\mu_{\gamma,water}$= 19.6 m⁻¹ and $\mu_{\gamma,TiO2}$= 189 m⁻¹ were obtained for the titanium dioxide experiments. The deviation in local solidosity in the case of titanium dioxide, based on a 95 % confidence interval, was found to be ≤ 0.006 m³/m³ in absolute value (for local measurements performed every 5 min).

4.2.3.2 Local filtration resistance

The local filtration resistance was determined using Eq. 8 because the materials investigated formed weakly to moderately compressible filter cakes, and the solid particle velocity was negligible compared to the liquid velocity in the flow direction for the thin slice of filter cake investigated in the local study. The pressure gradient $\frac{dp_l}{dz}$ was estimated from the difference between two local liquid pressures measured at heights corresponding to those chosen for the γ-attenuation measurements, i.e. 12 and 9 mm above the filter medium. The pressure measurements used were therefore made at either 12 & 9 mm or 9 & 7 mm above the filter medium. Furthermore, the superficial flow velocity, v, is constant through the whole filter cake and equals the superficial filtrate velocity. The filtration experiments were relatively fast for LignoBoost lignin suspended in acid water (Slurry 1, see Section 5.1.2), so the flow velocity was calculated based on the filtrate mass that was recorded continuously during the experiments. For all other cases, the flow velocity was determined from the position of the piston which was also recorded continuously for the duration of the experiments. This method of calculation was preferred generally over the use of the filtrate mass because of the possible loss of filtrate due either to evaporation from the vessel placed on the mass balance (Figure 6) and/or to contact with the edges of the equipment (i.e. the perforated bottom plate and wires connecting the capillary tubes to the pressure transducers).

The relative experimental uncertainty of the local filtration resistance $\Delta_{rel}\alpha$ was approximated to equal the experimental deviation induced by the local solidosity: $\Delta_{rel}\phi = \frac{|\Delta\phi|}{\phi}$ (the deviation introduced by the local hydrostatic pressure measurements was negligible compared to that introduced by the local solidosity). The relative experimental uncertainty of the local filtration resistance $\Delta_{rel}\alpha$ was approximated to equal the experimental deviation induced by the local solidosity: $\Delta_{rel}\phi = \frac{|\Delta\phi|}{\phi}$ (the deviation introduced by the local hydrostatic pressure measurements was negligible compared to that introduced by the local solidosity). The uncertainties obtained were averaged over all the measurements made for each slurry, $\overline{\Delta_{rel}\alpha}$, and are given in Table 8 for the presented data (Section 5.1.3). Deviations between 6.8 % and 19.2 % were found for the LignoBoost lignin experiments and uncertainties below 1.3 % were obtained for the titanium dioxide experiments.

5. Experimental Conditions and Procedure

5.1 LignoBoost lignin experiments

5.1.1 Materials

The lignins used in this work were softwood Kraft lignins extracted from black liquor using the LignoBoost process. Sourced from two different Nordic pulp mills, they are referred to as Batch A and Batch B, respectively. The contents of phenolic and carboxylic groups found in one of the LignoBoost lignins investigated (Batch B) were determined elsewhere and found to be 4.27 mmol/g and 0.45 mmol/g, respectively (Aminzadeh *et al.,* 2017).

The xylan used was a xylan powder from beechwood, with three batches from three different producers being used: a Megazyme batch, a TCI (Tokyo Chemical Industry) batch and a Sigma Aldrich batch. The glucuronic acid content of the Megazyme batch of xylan was stated by the producer as being 13.0 wt%. At the conditions investigated in this study, the glucuronic acid groups of xylan are not likely to be degraded into hexenuronic acid, nor to be alkaline or acid hydrolyzed (see Sections 2.4.2. and 2.6.4).

Sodium sulphate (Fisher Chemical, purity > 99.5 %) was added during the preparation of some slurries to increase the ionic strength. The pH of the slurries was adjusted using sodium hydroxide (Sigma Aldrich, purity ≥ 98%) for dissolution, and sulphuric acid (Scharlau, 95-97 % and Emsure, 95-97 %) for precipitation.

The fluorescent dye used to stain xylan was Remazol Brilliant Blue R (Sigma Aldrich R-8001), and is referred to here as RBBR (see Appendix A of Paper III for further information).

5.1.2 Slurry composition and preparation

Two different procedures were used to prepare the model liquors investigated, namely a suspension procedure and a dissolution & re-precipitation procedure. Two different acidification protocols were used in the latter: fast and slow. The cases are all described in the sections below; a summary of the experimental conditions used are shown in Table 7, along with the concentrations of the components. When xylan was added to lignin, the lignin/xylan ratio was 95 g/ 5 g (lignin/xylose ratio of 95 g/ ~3.8 g), which corresponds to the ratio found in Swedish hardwood Kraft black liquor (Wallmo *et al.,* 2009).

The ionic strength of the slurries (IS), given in Table 7, was calculated from the relation $IS=\frac{1}{2}([Na^+] + [H^+] + 4[SO_4^{2-}])$, where $[H^+]$ is the concentration of the remaining protons that has been estimated after acid base reaction during acidification.

Following preparation, all slurries were left under continuous stirring and at room temperature (approx. 20°C) for a minimum of 12 h before filtration, which was also performed at room temperature. When the rate of stirring was too high, a foam-like layer was observed at the top of the lignin slurry, so a moderate stirring rate was used to prevent gas bubbles from forming in the suspension feed. A down-flow pitch-blade impeller, angled at 45°, was used as the stirrer.

Table 7. The various lignin slurries investigated. L: lignin, X: xylan, dX: dyed xylan, S: extra salt added, Prec.: precipitation, T: temperature and IS: ionic strength. The relative uncertainty in ion concentration is estimated to be ≤ 4%.

No.	Slurry	IS [mol/L]	Prec. T [°C]	pH	Lignin [wt%]	Na$^+$ [mol/L]	SO$_4^{2-}$ [mol/L]
Suspension							
1.a					8.8		
1.b	L$_A$	<0.01	-	2.8	12.0	0.00	<0.01
1.c					19.8		
1.d					21.6		
2	L$_A$ + X$_{Sigma}$	<0.01	-	2.3	9.1	0.00	<0.01
3	L$_A$ + X$_{TCI}$ + S	0.94	-	2.8	8.5	0.62	0.31
Dissolution & re-precipitation: fast acidification							
4	L$_A$	0.67	80	2.1	8.4	0.4	0.2
5	L$_A$ + X$_{TCI}$	0.68	80	2.7	8.4	0.4	0.2
6	L$_A$ + X$_{TCI}$ + S	0.94	80	2.8	8.4	0.6	0.3
7	L$_A$	1.15	80	1.1	8.3	0.4	0.4
8	L$_A$ + X$_{Sigma}$	1.15	80	1.1	8.3	0.4	0.4
9	L	1.67	77	3.9	8.5	0.95	0.60
9'	L	1.70	77	4.2	8.6	0.97	0.61
10	L + X$_{TCI}$	1.69	77	4.0	8.5	0.97	0.60
10'	L + X$_{Sigma}$	1.67	77	3.9	8.4	0.96	0.60
11	L	1.11	77	4.2	9.1	0.75	0.37
12	L + X	1.10	77	4.2	9.0	0.75	0.36
13	L + dX	1.06	77	4.3	8.8	0.74	0.35
14	L	1.32	77	4.1	9.0	0.75	0.47
15	L + dX	0.98	77	4.0	8.7	0.67	0.32
16	L + X	0.95	77	2.8	7.9	0.63	0.32
16'	L + X	0.95	77	3.0	7.9	0.63	0.32
17	L + dX	1.05	77	2.9	8.6	0.72	0.34
18	L + X$_{TCI}$	1.84	77	2.2	8.6	0.98	0.67
Dissolution & re-precipitation: slow acidification							
19	L	1.82	77	4.1	9.8	1.08	0.64
20	L + X	1.88	77	4.1	10.0	1.09	0.66
20'	L + X	1.71	77	4.1	8.9	0.99	0.61
20''	L + X	1.88	77	4.1	9.4	1.08	0.67
21	L + X + S	6.72	77	4.0	7.8	4.37	2.27
22	L	1.77	65	4.1	9.0	1.01	0.63
22'	L	2.11	65	4.1	10.7	1.29	0.73
23	L + X	1.69	65	4.0	8.8	1.00	0.60
24	L	1.51	45	4.7	8.2	0.90	0.53
25	L + X	1.51	45	4.7	8.1	0.90	0.53

L$_A$ refers to Batch A of LignoBoost lignin; all other lignin is from the Batch B. X$_{Sigma}$ and X$_{TCI}$ refer to the Sigma Aldrich and TCI xylan batches, respectively; all other xylan is from the Megazyme batch.

5.1.2.1 Suspension procedure

Slurries 1-3: solid lignin, with or without the addition of xylan powder, were mixed and suspended at room temperature (approx. 20 °C) in distilled water at a pH not exceeding 2.8. Each slurry was acidified using sulphuric acid to avoid any dissolution of the solids into the water due to deprotonation of the phenolic/acid carboxylic groups. In the case of Slurry 3, the ionic strength of a lignin-xylan suspension was increased to 0.9 mol/L by the addition of sodium sulphate. In the case of the lignin suspension without an addition of xylan or extra salt, four different lignin concentrations were considered: Slurries 1 a-b-c-d, see Table 7. A volume of 3 L of slurry was prepared for each suspension investigated and a down-flow pitch-blade impeller, 10 cm in diameter and angled at 45°, was used for mixing. A stainless-steel vessel, with a volume of 8.5 L and an inner diameter of 21 cm, was used.

5.1.2.2 Dissolution & re-precipitation procedure

All the pH adjustments were made using sodium hydroxide for dissolution and sulphuric acid for precipitation.

5.1.2.2.1 Precipitation vessel

- Slurries 4-8: a stainless-steel precipitation vessel was used, with a volume of 5.6 L and an inner diameter of 19 cm. It was equipped with a stainless-steel lid to limit evaporation, as well as stainless-steel baffles positioned along the walls to enhance mixing. A Rushton impeller (8 cm in diameter) was mounted at approximately 3 cm from the bottom of the vessel. Furthermore, the precipitation vessel was immersed into a thermostatic oil bath. A volume of 3.8 L of slurry was prepared for each case investigated.

- Slurries 9-25: the precipitation vessel used was a 0.5 L jacketed glass vessel with an inner diameter of 9.6 cm. It was equipped with a plastic lid to limit evaporation, as well as stainless-steel baffles positioned along the walls to enhance mixing. At approximately 1.5 cm from the bottom of the vessel, a down-flow pitch-blade impeller was mounted that was 5 cm in diameter and angled at 45°. The interior temperature of the jacketed glass was controlled by a connected heating-circuit. A volume of 0.45 L of slurry was prepared for each case investigated.

5.1.2.2.2 Fast acidification

- Slurries 4-8: solid lignin, with or without the addition of xylan powder, was dissolved in distilled water with its pH adjusted to 13.8. Dissolution was performed at a temperature of 80 °C and under stirring (250 rpm) for about 1.5 h. The solids were then re-precipitated by one main addition of acid to about neutral pH, which was directly followed by the dilution of the resulting suspension in acid water. Thus, a final pH of 2.1-2.8 was achieved for one series of slurries (Nos. 4-6) and a final pH of 1.1 was obtained for a second series (Nos. 7-8). Precipitation (and dilution) were performed at a temperature of 80 °C and under continuous stirring for about 1.5 h.
  The NaOH and H_2SO_4 added gave the slurries a final ionic strength of about 0.7 mol/L for the pH 2.1-2.8 series and about 1.2 mol/L for the pH 1.1 series. In one particular case of a lignin–xylan slurry with a pH of 2.8 (Slurry 6), the ionic strength was increased to about 0.9 mol/L by adding sodium sulphate during the dissolution procedure and the final stage of dilution.

- Slurries 9-18:
  Slurries 9- 10' and 18: a significantly higher final ionic strength was achieved in these cases compared to the other slurries subjected to fast acidification. This was done in order to reach

similar ionic strengths as those obtained in the case of a slow acidification. The lignin powder was first dissolved in a distilled water solution at room temperature and a pH of about 13.4 for a minimum of 2 h. The pH of the solution was then decreased to about 12.6 before being left under continuous stirring (250 rpm) for about 40 min, prior to the addition of xylan and the temperature being raised.

Slurries 11-17: lignin powder, with or without the addition of xylan powder, was dissolved in a distilled water solution at room temperature at a pH of about 12.

In all cases (Nos. 9-18), the temperature was then raised to 77°C before the slurries were left to dissolve under stirring (250 rpm) for a minimum of 2 h. Thereafter, the solids were re-precipitated and the resulting suspension was diluted by a single main addition of acid with water: a final pH of about 4.1 was achieved for one series of slurries (Nos. 9-15) and a pH of 2.2–3 was obtained for a second series (Nos. 16-18). Precipitation (and dilution) was performed at a temperature of 77°C and under continuous stirring (250 rpm) for a minimum of 1.5 h and maximum of 3 h. The NaOH and H_2SO_4 that were added gave the slurries a final ionic strength of about 1.0-1.3 mol/L for Nos. 11-17, and to a significantly higher value of about 1.7-1.8 mol/L for Nos. 9-10' and 18.

▪ Slurries 13, 15 and 17: a fluorescent dye (RBBR) was attached to the xylan prior to the preparation of each slurry (see Appendix A, Paper III). After the dyed xylan was synthesized and washed, small amounts of sodium sulphate (Na_2SO_4) and sodium phosphate (Na_3PO_4) were still present in the dyed xylan precipitate obtained. Corresponding amounts of salts were therefore added, before acidification, when Slurries 11-16 (which did not contain dyed xylan) were being prepared to compensate for the amount of salts introduced by the dyed xylan. In these cases, the resulting concentration of phosphate ions was about 0.01 mol/L, which is not reported in Table 7 and neglected in the calculation of the ionic strength.

▪ Slurries 9 and 10': a pH of around 3.6 was first achieved after the one-stage addition of sulphuric acid with water. A negligible amount of sodium phosphate (Na_2HPO_4) was therefore also added during the end of the precipitation stage (at 77°C) in order to adjust the pH of the suspension to a value closer to the target value of 4.1. A final concentration of phosphate ions lower than 0.01 mol/L was achieved in these cases, which is not reported in Table 7 and neglected in the calculation of the ionic strength.

5.1.2.2.3 Slow acidification

Lignin powder was dissolved in a distilled water solution, the pH of which was adjusted to about 13.4. Dissolution was performed at room temperature, overnight and under continuous stirring (250 rpm). In the case of xylan being added to the lignin, the pH of the solution was first decreased to about 12.6 before the temperature was raised. The temperature of the slurry was then increased to either 77°C, 65°C or 45°C and left under continuous stirring (250 rpm) for about 2 h. The solids were thereafter re-precipitated by adding diluted acid (6M) dropwise, over a minimum of 10 hours: this was done to ensure conditions close to chemical equilibrium during the entire acidification process. A final pH of about 4.1 was reached for Slurries 19-23, and 4.7 for Slurries 24-25. Precipitation was performed at a constant temperature of either 77°C, 65°C or 45°C and under continuous stirring (250 rpm).

The NaOH and H_2SO_4 that were added led to the slurries having a final ionic strength of about 1.5–2.1 mol/L (the initial sodium ion concentration was 1 M). In one particular case of a lignin–xylan slurry (No. 21), the ionic strength was increased to about 6.7 mol/L by adding sodium sulphate before the temperature was raised (the initial sodium ion concentration was 4 M in this case).

- Slurries 19, 20, 21, 22', 23, 24 & 25: these were subjected to FBRM measurements during acidification in order to evaluate the formation of particles/agglomerates, and their size, during precipitation (see Section 6.2.2). In these cases, the lignin mixture was first filtered after the dissolution procedure to remove the non-dissolved/insoluble material, as this had the potential of affecting the precipitation behaviours monitored using FBRM[10]. Less than 1 wt% of the original lignin was filtered off using vacuum filtration and a regenerated cellulose membrane was used as the filter medium (Sartorius stedim, Type 184, 0.45 µm in pore size). The pre-filtered solution, with a pH value of 13.4, was then added to the precipitation vessel. In these experiments, the pH of each slurry was also measured several times during acidification: a sample of about 10 ml was withdrawn from the precipitation vessel and cooled down to 25 °C prior to the pH being measured by a Mettler Toledo Seven Compact™ S220 pH meter, which had been calibrated previously at room temperature. After the pH measurement was complete, the sample was reheated to the corresponding experimental temperature and returned to the precipitation vessel. This pH sampling method (including the return of the sample) did not show any measurable influence on the formation or agglomeration of particles.

- Slurries 24 and 25: in these cases, in which the slurries were subjected to a precipitation temperature of 45 °C, a gel-like structure was obtained during precipitation.

5.1.3 Filtration conditions and procedure

The slurries investigated differ in concentration, preparation procedure, ionic strength, pH and precipitation temperature, see Table 7. All these parameters were studied with regards to their influence on the filtration properties of lignin. The influence of the applied filtration pressure (Slurries 1-8) and of the filter media were also investigated.

A summary of the piston pressures applied and the filter media used for the various slurries are presented in Table 8. The precise pressures applied in the filter cell were determined from the value recorded by the local pressure probes at the beginning of each filtration experiment, see Section 4.2.1.

A large range of local solid compressive pressures could be covered by combining the results obtained from the different filtration experiments performed at various constant applied piston pressures in case of Slurries1-8. The local filtration properties were determined from the local data measured every 2 min during the filtration experiments and at a given position in the filter cake: 12 mm from the filter media for Slurries1-8 and 9 mm from the filter medium for the rest. Local properties were also calculated based on a time interval of 1 min in the case of Slurry 1 (very fast to filter).

The attenuation coefficients calculated for the solid and the liquid phases ($\mu_{\gamma,s}$ and $\mu_{\gamma,l}$), absolute deviations in local solidosity, $|\Delta\phi|$, averaged relative deviation in local filtration resistance, $\overline{\Delta_{rel}\alpha}$, are also given in Table 8 (see Section 4.2.3 for determination of the values).

Three different filter media were used: a regenerated cellulose membrane filter (Sartorius stedim, Type 184, pore size 0.45 μm); a cellulose nitrate filter (Sartorius stedim, Type 113, pore

---

[10] No pre-filtration was performed on Slurry 20', for which FBRM measurements were only made after acidification (under stirring at 250 rpm) once its temperature had reached room temperature.

size 0.45 μm) and referred to as NC in Table 8; a polyethersulphone membrane (Supor, pore size 0.45 μm for Slurry 20' and 0.1 μm for Slurries 20''- 23) and referred to as PES in Table 8. All filters were placed on a Grade 5 Munktell paper filter for support.

The filtration experiments were performed at room temperature (i.e. about 20° C). Following filtration, the filter cakes were subjected to expression at the applied filtration pressure for a minimum of 1 hour for Slurry 1, and 3-12 hours for the other filtered slurries. In the case of Slurry 1, no significant variation in the average solidosity was obtained after one hour of expression: the relative difference was less than 2%. Finally, the filter cakes were collected, weighed and placed in an oven for a minimum of 24 h at 105 °C for Slurries 1-8 and 45 °C for Slurries 9-23. The cakes were also weighed, and the weights of the wet and dry cake used to determine the average filtration properties.

The replicate Slurry 22' was not filtered; neither were Slurries 24 and 25, which were subjected to acidification at a temperature of 45 °C, because of the gel-like structure that was formed in these cases.

Table 8. Applied filtration pressure, filter media investigated, attenuation coefficients of the solid and liquid phases and deviations determined in local properties, in the case of the different slurries studied. L: lignin, X: xylan, dX: dyed xylan, S: extra salt added; NC: nitrate cellulose and PES: polyethersulphone membrane. A regenerated cellulose membrane was used unless otherwise specified.

No.	Slurry	Constant filtration pressure applied [MPa]	$\mu_{\gamma,s}$ [m⁻¹]	$\mu_{\gamma,l}$ [m⁻¹]	$|\Delta\phi|$ [m³/m³]	$\overline{\Delta_{rel}\alpha}$ [%]
Suspension						
1.a		0.20 0.50 0.60			1 min interval:	
1.b		0.34 0.85 1.17 1.70 (NC) 2.78 (NC)			0.040	9.2
1.c	L	1.90 2.15 2.36 2.57	24.6	19.6	2 min interval:	
1.d		0.30 (NC) 1.17 2.26			0.028	6.8
2	L + X	2.25 1.29 0.96 0.30	24.6	19.8	0.034	8.7
3	L + X + S	2.25 1.83 0.95 0.31	24.1	20.9	0.041	11.0
Dissolution and re-precipitation: fast acidification						
4	L	2.32 1.87 0.98 0.45[a]	23.1	20.6	0.046	12.7
5	L + X	2.23 1.86[a] 1.03[a] 0.42[a]	24.1	20.6	0.036	16.8
6	L + X + S	2.31 1.88 1.19 0.58[a]	23.8	21.0	0.046	19.2
7	L	2.26 1.71 0.94 0.31				
8	L + X	2.25 1.73 0.97 0.33				
9	L	1.06	23.4	21.2	0.062	
9'	L	1.05				
10	L + X	1.06 [a]				
10'	L + X	1.09	24.1	21.2	0.047	
11	L	1.08	24.0	21.0	0.044	
12	L + X	1.09				
13	L + dX	1.06[a]				
14	L	1.13				
15	L + dX	0.96[a]				
16	L + X	1.10[a]				
16'	L + X	1.18				
17	L + dX	1.11[a]				
18	L + X	1.09				
Dissolution and re-precipitation: slow acidification						
19	L	1.03	24.1	21.4	0.050	
20	L + X	1.12	24.2	21.4	0.048	
20'	L + X	1.10 (PES: 0.45 µm)	24.3	21.2	0.043	
20''	L + X	1.11 (PES: 0.1 µm)				
21	L + X + S	1.05 (PES: 0.1 µm)				
22	L	1.09 (PES: 0.1 µm)				
23	L + X	1.08 (PES: 0.1 µm)				

[a] Only average data was collected for these tests.

5.2 Titanium dioxide experiments

5.2.1 Material
The titanium dioxide used in this work was a 98% pure anatase powder. Anatase is one of the three natural mineral structures of titanium dioxide and is commonly used as a model material in filtration experiments. Sodium chloride (Sigma Aldrich, purity > 99.5 %) was used to adjust the ionic strength of the anatase suspensions.

5.2.2 Slurry preparation and experimental procedure
The influence of ionic strength on the local filtration properties of titanium dioxide was investigated using slurries of three different salt concentrations: 0, 2 and 10 kg NaCl/m^3. Four litres of slurry, with a titanium dioxide concentration of 10 vol. %, were prepared for each of the ionic strength levels investigated using deionized water. The slurry was left under continuous stirring for a minimum of 12 h before the series of filtration experiments began: these were performed at room temperature, i.e. 20 °C. A down-flow pitch-blade impeller, 10 cm in diameter and angled at 45°, was used for mixing purposes. A stainless-steel vessel of volume 8.5 L and inner diameter 21 cm was employed. The filter medium was a regenerated cellulose membrane (Sartorius stedim, Type 184, nominal pore size 0.2 μm) placed on a Grade 5 Munktell filter paper for support.

Three filtration experiments were performed for each ionic strength level corresponding to constant applied pressures of 0.7, 1.4 and 2.1 MPa, respectively. A large range of local solid compressive pressures was covered for each ionic strength level by combining the results obtained from the three applied pressure filtration experiments. The local filtration properties were calculated from the local measurements performed every 5 min at a height of 12 mm above the filter medium. After filtration, the filter cakes were subjected to expression at the applied filtration pressure for a period of 4 to 12 h. Finally, the filter cakes were collected, weighed and placed in an oven for a minimum of 24 h at 105 °C before being weighed again. The weights of the wet and dry cake were used to determine the average filtration properties, see Section 4.2.2.

5.3 Fitting the filtration models to the experimental data

The pressure dependency of the filter cakes formed was evaluated by fitting the empirical constitutive relationships, Eqs. 14 and 15 and the average filtration resistance expressed by Eq. 16 simultaneously to the local filtration properties, local pressure data and average filtration resistance obtained from filtration of Slurries 1-6[11]. The software used for the mathematical regression was Matlab and the optimization routine used was *fmincon*. The residual was scaled in order to obtain comparable contributions from the three filtration properties. Furthermore, the pressure drop over the filter cake, P_c in Eq. 18, was taken as the applied filtration pressure because the resistance of the filter media evaluated using Eq. 12 was found to be negligible compared to that of the filter cake.

There are large interactions between the 5 fitted parameters (n, β, α_0, ϕ_0 and P_a) so the scaling parameter P_a was set to the value obtained for the fit of one arbitrarily chosen slurry (No. 4), which allowed for a direct comparison of the parameters n and β to be made between the slurries. Also, the value of the parameter α_0 was set to the value obtained for the fit of the corresponding slurry containing only lignin: α_0 obtained from the data fit of Slurry 1 was used

---

[11] The fitting of the empirical constitutive relationships performed in the case of the titanium dioxide filtration experiments can be found in Paper V.

for Slurries 2 and 3 (with suspended solids) and that obtained from Slurry 4 was used for Slurries 5 and 6 (with re-precipitated solids).

A direct comparison between the average and local experimental measurements was made in the case of Slurry 1 (for which a large amount of local data was collected). The empirical constitutive relationships, Eqs. 14 and 15, were fitted simultaneously to the local data only (i.e. local filtration properties and local pressure) calculated every 1 min during the filtration experiments. The average filtration resistance was then calculated using Eq. 16, based on the parameters obtained from the fitting to the local data, and then compared to the average filtration resistance obtained experimentally using Eq. 12[12].

Finally, the local filtration data obtained for Slurry 1 (recorded every 2 min) and for titanium dioxide were also used to evaluate the performance of the three filtration models described in Section 3.3.2: the Kozeny-Carman equation, Happel's cell model and the cell model with a porous sphere core. The optimization routine used was *fmincon*. The fitting parameter for the Kozeny-Carman equation (Eq. 20) was the particle diameter. The parameter estimated in the Happel's cell model (Eq. 23) and the cell model with a porous core (Eq. 28) was the inner solid sphere of a diameter of $2a$. The permeability of the inner sphere, k_i, for the latter model was estimated using the Kozeny-Carman equation, Eq. 19; the inner sphere was also assumed to have a solidosity corresponding to a rhombohedral close-packing configuration, i.e. $\phi_i = 0.74$, and to be built up of spherical solid particles, the diameters of which correspond to the size of the single particles seen in the ESEM images for lignin (see Section 7.1.1.1) and to the B.E.T. measurements for titanium dioxide (see Section 7.2.1).

---

[12] A similar comparison between the local and average measurements was made for the titanium dioxide experiments and is only presented in Paper V. Furthermore, for LignoBoost lignin, the average solidosity was calculated using Eq. 17, based on the parameters obtained from the fitting to the local data, and then compared to the average solidosity obtained experimentally: only presented in Paper I.

6. Characterization Techniques

6.1 Environmental Scanning Electron Microscope (ESEM)

The shape and sizes of the particles/agglomerates were evaluated by employing an Environmental Scanning Electron Microscope (ESEM), a Zeiss EVO HD15, to take micrograph images of LignoBoost lignin and titanium dioxide in a moist and a dry environment, respectively. An ESEM has the advantage that it can be operated in humid conditions, which is not possible with a Scanning Electron Microscope (SEM). This is especially beneficial in the case of porous organic materials such as lignin, where drying might impact the structure of the agglomerates significantly, see Section 7.1.1.1. On the other hand, a dry mode is preferred for inorganic crystals such as titanium dioxide, since the images produced are sharper.

6.2 Size of particles/agglomerates

6.2.1 Laser diffraction measurements

The sizes of the particles/agglomerates were determined using a laser diffraction technique performed in highly diluted conditions (distilled water) with a Malvern Instruments Mastersizer 2000 capable of detecting particle sizes between 0.02 and 2000 μm.

The slurry samples in the LignoBoost lignin experiments were diluted in acid water (pH about 2.5) and refraction indexes of 1.60 for the solid and 1.33 for the acid water reference solution were used. The diluted slurries were also subjected to 10 min of ultrasound treatment prior to measurement in order to disintegrate any loose flocs that may be present. Furthermore, in some representative cases, the pH and the salt content of the reference acid water used to dilute the samples were also adjusted to match those of the corresponding slurry being investigated. No influence on the particle size distribution could be observed when compared to the use of acid water (pH about 2.5) with no salt addition.

In the titanium dioxide experiments, the refraction indexes used were 2.74 for the solid and 1.33 for the water reference solution. Ultrasound treatment was not found to influence the system.

6.2.2 Focused Beam Reflectance Measurements (FBRM)

The number and size of the particles were also measured using a Mettler-Toledo Focused Beam Reflectance Measurement (FBRM) G400 probe. This probe employs a rotating laser beam with high speed optics that scans a circular path of the sample. It provides a chord length distribution by crossing particles on any straight line between two edge points; measurements are performed using a backscattered light technique. The chord lengths reported range from 1 to 1000 μm.

In the case of lignin, the influence of the precipitation temperature, addition of xylan and ionic strength on the formation and size of particles/agglomerates was evaluated during preparation of each slurry: measurements were made under stirring (250 rpm) as the slow acidification of Slurries 19, 20, 21, 22', 23, 24 and 25 was being carried out (see Section 5.1.2). Measurements were also made for Slurry 20' but only after acidification, and after it had reached room temperature (still under stirring at 250 rpm).

Furthermore, the probe was positioned with its tip pointing towards the leading side of one of the cell baffles (see Section 5.1.2.2.1), at an angle of about 35 º to the direction of the flow and relatively close to the impeller blades.

In the case of titanium dioxide, the influence of the addition of salt on the sizes of the particles/agglomerates was evaluated using the FBRM probe on a solution having a solid concentration of 1 vol%. Furthermore, the probe was positioned vertically, perpendicular to the direction of the flow.

6.3   Content and distribution of xylan in the cake

6.3.1   High performance anion exchange chromatography

The amount of monomeric sugar xylose present in the filter cake was determined by High Performance Anion Exchange Chromatography (HPAEC), performed after the dry cake sample has been hydrolysed with sulphuric acid, according to the Klason method (Theander and Westerlund, 1986).

The HPAEC set-up comprised of a Dionex ICS-5000 system equipped with CarboPacTM PA1 columns and an electrochemical detector. The software used was Chromeleon 7, Chromatography Data System, Vers. 7.1.0.898, and NaOH and NaOH+NaAc (0.2 M) were used as eluents.

The amount of xylose present in the filtrate was also determined for Slurries 2, 3, 5, 6 and 8. This was done by first removing the salt from the filtrate by dialysis tubing (Spectra Por, molecular weight cut-off of 3.5 kDa) before subjecting it to evaporation using a rotary vacuum evaporator (Büchi, R) at a temperature not exceeding 35 °C. The remaining organic residue was then dried at 40 °C for one week before acid hydrolysis and HPAEC analysis were performed. In the case of Slurries 16', 17 and 18, the distribution of xylose through the cake was investigated by making measurements on slices of the filter cake taken at different positions across its thickness.

6.3.2   Fluorescent microscopy analysis

The localization of the xylan stained with Remazol Brilliant Blue R (RBBR) on the lignin particles that formed the filter cake was investigated by means of a Confocal Laser Scanning Microscope (CLSM) (Leica TCS SP5 II Wetzlar, Germany). The laser used was a 488 nm argon laser and the scanning layer was about 0.8 µm in depth. Lignin is a fluorescent material so a co-localization method was used: emission spectra of the dyed xylan and the samples of filter cake containing only lignin were thus first investigated separately (reported in Paper III, Appendix B). The specific wavelength emission ranges found to be predominant for each compound were thereafter assigned to the lignin and dyed xylan: emission wavelengths collected between 500 and 540 nm were therefore assigned to lignin, and those collected between 620 and 722 nm to stained xylan. Furthermore, an arbitrarily chosen colour was also assigned to each collection range of wavelengths for use in further image analysis involving both components: green was chosen for lignin and red for xylan.

6.4   Other particles properties

Various other techniques were used to characterize the properties of the particles. The solid density of the dried materials was measured by a gas displacement pycnometry system (Micromeritics Accupyc 1330). Also, the molecular weights of lignin and xylan were measured with gel-permeation-chromatography (GPC), (PL-GPC 50 plus) using both refractive index and ultraviolet (280nm) detectors (Polymer Laboratories, Varian, Inc.). DMSO/LiBr (10mM) was used as the mobile phase, and a PolarGel-M column and a guard column (300 × 7.5 mm and 50 × 7.5 mm, 8 µm) coupled in series were utilized. The molecular weight (Mw) was determined using a 10-point calibration curve with Pullulan standards (polysaccharide calibration kit,

PL2090-0100, Varian). After repeating the measurements twice, the average mass Mw obtained was reported. Finally, the B.E.T. surface area of the air-dried (105 °C) as well as freeze-dried lignin and titanium dioxide was determined using a Micromeritics Tristar 3000, with nitrogen as the adsorption gas.

7. Results and Discussion

The results obtained from the five studies on which this thesis is based are summarized in this chapter. The first section presents and discusses the characterization, experimental data and modelling results obtained from the LignoBoost lignin filtration experiments (Papers I-IV). In the second section, the influence of ionic strength on agglomeration and filtration of a model material commonly used for filtration, i.e. titanium dioxide, is discussed (Paper V) and compared to the findings of the LignoBoost lignin experiments; it also includes the result of the fitting of various filtration models to the experimental data obtained. All the results are presented as a continuous discussion, with the papers corresponding to the different sections indicated in parenthesis.

7.1 LignoBoost lignin experiments

7.1.1 Characterisation

7.1.1.1 Properties of the solids and suspensions (Papers I-III)

The micrograph images of moist LignoBoost lignin (Batch A) obtained using ESEM revealed that the lignin agglomerates are built up of small, non-spherical particles measuring about 2 μm in length, Figure 9 (a). This is in good agreement with the size of primary particles of Kraft lignin, i.e. 1-2 μm, found in other studies (e.g. Kannangara *et al.,* 2016). It could also be observed that the size of the agglomerates varies from about 10 μm to several hundred μm, Figure 9 (b).
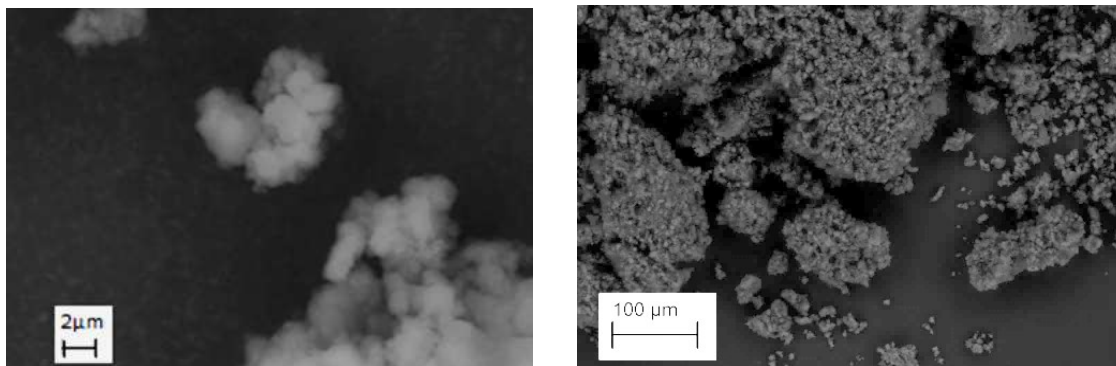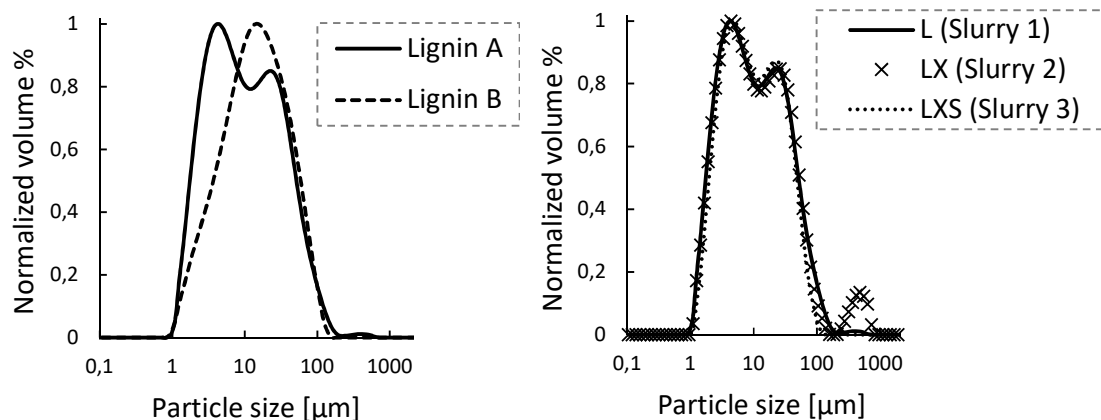

Figure 9 a (left), b (right). ESEM micrographs of moist LignoBoost lignin powder (Batch A) at two magnifications.

The results obtained from laser diffraction, B.E.T surface area, dry content, solid density, average molecular weight and measurements of xylose content performed on the two batches of LignoBoost lignin investigated are shown in Table 9. The particle size distribution (PSD) of the two batches of LignoBoost lignin in acid water suspension determined by laser diffraction are shown in Figure 10 (a), while the PSD of Slurries 1-3 (suspensions of LignoBoost Lignin A (Slurry 1) with added xylan (Slurry 2) and added xylan with extra salt (Slurry 3)) are shown in Figure 10 (b).

Table 9. Properties of the two batches of softwood LignoBoost lignin investigated. $D_{(x)}$ indicates that x % of the particles by volume are smaller than the value stated.

LignoBoost lignin	Laser diffraction measurements			Solid density [kg/m3]	Average molecular weight [kDa]	Xylose content [wt%]
	$D_{(10)}$ [μm]	$D_{(50)}$ [μm]	$D_{(90)}$ [μm]			
A	2.5	8.9	43.9	1346	17.8	0.3
B	3.0	13.0	47.6	1324	14.8	0.3

Figure 10: a (left) and b (right). Normalized volume-based particle size distribution obtained for (**a**) the two batches of LignoBoost lignin investigated and (**b**) Slurries 1-3 (with suspended solids). L: lignin, X: xylan and S: additional salt.

The results from the characterization showed that both LignoBoost lignin batches have very similar properties, even though they were produced in two different Nordic pulp mills. The laser diffraction measurements revealed that both lignins had a volume-based average size of about 10 μm for particles/agglomerates in suspension. Moreover, the sizes presented in Table 9 and Figure 10 (a) are in accordance with those observed in the micrographs image of moist lignin taken using ESEM, Figure 9 (a) & (b). It can be noted that the smallest 10% of the particles of the lignin Batch A were found to measure between 0.95 and 2.5 μm by laser diffraction, (Figure 10 (a) and Table 9), which corresponds well to the size-range of single particles observed in the images, Figure 9 (a).

The amount of residual xylan found in the two batches of softwood LignoBoost lignin investigated is very low, Table 9. These lignins are therefore suitable for studying the influence that an addition of xylan has on the precipitation and filtration of lignin.

Apart from a few larger agglomerates that were found for the lignin suspension containing xylan and without an extra addition of salt (Slurry 2), the addition of neither xylan nor extra salt was observed as having any significant influence on the PSD of the lignin suspension, Figure 10 (b). In addition, the concentration of the slurry (i.e. 8.8-21.6 wt%) was not found to affect the PSD of the particles/agglomerates in diluted suspension when measured by laser diffraction.

The B.E.T. surface area of air-dried and freeze-dried samples of LignoBoost lignin powder (Batch A) was also measured: the results obtained were 15.4 m^2/g and 33.4 m^2/g, respectively. These surface areas correspond to particle diameters of 0.28 μm and 0.13 μm, respectively, assuming perfectly smooth and spherical particles. These are significantly smaller than the diameters observed and measured by ESEM and laser diffraction: about 2 μm for the single

lignin particles. The difference in the size of the particles based on the B.E.T. surface area measurement is a consequence of both the irregularities in shape and the porosity of the lignin particles and particles agglomerates (which are neither perfectly spherical nor perfectly smooth). Furthermore, the specific surface area obtained for the freeze-dried lignin was twice as large as the area obtained for air-dried lignin. These results are also a consequence of the porosity of the lignin particles and agglomerates, as illustrated in Figure 11. When it is air-dried, the structure of an organic porous agglomerate tends to collapse: the water capillary forces between the solid particles that compose the agglomerate increase while the water trapped inside is evaporating. However, this behaviour does not occur if the agglomerate is freeze-dried: the water trapped between the particles increases slightly in volume instead while freezing, before being sublimated, which also possibly makes the single particles move apart. These behaviours therefore lead to a freeze-dried sample having a higher specific surface area than an air-dried sample, Figure 11.
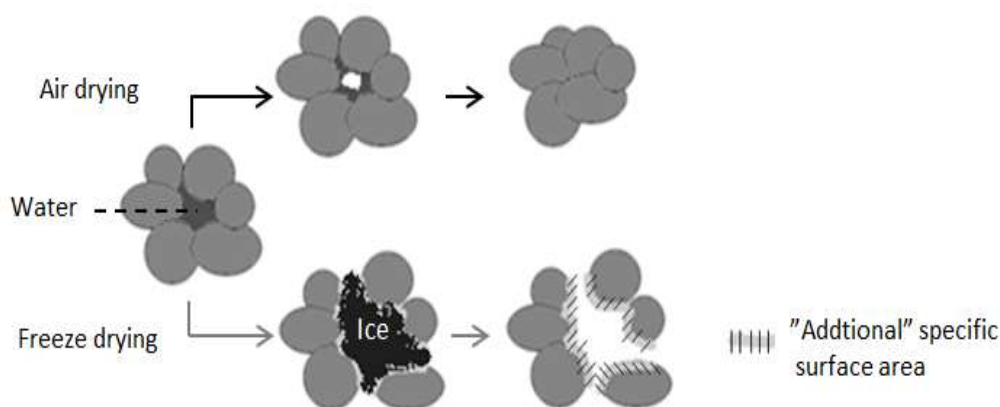

Figure 11. A porous agglomerate structure subjected to two drying techniques.

The solid densities and average molecular weights that were measured for the three different batches of beechwood xylan investigated are presented in Table 10, along with the composition of the xylan in sugars determined by HPAEC. The properties obtained for these three batches were very similar, and it was therefore assumed that the xylans have a comparable influence when they are added to lignin. Further results will therefore not be differentiated based on the batch of xylan used.

Table 10. Properties of the three batches of beechwood xylans investigated.

		Xylan		
		Megazyme	**Sigma**	**TCI**
Solid density [g/cm³]		1.52	1.49	1.49
Average molecular weight [kDa]		24.0	21.8	22.6
[wt% of total sugars]	**Xylose**	94.8	91.6	92.4
	Arabinose	1.1*	1.0*	1.1*
	Rhamnose	1.5	1.9	1.7
	Galactose	1.2	1.5	1.6
	Glucose	1.3*	4.1*	3.2*
	Mannose	-	-	-

* Close to/below the calibrated lower limit.

7.1.1.2   *Content and distribution of xylan in the filter cake (Papers II and III)*

7.1.1.2.1   HPAEC analysis

The amount of xylose found in the filter cakes determined using HPAEC measurement is reported in Table 11, together with some characteristic of the slurries. The content of xylose in the cakes formed by Slurries 2-8 is based on analysis of the filtrate: the xylose content determined from the filter cake analysis for these samples was low and very scattered. The reason for this is unknown but may partly be a result of the high temperature used while the cake was being oven-dried (oxidation at elevated temperature, i.e. 105 °C for 24-48 h). Reasonable data was obtained for the cakes formed by Slurries 10-23, for which a lower temperature of 45 °C was used to dry the cakes.

The xylose content at different positions in the filter cake, determined by the analysis of different cake slices (dried at 45 °C) obtained after the filtration of Slurries 16', 17 and 18, is given in Figure 12 (a), while Figure 12 (b) illustrates the position of each slice investigated. The bottom slice of the filter cake obtained after Slurry 16' was filtered was analysed in triplicate: a standard deviation of 0.13 wt% was found between the samples.

Table 11. Xylose content of the filter cakes measured using HPAEC. T: temperature.

No.	Slurry	IS [mol/L]	Precipitation T [° C]	pH	% of total xylose found in the filter cake
Suspension					
2	L + X	<0.01	-	2.3	89*
3	L + X + S	0.94	-	2.8	99*
Dissolution & re-precipitation: fast acidification					
5	L + X	0.68	80	2.7	99*
6	L + X + S	0.94	80	2.8	99*
8	L + X	1.15	80	1.1	82*
10	L + X	1.69	77	4.0	75
10'	L + X	1.67	77	3.9	62
12	L + X	1.10	77	4.2	70
13	L + dX	1.06	77	4.3	86
15	L + dX	0.98	77	4.0	75
16	L + X	0.95	77	2.8	73
16'	L + X	0.95	77	3.0	77
17	L + dX	1.05	77	2.9	86
18	L + X	1.84	77	2.2	85
Dissolution & re-precipitation: slow acidification					
20	L + X	1.88	77	4.1	72
20'	L + X	1.71	77	4.1	77
20''	L + X	1.88	77	4.1	82
21	L + X + S	6.72	77	4.0	78
23	L + X	1.69	65	4.0	72

* Based on analysis of the filtrate. All other data is based on analysis of the cake.
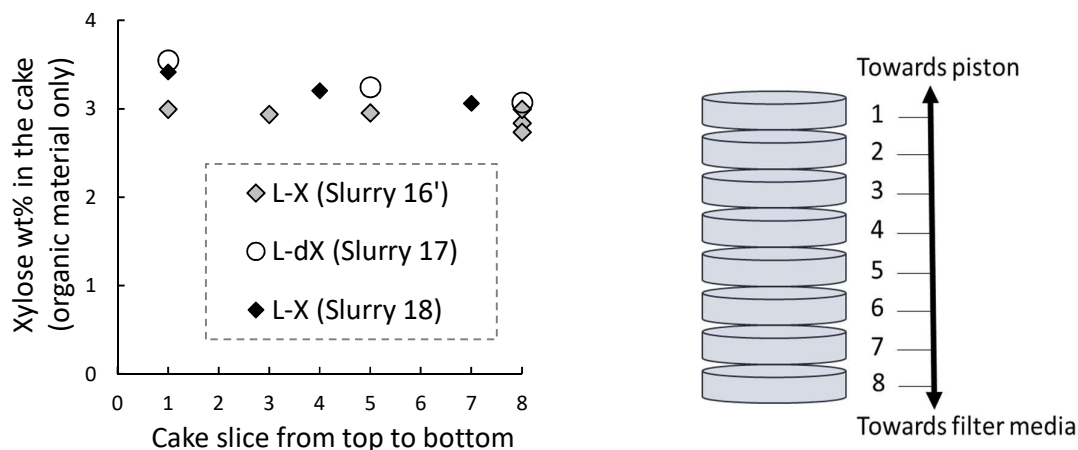
Figure 12: a (left) and b (right). (**a**) Xylose content of the slices of filter cake obtained from HPAEC analysis with only the organic material considered (i.e. salt is excluded). The xylose content of the initial slurry is about 3.8 wt% of the organic material. L: lignin, X: xylan and dX: dyed xylan. These slurries have a pH between 2-3 and an ionic strength between 1-2 mol/L. (**b**): Location of the slices of cake investigated.

A large majority of the xylose added was found in the filter cake. Furthermore, the results show that the content of xylose in the filter cake was not influenced by the pH, ionic strengths and preparation procedures of the original slurry that were investigated, Table 11. However, the data obtained based on the filtrate analysis gave significantly higher amounts of xylose in the filter cake compared to that based on the cake analysis. This was especially true for the filtrates subjected to dialysis (salt removal): Slurries 3-8. A partial loss of xylan during dialysis of the filtrates may therefore explain the higher amount of xylose present in the cake that was calculated in these particular cases: it was based on an underestimated value of xylose in the filtrate. Furthermore, slightly less xylose was found in the cake obtained from Slurry 8 (i.e. more xylose was found in the filtrate) compared to that of Slurries 3-6, even though its filtrate was also subjected to dialysis. This might possibly be explained by the relatively harsher conditions used during precipitation in this case (lower pH): a partial cleavage of xylan by acid hydrolysis could have resulted in a more soluble xylan, i.e. more xylan is dissolved in the filtrate.

It was also found that the xylose was distributed evenly over the filter cake (obtained from slurries subjected to the dissolution & re-precipitation procedure), Figure 12 (a). The small deviations in xylose content found between the cake slices located at different positions (especially in the case of Slurries 17 and 18) remain within the experimental error (i.e. ± 0.13 wt%).

These results imply that xylan is being incorporated (possibly sorbed) evenly within the lignin particles/agglomerates that are formed during the re-precipitation of both solids.

7.1.1.2.2 Fluorescent microscopy analysis

Even though the samples of filter cake were probed for several hours using a confocal laser scanning microscope, only two "hot spots" could be detected, for which the light emitted in the wavelength collection range assigned to the RBBR dye (marking xylan) was found to be dominant over that assigned to lignin. One of these cases is presented in Figure 13 (a)-(c), with a red hot spot surrounded by a white dotted square (the filter cake was obtained after filtration of Slurry 15). The "red light" collected over the whole cake (Figure 13 (a)) is mainly that emitted by lignin in the emission range for which the light emitted by stained xylan should be predominant for similar concentrations of fluorescent material, see Paper III, Appendix B.
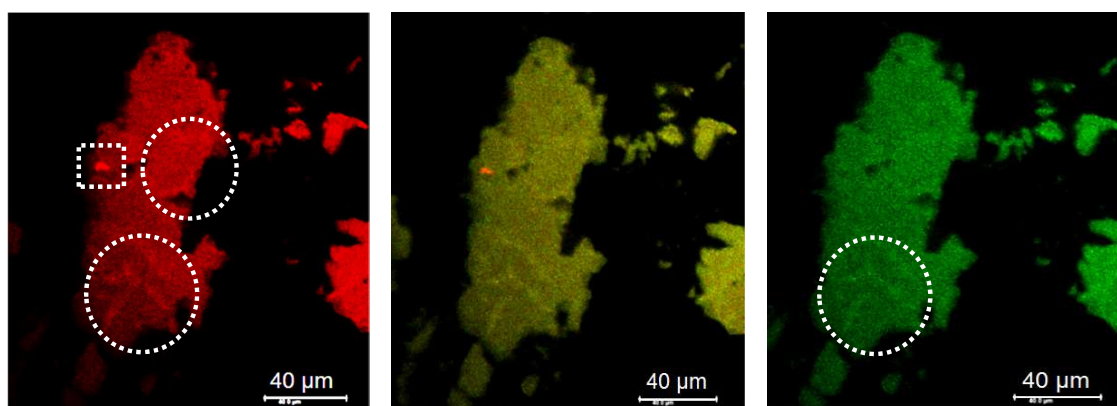
(a) Emission range assigned to dyed xylan: 620-722 nm.   **(b)** Co-localization of both emission ranges collected.   **(c)** Emission range assigned to lignin: 500-540 nm.

Figure 13. Images of the filter cake obtained after filtration of Slurry 15, taken by a confocal laser scanning microscope. Dotted square: red "hot spot" and dotted circles: "bright spots".

The presence of dyed xylan on the lignin particles/agglomerates could be confirmed by the hot spots that were found. However, very few hot spots were detected and they cannot account for the content of xylose in the filter cake: about 3 wt% of the total organic material distributed evenly throughout the cake, as determined using HPAEC. The most plausible explanation is therefore that the distribution of xylan is so even throughout the cake that, in general, the intensity of the light emitted by the dispersed, but small amounts of, dyed xylan remains below the level for which it can be differentiated from the light emitted by the lignin.

Furthermore, some more frequently occurring "bright spots" were also observed in the emission range image assigned to stained xylan (Figure 13 (a)) that were not always detectable in that assigned to lignin (Figure 13 (c)). These are likely to be caused by the relief present on the structure of the samples of lignin cake analysed. More emitted light can reach the detector if the layer of cake it has to cross is thinner locally: the light attenuation caused by the surrounding material is lower, leading to slightly higher emission. In the case of the bright spots that are difficult to detect in the emission range image assigned to lignin, however, it cannot be ruled out completely that these areas do, in fact, have a higher concentration of dyed xylan.

7.1.2 Lignin precipitation

7.1.2.1 Onset of precipitation (Paper IV)

The FBRM measurements performed during slow acidification revealed that the onset of precipitation (for particles with chord lengths > 1µm) was not influenced significantly by either the precipitation temperature (45, 65 and 77 °C) or the addition of xylan at the conditions investigated, i.e. an initial sodium ion concentration of 1 M. The average onset pH obtained was 9.3 (measured at 25 °C), which is in the range of apparent pKa values expected for Kraft lignin (Norgren *et al.,* 2000), and corresponds to the protonation of the phenolic groups.

Increasing the ionic strength of the solution to an initial sodium ion concentration of 4 M (Slurry 21) did, however, have an important impact on the onset of precipitation: an onset pH above 11.3 was found in this case. This result is expected (see Section 2.6.3) and can be explained by the extra salt that was added screening the charge of the ionized phenolic groups on the lignin molecules, which favours lignin aggregation. This is because the repulsive electrostatic

interactions between the molecules are considerably reduced: a smaller amount of acid is thereby necessary to precipitate lignin.

7.1.2.2 *Influences of additions of acid and xylan during precipitation (Paper IV)*

The evolution of the chord length distribution of the particles during the course of precipitation performed at 77 °C for an initial sodium ion concentration of (a) 1 M (Slurries 19 and 20: without and with the addition of xylan) and (b) 4 M (Slurry 21: with the addition of xylan), are presented in Figure 14 (a) and (b), respectively. The data obtained in the case of a precipitation temperature of 65 °C is only discussed in the text and can be found in Paper IV. Furthermore, the case of a precipitation temperature of 45 °C, for which gelation occurred close to the onset pH during precipitation, is only discussed in Paper IV.
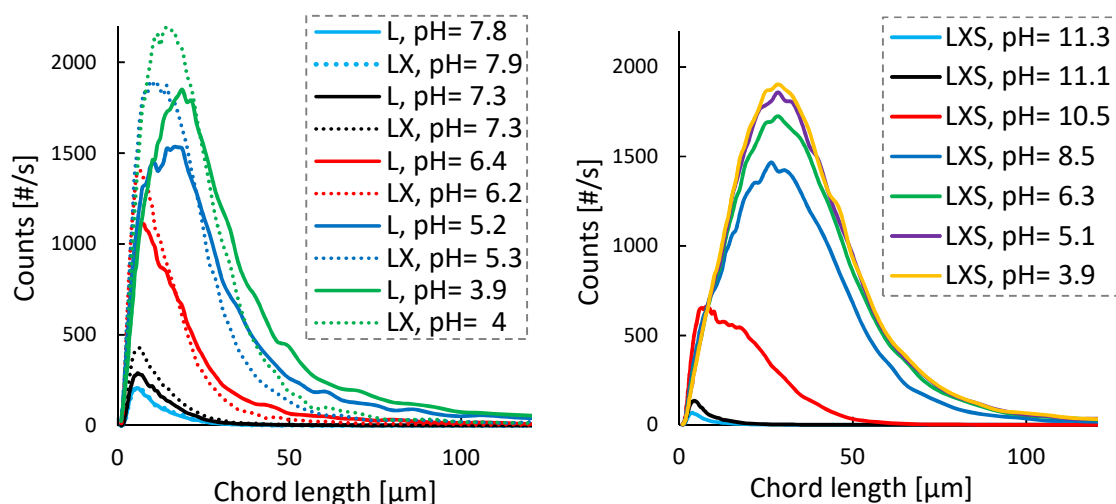
Figure 14: a (left) and b (right). Profiles of chord length distributions at 77 °C and an initial sodium ion concentration of (**a**): 1 M (L: Slurries 19 & LX: Slurry 20) and (**b**) 4 M (Slurry 21). L: lignin; X: xylan and S: extra salt added.

For both precipitation temperatures (65 and 77 °C), independent of the addition of xylan, and at an initial sodium ion concentration of 1 M, the precipitation process was found to be highly pH sensitive over the neutral to acidic pH range, e.g. at 77 °C, Figure 14 (a). Both the number (i.e. counts) and size of the particles/agglomerates were found to increase gradually as the pH was decreased from 7.9 to 3.9, i.e. once the protonation of the phenolic groups can be considered as being complete. These results may indicate that, at these conditions, the precipitation of lignin is not only influenced by the protonation of its phenolic groups but also of its carboxylic groups: pKa values around 5.5 have been reported (Laine *et al.,* 1994). The surface charge of the lignin molecules and particles that are formed is higher because of the greater amount of unprotonated carboxylic groups that are present at pH 7.9 than at 3.9. This makes the lignin more soluble at pH 7.9 compared to a lower pH; the agglomeration of particles may also be limited due to the higher electrostatic repulsive interactions between the particles/agglomerates that are formed.

At higher ionic strengths, i.e. an initial sodium ion concentration of 4 M, however, the amount of particles/agglomerates that are formed increased only slightly when the pH was decreased from pH 8.5 to 3.9, and their size (i.e. chord length distribution) was not found to be affected, see Figure 14 (b). The impact of the carboxylic groups on the precipitation of lignin is thus likely to be cancelled out at high ionic strengths due to the sufficient screening of their charges caused by the extra amount of salt added.

A slight shift towards smaller sizes was also found to occur when xylan was added to lignin during precipitation performed at a temperature of 77 & 65 °C and a 1 M initial sodium ion concentration, and around pH 6-4, e.g. at 77 °C, see Figure 14 (a). These results are possibly in line with the influence of the carboxylic groups described above. Xylan is also substituted by carboxylic groups, so the agglomeration of the solids would possibly be more limited in suspensions of lignin-xylan than in those containing only lignin due to the higher content of carboxylic groups introduced by the xylan.

Furthermore, the difference in the chord lengths of the particles between the lignin and the lignin-xylan suspensions was found to be much more pronounced at a precipitation temperature of 77 °C when compared to 65 °C, at which the sizes were almost unaffected and a change in count number was the main effect recorded, with lower values being obtained when xylan was added to lignin.

As the slurry was left to cool down to room temperature following preparation, a slight shift towards smaller sizes was recorded in all cases, i.e. independent of the precipitation temperature, addition of xylan and ionic strength. This is shown in Figure 15 for Slurries 19 & 20, i.e. precipitation at 77 °C. The shift observed was however less significant for a precipitation temperature of 65 °C, and even lesser at 45 °C. Furthermore, the decrease in size that was observed started exactly when the heating device was turned off and lasted for only 2-3 h, i.e. no significant change in size was observed between 3-10 h after the heat was shut off, even though the slurries were always left under continuous stirring. Particle breakage due to prolonged stirring is thus not likely to be related to the slight decrease in size described: it should be attributed instead to an effect of the temperature which indicates that, for the conditions investigated, the agglomeration of lignin is slightly favoured at higher temperatures. Figure 15 also shows that the difference in the chord length distribution between the lignin and the lignin-xylan suspensions was reduced when the slurry reached room temperature.

Additional information about the results presented here, and the kinetics of formation of the particles, can be found in Paper IV.
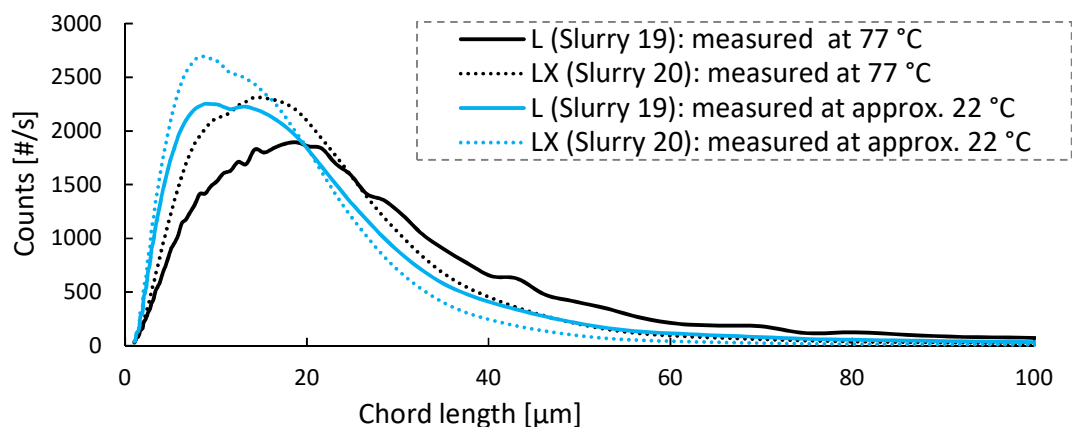

Figure 15. Chord length distribution after preparation of Slurries 19 & 20 measured at the actual precipitation temperature (77 °C) and after they were left to cool down to room temperature (approx. 22 °C). L: lignin and X: xylan.

7.1.2.3 *Size of the re-precipitated solids (Papers II, III and IV)*

7.1.2.3.1 Slow acidification: influences of the precipitation temperature, addition of xylan and ionic strength

Following preparation of the slurries subjected to slow acidification at different precipitation temperatures, the particle size distribution (PSD) and chord length distribution (CLD) of the particles/agglomerates formed were measured using laser diffraction and FBRM, respectively. The PSD obtained are presented in Figure 16 (a) and the corresponding CLD in Figure 16 (b). The measurements presented here were made once the slurry had reached room temperature. The laser diffraction measurements in Figure 16 (a) revealed that the major part of the particles/agglomerates formed at a precipitation temperature of 45 °C measured less than 1 µm. The CLD obtained for the slurry subjected to a precipitation temperature of 45 °C is thus excluded from Figure 16 (b).
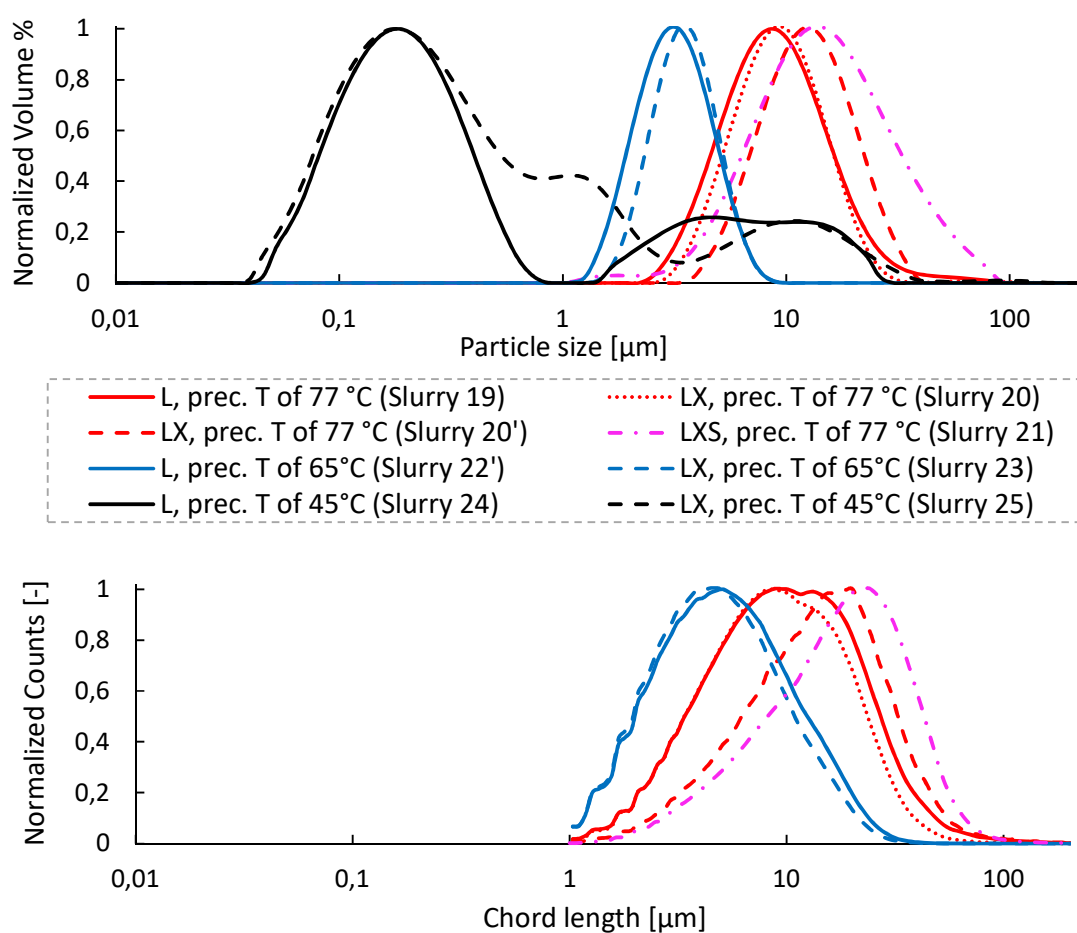

Figure 16: a (above) and b (below). Normalized (**a**) PSD and (**b**) CLD of the slurries investigated by both FBRM and laser diffraction. L: lignin, X: xylan, S: extra salt, T: temperature and prec.: precipitation. The slurries have a relatively similar pH (4.1-4.7) and ionic strength (1.5-1.9 mol/l) apart from Slurry 21 (6.7 mol/l). All measurements were performed at room temperature.

The absolute sizes obtained from the two instruments cannot be compared directly because different theoretical methodologies are used, but the trends observed using the laser diffraction

and FBRM measurements were nevertheless in good agreement. Increasing the precipitation temperature led to the formation of larger particles/agglomerates, Figure 16 (a) & (b). A similar result was also obtained in a previous study (Öhman and Theliander, 2007b) performed at different conditions and for which the pH of black liquor was decreased, at most, to 9.5.

Furthermore, slightly larger particles/agglomerates were obtained when the ionic strength was increased from 1.9 to 6.7 mol/L: Slurries 20-20' vs 21, Figure 16 (a) and (b). This may be explained by the lower electrostatic repulsive interactions that occur between the solids if a higher amount of salt is present in the slurries: the surface charge of the particles is being shielded which, in turn, allows for more extensive agglomeration.

The same influences of the precipitation temperature and ionic strength were observed during precipitation (data presented in Paper IV). However, the addition of xylan was found to have neither a systematic nor a significant influence on the size of the particles/agglomerates when measured at room temperature after preparation, Figure 16 (a) & (b), even though slightly smaller sizes were recorded during precipitation (see Section 7.1.2.2). The duplicate slurry, Slurry 20' (for which FBRM data was recorded after preparation only), showed instead larger sizes when xylan was added to lignin.

A small deviation in the CLD and PSD was found between the duplicates, i.e. Slurry 20 vs 20' & 20'' and Slurry 22 vs 22'. Slurries 20 vs 20' are shown in Figure 16 (a) and (b). The reason behind this is still unknown and requires further investigation.

7.1.2.3.2 Influences of the preparation procedure and slurry conditions

The volume-based particle-size distribution of representative examples of slurries subjected to fast acidification (performed at a precipitation temperature close to 80 °C) are presented in Figure 17 (a) & (b); the PSD of lignin suspended in acid water is also shown in Figure 17 (b) for purposes of comparison. The PSD of two slurries subjected to fast and slow acidification, respectively, are presented in Figure 18: both have a similar ionic strength and pH, and a precipitation temperature of 77 °C.
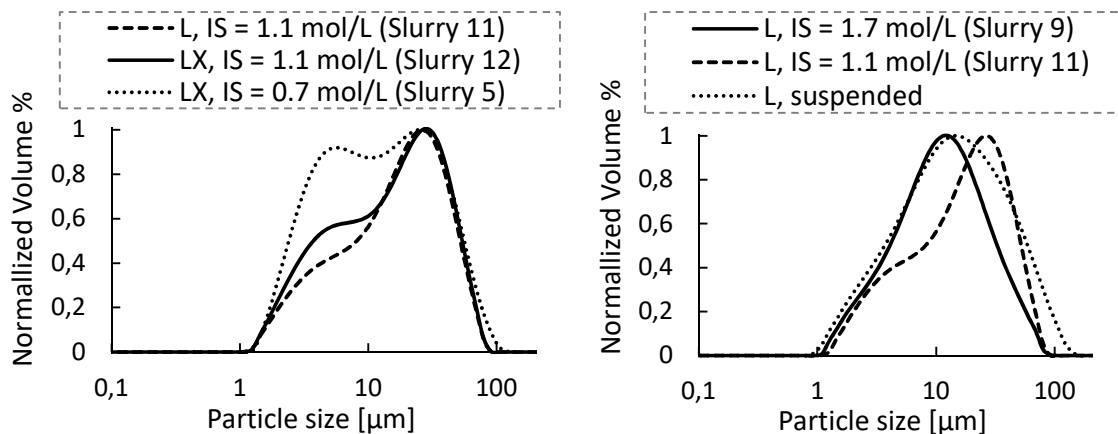

Figure 17: a (left) and b (right). (a) & (**b**) Normalized volume-based PSD of slurries subjected to fast acidification together with (**b**) the PSD of suspended lignin (Batch B). L: lignin, X: xylan and IS: ionic strength. The slurries subjected to dissolution and re-precipitation have a precipitation temperature close to 80 °C and a similar pH close to 4.1 apart from Slurry 5, with a pH 2.7. All measurements were performed at room temperature.
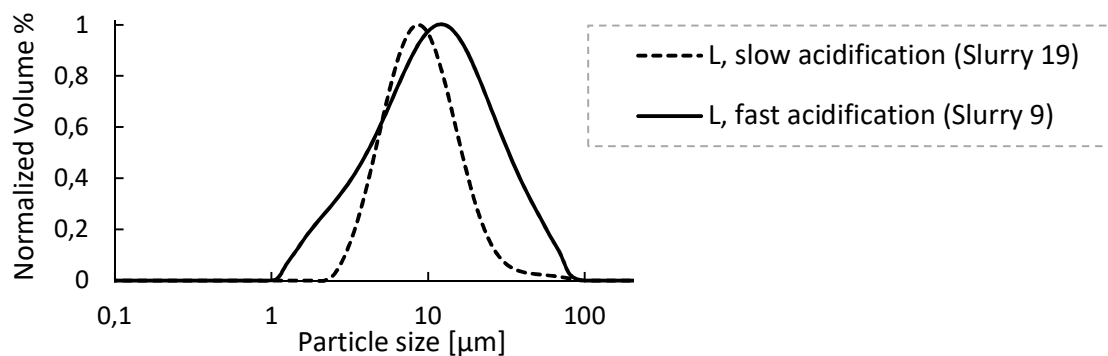
Figure 18. Normalized volume-based PSD of two slurries subjected to slow and fast acidification. L: lignin, X: xylan. The slurries subjected to dissolution and acidification have a similar pH and ionic strength, and a precipitation temperature of 77 °C. All measurements were performed at room temperature. Similar differences in PSD were recorded for Slurries 10 (slow acidification) and 20 (fast acidification), in which xylan was added to the lignin.

Although the shape of the distributions of the slurries subjected to fast acidification was found to vary between the slurries, no systematic influence on the PSD could be attributed to any of the parameters investigated, i.e. ionic strength (0.7-1.8 mol/L), pH, addition of xylan or after attaching a dye to the xylan, Figure 17 (a) & (b). Furthermore, similar ranges of particle sizes were obtained for the re-precipitated solids for the different batches of lignin and xylan used, e.g. Slurries 12 vs 5, Figure 17 (a). This is in line with the characterization results: rather similar properties were found for the solid materials investigated.

Furthermore, even though slightly larger particles were observed for suspended solids, relatively similar PSD were still obtained when the slurries containing suspended solids were compared to those subjected to fast acidification (performed at a temperature close to 80 °C), Figure 17. This might be expected, considering the fact that the suspended solids were extracted using the LignoBoost process: they were also formed after a fast acidification performed at a temperature close to 80 °C.

Significantly broader volume-based PSD were, however, obtained for fast acidification compared to slow acidification: both smaller and larger particles were formed, Figure 18. The large changes in pH that occur in a short period of time within the slurry when the acidification is performed in one step thus lead to a more heterogeneous formation of particles/agglomerates. These results also indicate that if industrial conditions are to be simulated in the laboratory, then fast acidification is preferable to slow acidification.

7.1.3 Filtration properties

The applied filtration pressure, the addition of xylan, the addition of salt, the pH of the slurry and the preparation procedure were all found to influence the filtration properties of the lignins investigated. The concentration of the slurry (8.8 to 21.6 wt%) and the filter medium used (having same nominal pore size), on the other hand, were not found to have a significant influence on the filtration properties of the systems studied.

The influences observed for the parameters investigated are summarized in Table 12, and described in the sections below. The influences observed between the different preparation procedures are only discussed in the text.

The empirical constitutive relationships, Eqs. 14 and 15, and the expression derived for the average filtration resistance, Eq. 16, could be fitted simultaneously and successfully to the experimental data. This indicates a good agreement between local and average properties

determination. The numerical values of the fitted parameters obtained are presented in Table 13 and discussed further in the sections below.

Table 12. Summary of the influences observed on the filtration properties of the lignins studied by the main parameters investigated. IS: ionic strength; conc.: concentration; RC: regenerated cellulose; NC: nitrate cellulose and PES: polyethersulphone (filter medium material).

	Effect on:		
Effect of:	α and α_{avg}	$\emptyset$ and $\emptyset_{avg}$	Pressure dependence of the filtration properties
Concentration of the lignin slurry (8.8 to 21.6 wt%)	→	→	→
Increase in applied pressure (0.2 to 2.78 MPa)	↗	↗	↘ (weakly compressible)
Filter medium: RC vs NC vs PES (0.45 µm pore size)	→	→	→
Addition of xylan	↗	↗ a ↘	↗
Increase in ionic strength (0.7 to 1.8 mol/l)	↘	b ↗ →	↘
Increase in pH (pH 1-2.9 vs pH 4)	c ↘ →	→	Not studied

Changes observed in the case of *a)* local solidosity before expression for re-precipitated solids and lower IS; *b)* re-precipitated solids; *c)* xylan added to lignin at lower IS.

Table 13. The parameters obtained fitted to the experimental data. L: lignin; X: xylan and S: additional salt.

No.	Slurry	$\alpha_0 \cdot 10^{-12}$ [m/kg]	$\emptyset_0$[-]	P_a [Pa]	n [-]	β[-]
Suspension						
1 (a-d)	L[a]	0.11[a]	0.315[a]	5210[a]	0.281[a]	0.074[a]
1 (a-d)	L	0.10	0.324	3157	0.278	0.060
2	L + X	0.10	0.301	3157	0.503	0.061
3	L + X + S	0.10	0.264	3157	0.314	0.095
Dissolution and re-precipitation: fast acidification						
4	L	0.36	0.220	3157	0.435	0.098
5	L + X	0.36	0.062	3157	0.601	0.227
6	L + X + S	0.36	0.096	3157	0.495	0.186

[a] Based on local measurements only, performed every 1 min. All other data is based on local measurements performed every 2 min, also using average filtration resistance data for fitting.

7.1.3.1 *Influences of slurry concentration, pressure and filter media (Paper I)*

The local filtration properties obtained from the filtration of the LignoBoost lignin suspensions are plotted versus the local solid compressive pressure in Figure 19 (a) and (b) for the different slurry concentrations investigated (8.8 wt% to 21.7 wt%). The corresponding average filtration properties are plotted as a function of the applied filtration pressure, and for the different slurry concentrations investigated, in Figure 20 (a) and (b). The empirical constitutive relationships (Eq. 14 and 15) fitted to the local data are presented as solid lines in Figure 19 (a) and (b): the corresponding fitted parameters are given in Table 13 (Slurry 1: L[a]). The average filtration resistance calculated using Eq. 16, and the parameters fitted to the local data (given in Table 13), is presented as a solid line in Figure 20 (a).
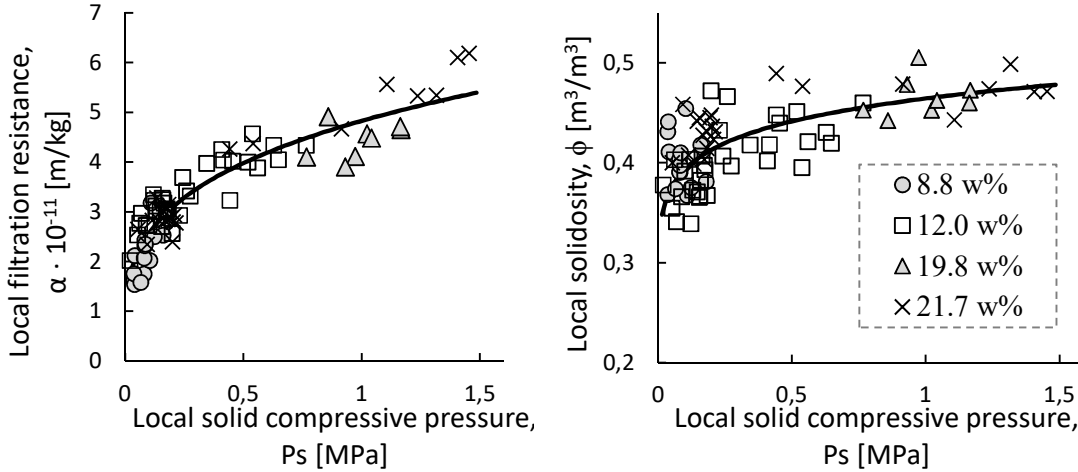

Figure 19: a (left) and b (right). Local filtration resistance and local solidosity as a function of the local solid pressure for the different concentrations of the lignin slurries investigated, obtained on filtration of Slurry 1 (a-d). The solid lines are the local filtration resistance and the local solidosity, respectively, calculated from Eqs. 14 and 15 fitted to the experimental local data. Measurements were performed every 1 min at a height of 12 mm from the filter medium; the final cake was about 22-62 mm thick.
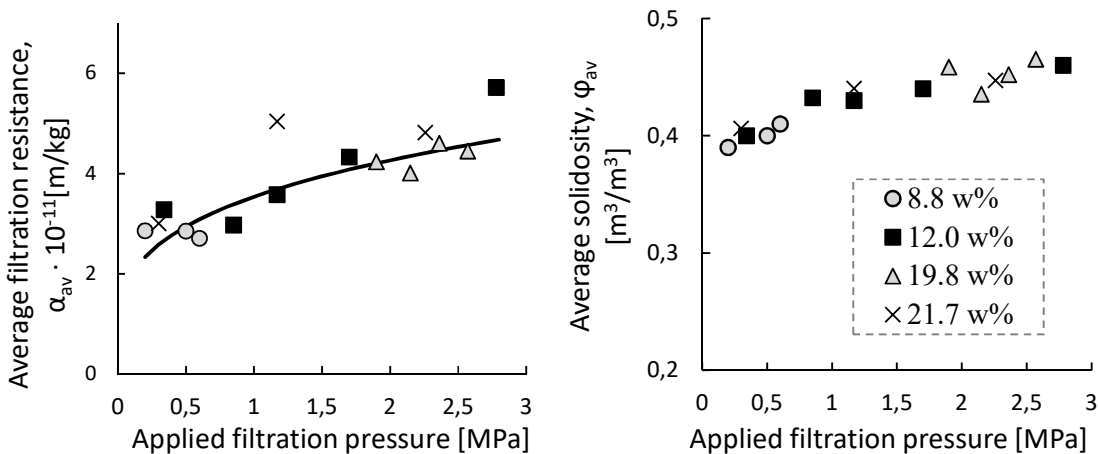

Figure 20: a (left) and b (right). Average filtration resistance and average solidosity (after expression) as a function of the applied filtration pressure for the different slurry concentrations, obtained on filtration of Slurry 1 (a-d). The solid line in (**a**) represents the average filtration resistance calculated using Eq. 16 and the obtained fitted parameters presented in Table 13 (L[a]).

Similar local and average filtration properties were obtained at similar solid compressive pressures and applied filtration pressures, respectively, regardless of the concentration of the slurry, Figure 19 (a) & (b) and Figure 20 (a) & (b). This shows that the concentration of the slurry does not significantly influence the filtration properties of lignin in the range investigated: 8.8 to 21.7 wt % (i.e. 6.7-17 vol%). Furthermore, it also shows that the height of the filter cake, which depends on the initial concentration of the slurry, does not influence the structure of the filter cake formed within the range investigated. The heights of the cakes obtained experimentally (23-62 mm) correspond to the range of heights obtained on an industrial scale, so the results obtained can therefore be considered in industrial applications.

Furthermore, the LignoBoost lignin suspensions investigated form weakly compressible filter cakes, based on the classification shown in Table 5 and taking the fitted parameters obtained (Slurry 1, Table 13) into consideration. Also, the values of the average filtration resistance obtained experimentally varied between 2 and $6 \cdot 10^{-11}$ m/kg: the LignoBoost lignin investigated is relatively easy to filter in the pressure range studied (0.2 to 2.8 MPa). Consequently, relatively high filtration pressures and a relatively small filter area can be used industrially.

The parameters of the empirical relationships in Eqs. 14 and 15 fitted only to the local data could be used successfully to describe the average properties obtained experimentally (applying the classical filtration equation), using Eq. 16, Figure 20 (a). In addition of showing a good agreement between the local and average measurements, this also implies that the average measurements can be used to estimate the filtration resistance of the weakly compressible cakes that are obtained using the investigated LignoBoost lignin, with a fairly high degree of accuracy.

Finally, no influence of the filter media was observed when comparing the filtration results obtained using the regenerated cellulose and the cellulose nitrate filters (see Figures 7 and 8 in Paper I). This indicates that the interactions between the lignin and the filter medium used are small and/or similar.

<p style="text-align:center">**************</p>

The results in the following sections are not differentiated according to the concentration of lignin since it was shown that the concentration of the slurry (8.8-21.6 wt%) did not influence the filtration properties of lignin.

7.1.3.2 Influences of the addition of xylan and ionic strength (Papers II and III)

7.1.3.2.1 Local and average filtration resistance

The local filtration resistance obtained from the filtration of slurries with suspended solids (Nos. 1-3) and of slurries with dissolved and re-precipitated solids (Nos. 4-6) are plotted against the local solid compressive pressure in Figure 21 (a) and (b), respectively. The corresponding average filtration resistance is shown as a function of the applied filtration pressure in Figure 22 (a) and (b). The results of the equations fitted to the experimental data (Eqs. 14, 15 and 16) are presented as dotted and solid lines in the figures (Eqs. 14 and 16), and the fitted parameters obtained are given in Table 13. The average filtration resistance obtained on filtration of Slurries 7 and 8 (with re-precipitated solids, at higher ionic strength) are presented as a function of the applied filtration pressure in Figure 23, together with the average filtration resistance of Slurries 4 and 5.
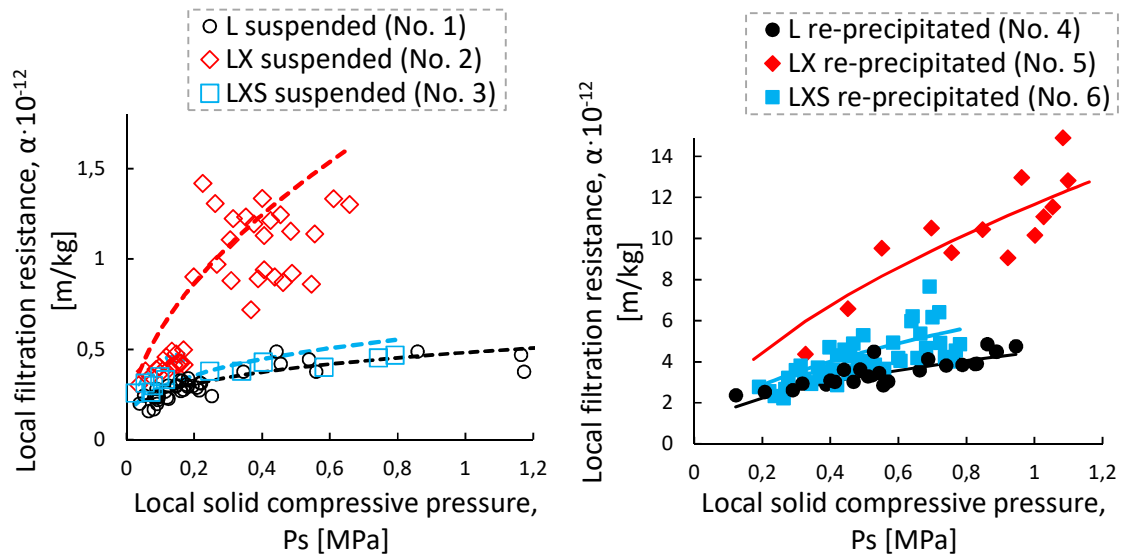
Figure 21: a (left) and b (right). Local filtration resistance as a function of the local solid compressive pressure obtained on filtration of slurries (**a**): with suspended solids (Nos. 1-3) and (**b**): with re-precipitated solids (Nos. 4-6). L: lignin, X: xylan and S: additional salt. Dotted and solid lines: local filtration resistances calculated from Eq. 14 fitted to the experimental data. Measurements were performed every 2 min at a height of 12 mm from the filter media; the final cake was about 22-62 mm thick (Slurries 1-3) and 30-45 mm thick (Slurries 4-6).
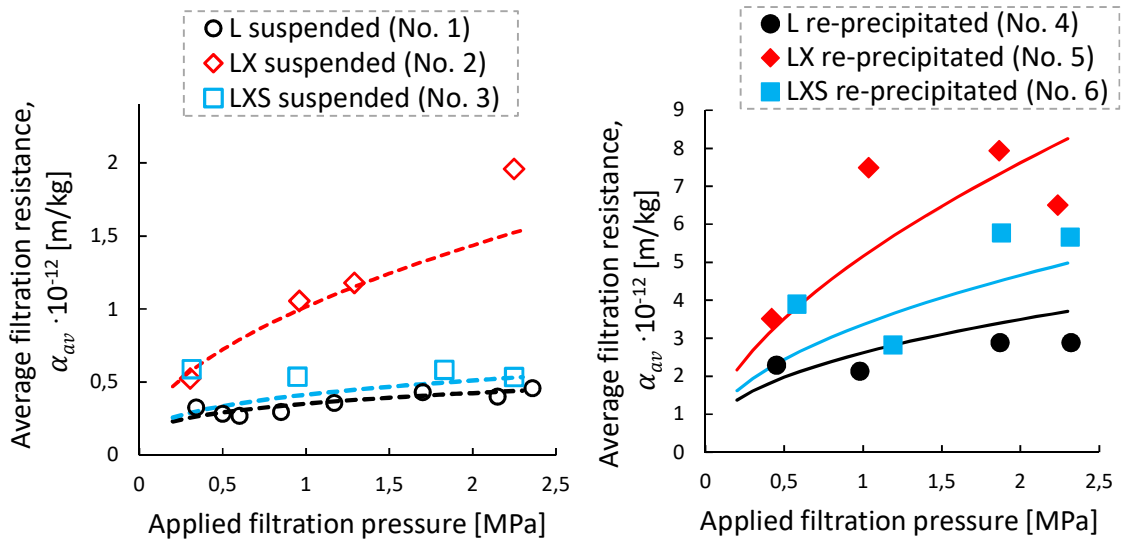

Figure 22: a (left) and b (right). Average filtration resistance as a function of the applied filtration pressure obtained on filtration of slurries (**a**): with suspended solids (Nos. 1-3) and (**b**): with re-precipitated solids (Nos. 4-6). L: lignin, X: xylan and S: additional salt. Dotted and solid lines: average filtration resistances calculated using Eq. 16 fitted to the experimental data. N.B. for the purpose of clarity, all the data for Slurry 1 is not presented here.
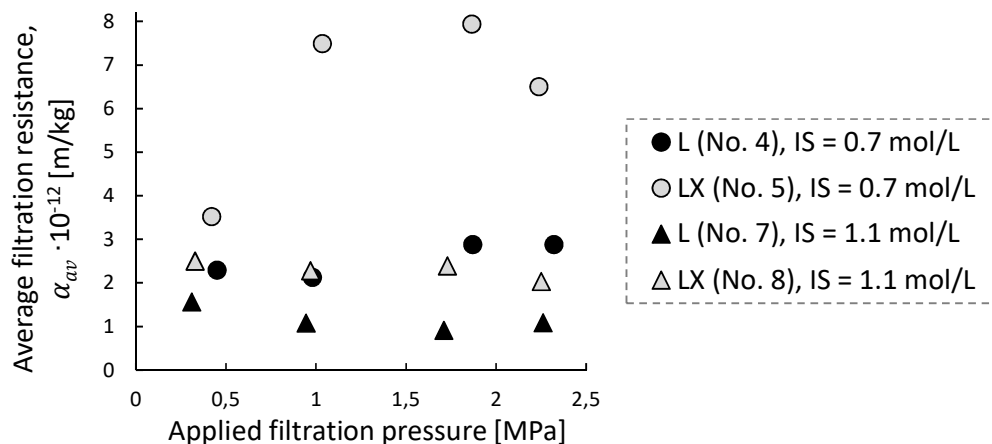
Figure 23. Average filtration resistance versus the applied filtration pressure obtained on filtration of Slurries 4, 5, 7 and 8 (with re-precipitated solids). L: lignin, X: xylan and IS: ionic strength.

Similar observations can be made for both cases, i.e. slurries with suspended solids and re-precipitated solids, with respect to the influence made by the addition of xylan and extra salt on the local and average filtration resistance. The addition of xylan was found to increase both the local and the average filtration resistance of the lignin slurries significantly: up to a factor of 3 for a similar salt concentration, Figure 21 (a) & (b) and Figure 22 (a) & (b). The pressure dependency of the local and average filtration resistance was also increased significantly, Table 13: the value of n is up to twice as high after xylan is added to lignin, with the same content of salt (Slurry 1 vs 2 and Slurry 4 vs 5).

Furthermore, it was found that the addition of salt resulted in a significant decrease in both the local and average filtration resistance in all cases, i.e. with or without the addition of xylan, and that it decreased the pressure dependency of the filtration resistance, Figure 21 (a) & (b), Figure 22 (a) & (b) and Figure 23, and Table 13.

Interpretation of the results

It has been shown previously that the removal of hemicelluloses from hardwood black liquor (i.e. mainly xylan) prior to the precipitation and filtration of lignin results in a significant decrease in the average filtration resistance, which then approaches the value obtained for softwood lignin precipitated in black liquor, Wallmo *et al.* (2009). Furthermore, this work has shown that both the local and the average filtration resistance increased significantly after xylan was added to softwood Kraft lignin. Thus, the conclusion drawn from these two studies is that xylan is likely to be one of the main causes for the higher filtration resistance generally obtained for hardwood lignin than for softwood lignin.

The increase in filtration resistance observed after the addition of xylan implies that the drag force that the liquid exerts on the solid has increased, i.e. the contact area between the liquid and the solid material is higher during the filtration process. Furthermore, it should also be kept in mind that the HPAEC measurements revealed that xylan is evenly distributed throughout the filter cake.

One of the possible explanations of the phenomenon described above, therefore, is that xylan is incorporated, possibly sorbed, onto the surface of agglomerates of lignin particles. Furthermore, the sorbed xylan interacts with lignin (e.g. through electrostatic and steric

repulsive interactions), thereby making the agglomerates become more open and porous locally. The particle agglomerates would consequently become more exposed to the flowing liquid, i.e. the resistance to the flow is increased; the phenomena described here are illustrated in Figure 24. Moreover, the particles size distribution would not be affected significantly by the dispersed xylan particles sorbed onto lignin, according to the results obtained from the laser diffraction and FBRM size measurements, Section 7.1.2.3. This explanation is particularly feasible for the case where lignin and xylan are dissolved and re-precipitated together. In the case of lignin and xylan being simply mixed together as solid materials in suspension, another possible mechanism may be involved is that small particles of xylan are formed without being incorporated into the lignin agglomerates: this would also lead to an increase of the flow resistance. It is nevertheless unlikely to be one of the main explanations, given that the size distributions measured are similar, i.e. independent of the addition of xylan.

When salt is added to the suspension, however, the negative surface charges of the lignin and xylan are shielded (i.e. carboxylic acid side groups at the pH levels investigated). This is likely the explanation for the influence of ionic strength that was observed, i.e. the decrease in filtration resistance when the ionic strength of the slurry was increased. When the surface charges are being shielded, the solid-solid electrostatic repulsive interactions decrease, which may allow for the formation of a denser structure of both the particle agglomerates during precipitation and the structure of the filter cake during filtration. As a consequence, the surface contact between the solid and the liquid during filtration decreases, and the resistance to the flow is reduced. The influence of ionic strength described here is also discussed in relation to another agglomerating system affected by ionic strength, i.e. titanium dioxide, in Section 7.2.3.
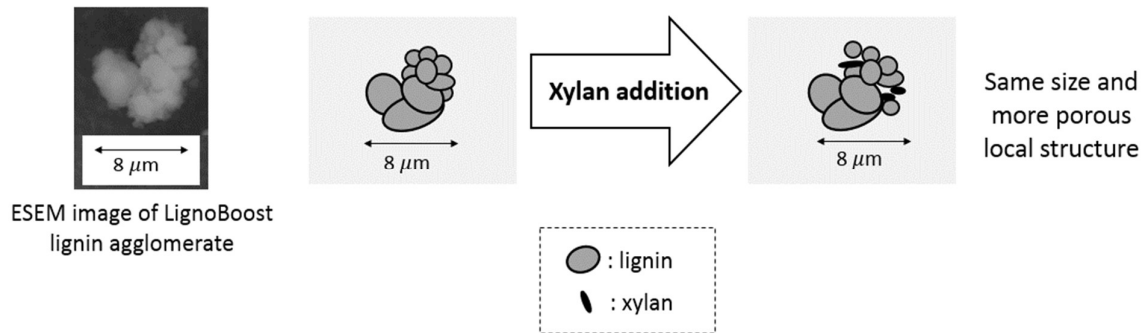

Figure 24. Illustration of the possible effect the addition of xylan has on an agglomerate of lignin particles in suspensions of the same ionic strength.

7.1.3.2.2 Local and average solidosity

The local solidosity obtained for slurries with suspended solids (Nos. 1-3) and of slurries with dissolved and re-precipitated solids (Nos. 4-6) are plotted against the local solid compressive pressure in Figure 25 (a) and (b), respectively. The corresponding average solidosity (after expression) are shown as a function of the applied filtration pressure in Figure 26 (a) and (b). The results of the equations (Eqs. 14, 15 and 16) fitted to the experimental data are presented as dotted and solid lines in the figures (Eq. 15) and the fitted parameters obtained are given in Table 13. The average solidosity of the cake (after expression) obtained on filtration of Slurries 7 and 8 (with re-precipitated solids and at higher ionic strength) are presented as a function of the applied filtration pressure in Figure 27, together with the average solidosity of Slurries 4 and 5.

Furthermore, the local solidosity obtained from the filtration of Slurries 9 and 10' (performed at a similar constant applied filtration pressure of about 0.1 MPa) are presented versus the filtrate volume and the experimental time in Figure 28 (a) and (b), respectively.
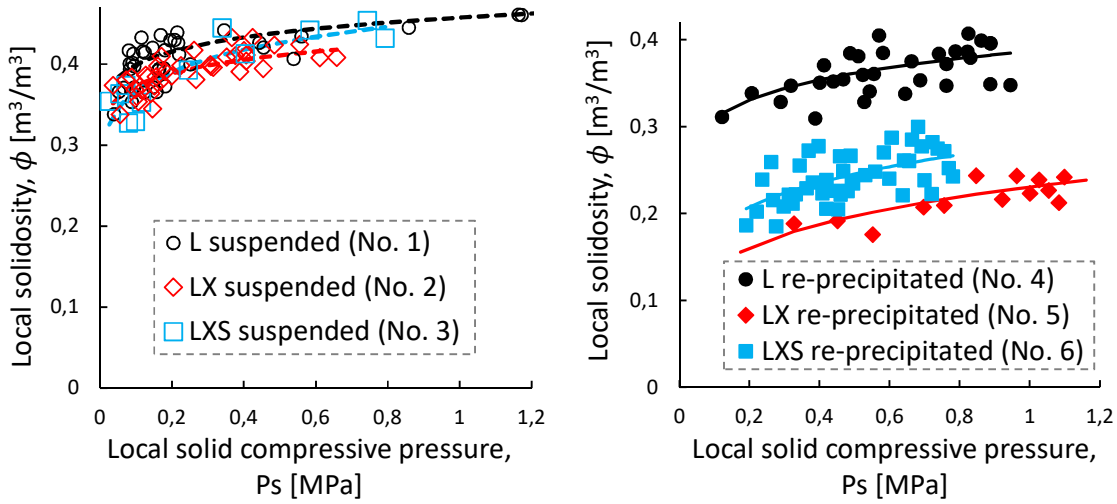

Figure 25: a (left) and b (right). Local solidosity as a function of the local solid compressive pressure obtained on filtration of slurries (**a**): with suspended solids (Nos. 1-3) and (**b**): with re-precipitated solids (Nos. 4-6). L: lignin, X: xylan and S: additional salt. The dotted and solid lines are the local filtration resistance calculated from Eq. 15 fitted to the experimental data. Measurements were performed every 2 min at a height of 12 mm from the filter media; the final cake was about 22-62 mm thick (Slurries 1-3) and 30-45 mm thick (Slurries 4-6).
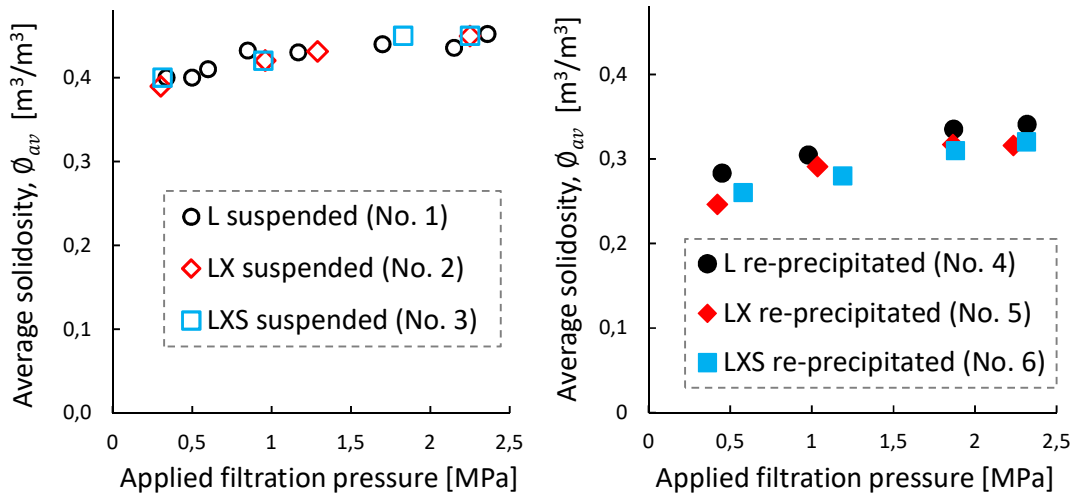

Figure 26: a (left) and b (right). Average solidosity of the cake (after expression) as a function of the applied filtration pressure obtained on filtration of slurries (**a**): with suspended solids (Nos. 1-3) and (**b**): with re-precipitated solids (Nos. 4-6). L: lignin, X: xylan and S: additional salt. N.B. for the purpose of clarity, all the data for Slurry 1 is not presented here.
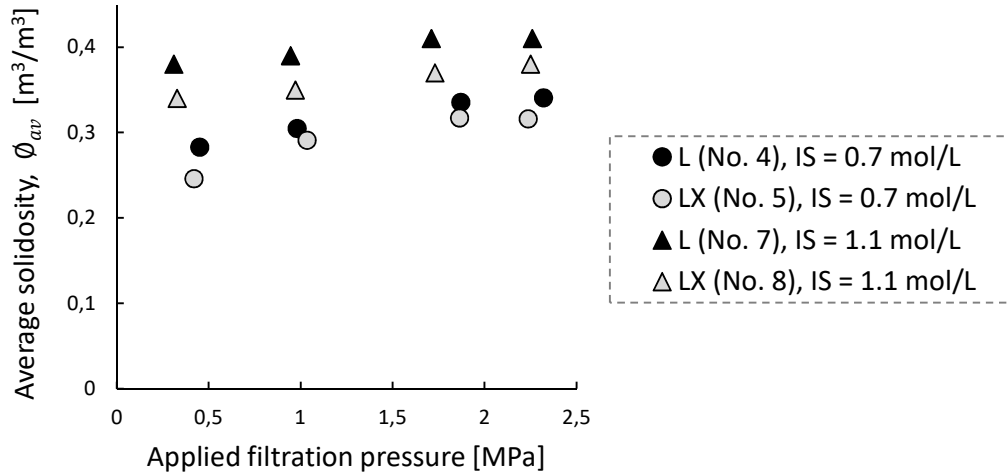
Figure 27: a (left) and b (right). Average solidosity (after expression) versus the applied filtration pressure obtained on filtration of Slurries 4, 5, 7 and 8 (with re-precipitated solids). L: lignin, X: xylan and IS: ionic strength.
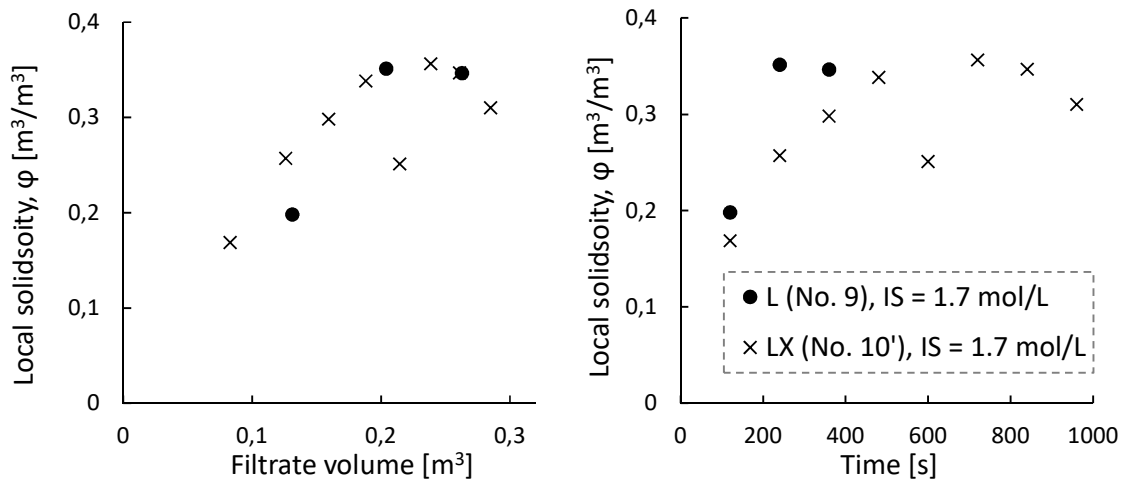

Figure 28: a (left) and b (right). Local solidosity during cake formation versus (**a**): filtrate volume and (**b**): experimental time obtained on filtration of Slurries 9 and 10' (with re-precipitated solids). L: lignin, X: xylan and IS: ionic strength. The slurries have a similar pH of about 4 and were filtered at a constant applied filtration pressure of about 0.1 MPa. Measurements were performed at 9 mm above the filter medium; the final cake was about 22-31 mm thick.

Regarding the ways in which the additions of xylan and extra salt influenced the local and average solidosity, observations made in some cases involving re-precipitated solids differed to those made for suspended solids, as discussed below.

The case of suspended solids
In the case of solids being suspended in acid water (Slurries 1-3), the addition of either xylan or extra salt was not found to influence the local and average solidosity of the filter cake, Figure 25 (a), Figure 26 (a) and Table 13.

The case of dissolved and re-precipitated solids
For the lower range of ionic strength investigated (i.e. Slurries 4-6: IS = 0.7 to 0.9 mol/L), the local solidosity during cake formation was found to decrease significantly after the addition of xylan (about 40% lower) and to increase slightly after the addition of salt, Figure 25 (b). Also, the pressure dependency of the local solidosity was found to increase after the addition of xylan (for slurries of the same ionic strength: Slurry 4 vs 5) and to decrease after the addition of salt (Slurry 5 vs 6), Table 13. However, for slurries of higher ionic strength (Nos. 10' and 9: IS = 1.1 to 1.7 mol/L), no significant influence was found after the addition of xylan, Figure 28 (a) and (b). The deviations observed between the slurries remain within the experimental error, i.e. $\pm$ 0.056 [m^3/m^3] in absolute local solidosity. These results indicate that, for a suspension with a sufficiently high concentration of ions, xylan does not influence the porosity of the structure of the cake during filtration.
Regarding the average solidosity obtained after the cake had been subjected to expression, no significant influence was found after the addition of either xylan or extra salt in the case of the lower range of ionic strength investigated: Slurries 4-6 (IS = 0.7 to 0.9 mol/L), Figure 26 (b). However, an increase of the average solidosity was observed at higher ionic strength: Slurries 7 and 8 (IS = 1.1 mol/L) compared to 4 and 5 (IS = 0.7 mol/L), Figure 27 (b), for all cases, i.e. with or without the addition of xylan. In the systems investigated, a certain concentration of ions was therefore required in the slurry before its ionic strength could be observed as having a significant influence on the average solidosity after expression.

Interpretation of the results
The lower solidosity obtained when xylan is added to lignin in the case of re-precipitated solids, and for slurries with lower ranges of ionic strength, implies that a larger volume of liquid is present between the particles: the average distance between the particles is greater in these cases.
One possible explanation for this phenomenon is that the repulsive interactions (i.e. electrostatic and steric) between lignin and the sorbed xylan lead to the formation of a more porous structure in the filter cake during filtration. When salt is added to the suspension, however, and as discussed in Section 7.1.3.2.1, the negative surface charges of the lignin and xylan particles are being shielded (i.e. carboxylic acid side groups at the pH levels investigated). This may allow for the formation of a denser structure of both the particles/agglomerates formed and the filter cake in all cases (i.e. with or without the addition of xylan), which increases the solidosity.

Furthermore, the lignin-xylan repulsive interactions may also be partly overcome during expression of the filter cake: the local solid compressive pressure increases drastically when the piston reaches the top of the cake, i.e. when expression starts (see Sections 3.1.2 and 4.2.1). This would explain why, in the case of Slurries 4-6 (IS = 0.7 to 0.9 mol/L), the solidosity of the lignin-xylan filter cakes increases drastically after expression, despite a much lower local solidosity being obtained during cake formation, to become almost similar to that of lignin filter cakes (Figure 25 (b) vs Figure 26 (b)). Relatively loose structures are therefore likely to be formed during cake formation in these cases: i.e. Slurries 4-6, IS = 0.7 to 0.9 mol/L. A more

compact structure is however expected to be formed for slurries of higher ionic strength during cake formation already, regardless of the presence of xylan, because of the lower electrostatic repulsive interactions that exist between the solids. The local solidosity during formation of the cake was found to be independent of the presence of xylan for Slurries 9 and 10' (IS = 1.7 mol/L), Figure 28 (a) and (b).

7.1.3.2.3   Comparison of dissolved & re-precipitated solids versus suspended solids

The average filtration resistance and average solidosity plotted as a function of the applied filtration pressures obtained from the filtration of Slurries 1-6 are presented in Figure 29 (a) and (b), respectively.
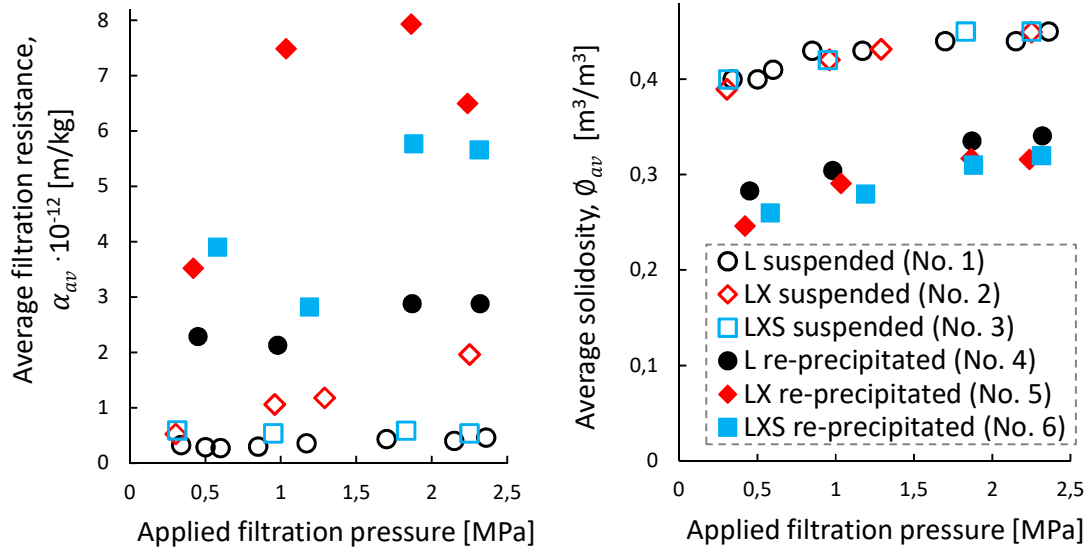

Figure 29: a (left) and b (right). Average filtration resistance and average solidosity (after expression) versus the applied filtration pressure obtained on filtration of Slurries 1-6. L: lignin, X: xylan and S: additional salt. N.B. for the purpose of clarity, all the data for Slurry 1 is not presented here.

Significantly lower filtration resistance and higher solidosity were obtained for slurries containing solids that were only suspended in acid water compared to those containing dissolved and re-precipitated solids, Figure 29 (a) and (b).

These differences are similar to those found between the slurries subjected to re-precipitation at higher ionic strength and at lower ionic strength, i.e. showing a decrease in filtration resistance and an increase in solidosity, Figure 23 and Figure 27. Therefore, the difference that was observed between the two preparation procedures (i.e. suspended vs re-precipitated solids) is likely to be explained by the high ionic strength of the original black liquor from which the lignin used in this study was precipitated and extracted before being suspended in acid water. A typical value of the ionic strength of black liquor prior to lignin extraction (dry content ~ 30 wt%) is about 2.3 mol/kg liq. (Zhu *et al.,* 2014) while a maximum of 1.0 mol/kg liq. (corresponding to 1.1 mol/L) was considered for the slurries discussed, i.e. for which the influence of the applied pressure was studied: Nos. 1-8.

7.1.3.3 *Influence of pH (Paper III)*

The average filtration resistance and the average solidosity after expression of the filter cake obtained on filtration of Slurries 4 to 18 (with re-precipitated solids) are plotted in Figure 30 (a) and (b), respectively, as a function of the ionic strength of the slurry and the pH values investigated. All the slurries were subjected to a fast acidification procedure and a precipitation temperature close to 77°C, and were filtered at a constant applied pressure close to 1.08 MPa.
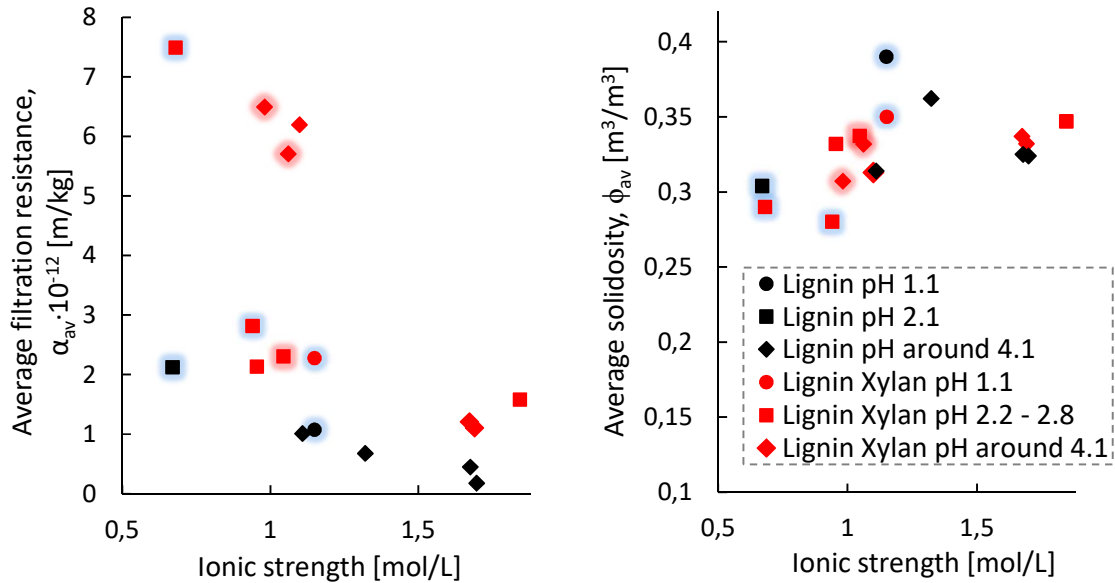

Figure 30: a (left) and b (right). Average filtration resistance and average solidosity (after expression) versus the ionic strength of the slurry and the different pH levels investigated for Slurries 4-18, filtered at a constant applied pressure close to 1.08 MPa. The data points with a blue halo were obtained using lignin Batch A (Slurries 4-8): all other data is from Batch B. The points with a pink halo correspond to dyed xylan. The results obtained for the duplicate Slurry 16' are not presented here[13].

Relatively similar filtration properties were obtained for the different batches of lignin (and xylan) used: this is coherent with the similar solid properties and particle size measurements also obtained for the different batches of materials investigated. Furthermore, attaching a dye to xylan was not found to have a significant influence on the filtration properties, Figure 30 (a) and (b).

No significant influence of the pH on the average solidosity after expression of the filter cake was observed for the slurries investigated, i.e. with or without the addition of xylan and for the pH and ionic strength ranges in question, Figure 30 (b).
However, when xylan was added to lignin, the filtration resistance was found to be significantly higher when the pH of the slurry was about 1-2.8 compared to pH 4. Furthermore, this was

---

[13]A technical issue occurred when the filter cell was being filled with Slurry 16': the slurry was recollected and left overnight without stirring before the experiment was repeated the next day. The average filtration resistance obtained was scattered compared to other data and is not considered reliable. The average solidosity obtained was equal to that of the duplicate Slurry 16.

found only if the ionic strength of the slurry was also relatively low, i.e. around 1.2 mol/l: no influence of the pH was observed at higher ionic strengths, i.e. around 1.7 mol/L, Figure 30 (a). The pKa value of the carboxylic acid groups of xylan, which is around 3.4 (Laine *et al.,* 1994), is the likely explanation for these results. A significantly higher amount of unprotonated carboxylic acid groups is present on xylan at pH 4 (i.e. $\geq$ pKa) compared to 2.8 or lower: the electrostatic repulsive interactions between the solids are increased at pH 4. As a consequence, the formation of a solid structure that is more open locally is likely to occur at the surface of the agglomerates, which is where xylan is possibly sorbed onto lignin: the surface area between the solid and the liquid becomes larger during filtration and the filtration resistance thus increases. However, if the concentration of ions in the suspension is sufficiently high, the additional surface charge induced by the unprotonated carboxylic groups of xylan is shielded and the influence of the pH on the filtration is thus reduced.

Furthermore, in the cases of lignin slurries that did not contain added xylan, increasing the pH from 1 to 4 was not found to influence the average filtration resistance, Figure 30 (a), even though lignin was also substituted by acid carboxylic groups. This might be explained by carboxylic groups on lignin having a higher pKa: values of around 5.5 have been reported in the literature (Laine *et al.,* 1994).

Similar observations to those made previously regarding the influences of xylan and ionic strength on the filtration of Slurries 1-8 were also made for Slurries 9-18: higher filtration resistances were obtained after the addition of xylan and at lower ionic strength of the slurry, Figure 30 (a). Furthermore, a slight tendency towards a higher average solidosity after expression of the cake was found when increasing the ionic strength of the slurry, while no significant influence of the addition of xylan was observed on solidosity, at the conditions investigated, Figure 30 (b).

7.1.3.4 *Influence of the precipitation conditions: rate of acidification and temperature (Paper III)*

Data of the average filtration resistance and the average solidosity after expression of cakes obtained from the filtration of slurries subjected to slow acidification is presented in Table 14, together with some properties of the slurries, the filter medium used and its pore size. Corresponding data obtained for slurries subjected to fast acidification, at similar pH and ionic strengths, is also presented in Table 14 for the purpose of comparison.

In addition, the local solidosity measured during cake formation and prior to expression in the case of Slurries 19-20' is plotted as a function of the experimental time and filtrate volume in Figure 31 (a) and (b), respectively.

Table 14. Average filtration properties obtained on filtration of Slurries 9-10′ & 19-23. L: lignin, X: xylan, dX: dyed xylan, S: additional salt, IS: ionic strength, T: temperature, RC: regenerated cellulose and PES: polyethersulphone. The slurries have a pH of about 4.1 and were filtered at a constant applied pressure close to 1.08 MPa.

No.	Slurry	Filter medium	Pore size [μm]	IS [mol/L]	Prec. T [°C]	$\emptyset_{av}$ [m³/m³] (after expression)	$\alpha_{av} \cdot 10^{-12}$ [m/kg]
						Dissolution & re-precipitation: fast acidification	
9	L	RC	0.45	1.67	77	0.33	0.45
9'	L	RC	0.45	1.70	77	0.32	0.18
10	L + X	RC	0.45	1.69	77	0.33	1.11
10'	L + X	RC	0.45	1.67	77	0.34	1.21
						Dissolution & re-precipitation: slow acidification	
19	L	RC	0.45	1.82	77	0.37	0.11
20	L + X	RC	0.45	1.88	77	0.35	6.79 & 1.60*
20'	L + X	PES	0.45	1.71	77	0.35	9.20 & 1.06*
20''	L + X	PES	0.1	1.88	77	0.35	1.95 & 0.05*
21	L+X+S	PES	0.1	6.72	77	0.33	0.06
22	L	PES	0.1	1.77	65	0.27	0.70
23	L + X	PES	0.1	1.69	65	0.31	1.27

*An unstable solid structure was formed and two distinct phases were observed during filtration, and therefore also two distinct apparent filtration resistances.
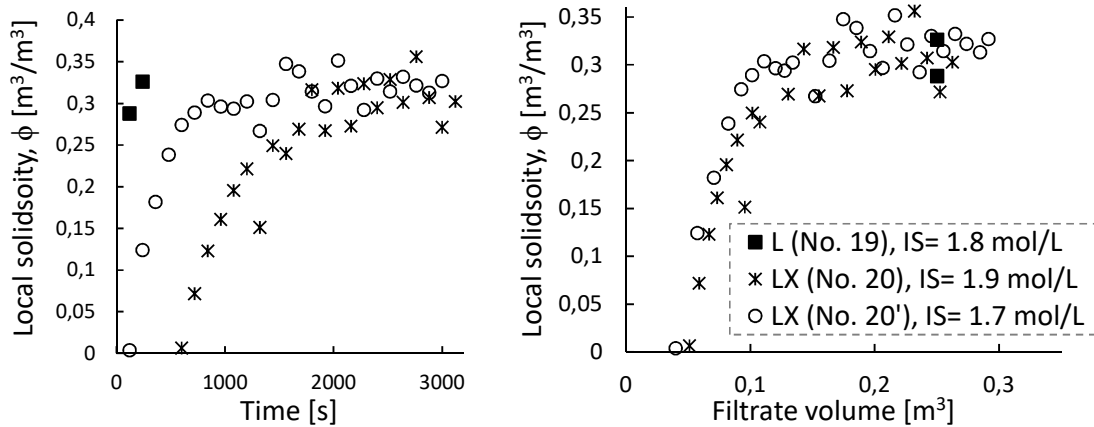

Figure 31: a (left) and b (right). Local solidosity during cake formation versus (**a**): experimental time and (**b**): filtrate volume, obtained on filtration of Slurries 19-20'. IS: ionic strength. Measurements were performed at 9 mm above the filter medium; the final cake was about 22-25 mm thick. NB: the initial local solidosity should correspond, at the very least, to the volumetric solid content of the slurries, i.e. about 7 vol%: the lower values observed remains in the range of the measurement uncertainty ($\pm$ 0.05 [m³/m³] in absolute solidosity).

Observations similar to those made for fast acidification could also be made for slow acidification. A significantly higher filtration resistance was found after the addition of xylan (Slurry 19 vs 20, 20' and Slurry 22 vs 23), and for slurries of lower ionic strength (Slurry 20'' vs 21), Table 14; the slurries in question were filtered using filter medium with the same pore size. Furthermore, the local and average solidosities of the filter cake were not found to be influenced significantly by the addition of xylan, Table 14 and Figure 31 (a) and (b).

No significant influence of the filter medium was observed when the filtration results obtained using the regenerated cellulose medium were compared to that of the polyethersulphone medium: Slurry 20 vs 20', Table 14, Figure 31 (a) and (b). It indicates that the interaction between the solids and the filter medium used is small or/and similar. However, when the pore size of the filter medium was decreased from 0.45 to 0.1 µm, a significantly lower filtration resistance was found: Slurry 20' vs 20'', Table 14. This could imply that the medium becomes partially blinded for a membrane pore size of 0.45 µm and at the conditions used for Slurries 20-20''.

Furthermore, a singular phenomenon was found to occur exclusively on filtration of Slurries 20, 20' & 20'': the formation of a filter cake with an unstable solid structure. Two distinct phases were observed during the filtration process, with a sudden acceleration of the filtration rate in the latter phase. Two distinct values of an apparent average filtration resistance were therefore reported: one for each of the two distinct phases of filtration observed, Table 14. It is likely that the phenomenon is partly related to both: a partial obstruction of the filter medium and cracking of the structure of the cake being formed. The phenomenon is still not fully understood; further discussion can be found in Paper III, Appendix F.

Comparing the values of the filtration properties obtained for the two acidification procedures, in the case where xylan was not added to lignin, similar average filtration resistances and local solidosities before expression were found: Slurries 9 & 9' vs 19: Table 14, Figure 28 and Figure 31 (a) & (b). This is despite the broader particles size distribution that was obtained for fast acidification, Figure 18. A higher average solidosity after expression of the filter cake was obtained for slow acidification, but no conclusion can be drawn due to the rather large spread of the average solidosity data found for fast acidification, Figure 30 (b).

When xylan was added to lignin, however, the slurries subjected to slow acidification (Nos. 20 & 20') were found to have a considerably lower filtration rate (i.e. more difficult to filter) compared to those subjected to fast acidification (Nos. 10 & 10'), Figure 28 (b) and Figure 31 (a). Moreover, the phenomenon of two distinct phases observed during the filtration of slurries subjected to slow acidification (Nos. 20-20'') did not occur in the corresponding slurries subjected to fast acidification (Nos. 10 & 10'). It is therefore likely that this phenomenon is responsible for the lower filtration rate obtained for slow acidification. Finally, both the local and the average solidosity of the cakes after expression were found to be similar for both acidification procedures when xylan was added to lignin.

When the precipitation temperature of the lignin slurry (with no addition of xylan) was decreased from 77 to 65°C, a significantly lower filter cake solidosity and a significantly higher filtration resistance were obtained: Slurry 19 vs 22, Table 14 (N.B. the filter media used had different pore sizes). These results are likely to be attributed to the smaller particles that are formed at lower precipitation temperatures, as shown by both the laser diffraction and FBRM measurements, Figure 16 (a) and (b). A peak in particle size of about 3-5 µm was measured at a precipitation temperature of 65 °C, i.e. close to the size of the primary particles (2.5 µm), implying that these do not form many/large agglomerates. The more porous solid structure of the cake that is formed by the smaller particles/agglomerates obtained at a precipitation temperature of 65 °C also leads to an increase in the solid/liquid contact area during filtration: the resistance to the flow is thus also higher; an illustration of the possible phenomenon described is shown in Figure 32. These results are in agreement with previous findings in the literature (Öhman and Theliander, 2007b): higher filtration resistance and higher porosity of the cake were obtained when filtering a black liquor, the precipitation temperature of which was decreased from 80 to 69 °C and the pH decreased, at most, to 9.5.

The case of the slurry with added xylan and a precipitation temperature of 65 °C (No. 23) is not discussed here, since it was seen that the slow acidification procedure possibly affects the

filterability of the lignin suspension (cf. the "two phase phenomenon" described for Slurries 20, 20' & 20'').
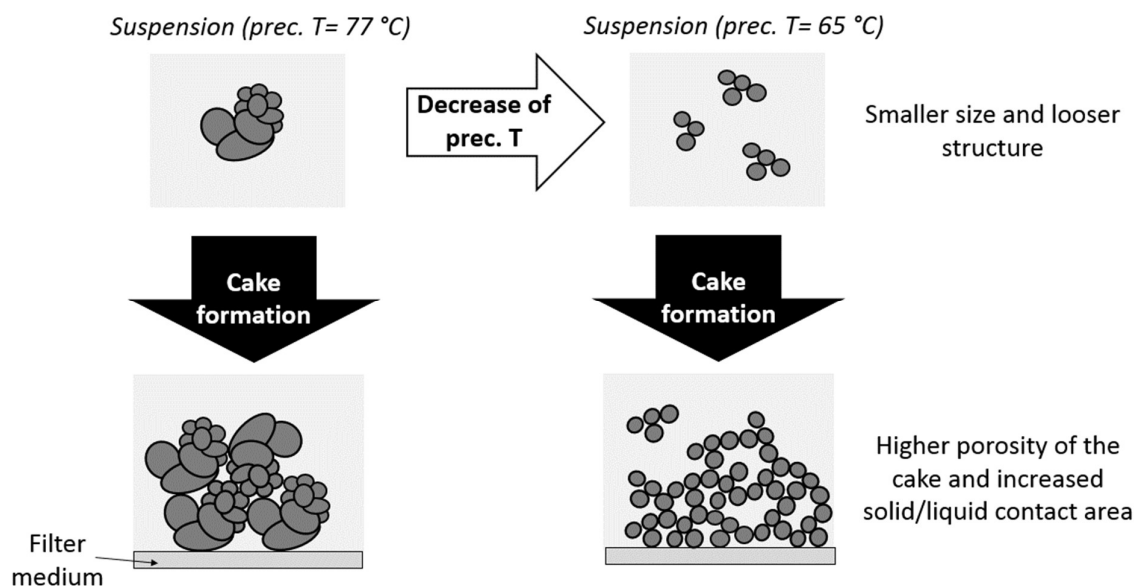

Figure 32. Illustration of the possible effect a decrease in the precipitation temperature (from 77 to 65 °C) may have on the agglomeration and filtration of lignin. T: temperature and prec.: precipitation.

7.2   Comparison of lignin and another agglomerating system: Titanium dioxide

7.2.1   Particle properties (Paper V)

The single particles of dry titanium dioxide powder visible in the micrograph images taken using ESEM, Figure 33 (a) and (b), appear to be around, or smaller than, 0.5 µm and the agglomerates in the size range of 2-20 µm.
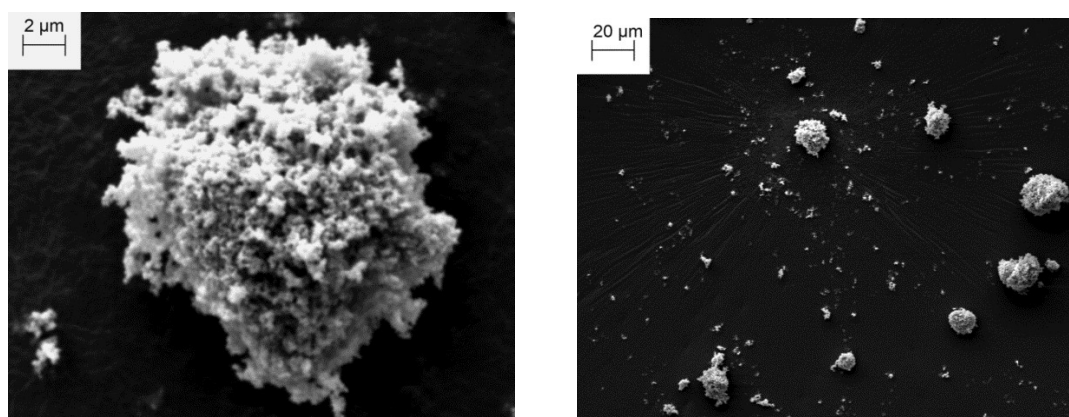

Figure 33: a (left) and b (right). ESEM micrographs of dried titanium dioxide powder at two different magnifications.

The results of the laser diffraction, B.E.T. and solid density measurements made on samples of titanium dioxide are shown in Table 15, along with the corresponding data obtained for LignoBoost lignin (Batch A) for the purpose of comparison.

Table 15. Properties and particle sizes of samples of titanium dioxide and LignoBoost lignin (Batch A). $D_{(x)}$ indicates that x % of the particles by volume are smaller than the value stated.

	Laser diffraction measurements			B.E.T. specific surface area [m2/g]		Solid density [kg/m3]
	$D_{(10)}$ [μm]	$D_{(50)}$ [μm]	$D_{(90)}$ [μm]	Air-dried	Freeze-dried	Air-dried
TiO₂	0.28	0.63	10.9	9.8	12.8	3810
Lignin (batch A)	2.5	8.9	43.9	15.4	33.4	1346

Based on the total volume, 80 % of the particles/agglomerates of titanium dioxide were shown to measure between 0.28 and 10.9 μm in diameter, with a volume-based average diameter of about 0.63 μm, Table 15. These results are in good accordance with the sizes observed in the micrograph images taken using ESEM (in dry conditions). The diameters of the particle corresponding to the B.E.T. specific surface area measurements performed on samples of both air-dried and freeze-dried titanium dioxide were 0.16 μm and 0.12 μm, respectively, assuming the particles to be perfectly smooth solid spheres. These values are smaller than for the agglomerates of particles measured and observed by laser diffraction and ESEM, respectively. Nevertheless, the particle sizes estimated from the B.E.T. measurements correspond well to the smallest particle sizes detected by laser diffraction (i.e. 0.16 μm: Figure 34 (a) in Section 7.2.2) and thus describe the size of the smallest primary particles that form the agglomerates with a relatively high degree of accuracy.

Furthermore, the samples of freeze-dried and air-dried titanium dioxide analysed had relatively similar B.E.T. surface areas, implying that the particles of TiO₂ are rigid enough so as not to be affected significantly by the drying technique. In comparison, a B.E.T. surface area twice as large was obtained for the freeze dried sample versus the air-dried sample in the case of lignin, which is a less rigid material, Table 15 (see Figure 11, Section 7.1.1.1). Furthermore, the primary particles and agglomerates formed in water suspension are significantly smaller for titanium dioxide than for lignin: primary particles close to ten times smaller were, for example, measured for TiO₂.

7.2.2 Influence of ionic strength on the size of particles/agglomerates (Paper V)

The size and chord length distribution of particles/agglomerates of titanium dioxide measured for slurries with varying initial concentrations of salt are presented in Figure 34 (a) and (b), respectively. The suspensions investigated had a significantly different concentration of solids, depending on the method employed: a highly diluted suspension was used for laser diffraction measurements while the suspension used for FBRM had a solid concentration of 1% by volume.
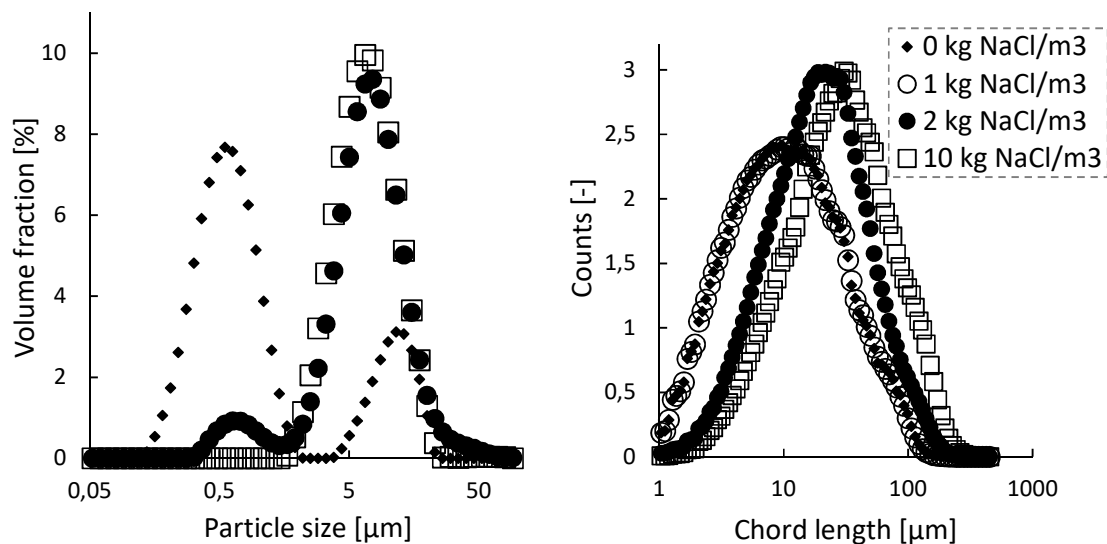
Figure 34: a (left) and b (right). Volume-based particle size distribution and chord length distribution measured using laser diffraction and FBRM for suspensions with varying contents of salt.

A clear increase in the size and chord length of the titanium dioxide particles/agglomerates can be observed after the addition of salt, Figure 34 (a) and (b), showing that an extensive agglomeration takes place in suspensions of higher ionic strength. This occurs when the electrical repulsive forces between the solid particles are sufficiently reduced due to the surface charge of the particles being shielded by the electrolytes added. The FBRM measurements revealed that the shift towards the attractive forces having a greater influence than the repulsive forces takes place between 1 and 2 kg NaCl/m^3. No difference in chord length distribution was recorded at lower ionic strength, i.e. between 0 and 1 kg NaCl/m^3, whereas a clear increase in size was seen between 1 and 2 kg NaCl/m^3, Figure 34 (b). Moreover, a further addition of salt was not found to have a significant impact on the sizes and chord length distributions of titanium dioxide particles: rather similar values were found between the two levels of salt, i.e. 2 and 10 kg NaCl/m^3, Figure 34 (a) and (b).

Furthermore, while the size distribution of the suspension with no salt addition shows two separate size ranges (first a dominant peak at about 0.6 μm and then a second peak at about 11 μm), Figure 34 (a), a shift towards a single, large size range peak can be observed after the addition of salt. This result also clearly shows the extensive agglomeration of particles that occurs at a higher ionic strength: the primary particles (and small agglomerates) measuring around 0.6 μm in diameter gather together to form larger agglomerates with an average diameter of about 8 μm in a diluted suspension.

The size ranges of the particles detected by laser diffraction are significantly smaller than those measured by FBRM, especially for the level where no salt was added. Although the absolute sizes obtained from the two instruments cannot be compared directly because they use different theoretical methodologies and solid concentrations, the large difference found between them is also due to the fact that the FBRM device does not report sizes smaller than 1 μm.

7.2.3 Influence of ionic strength on filtration (Papers III and V)
The local filtration resistance and the local solidosity of titanium dioxide filter cakes obtained from slurries with different initial concentrations of salt are presented in Figure 35 (a) and (b), respectively.
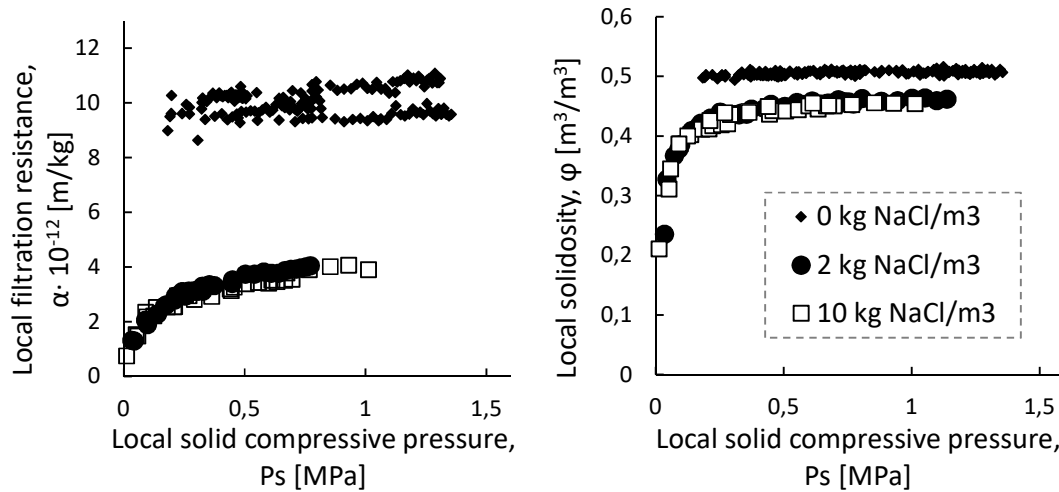
Figure 35: a (left) and b (right). Local specific filtration resistance and local solidosity as a function of the local solid pressure at varying ionic strengths obtained on filtration of titanium dioxide. Measurements were made at 12 mm from the filter medium; the final cake was about 31-35 mm thick.

The local filtration resistance and the local solidosity were found to decrease significantly after the addition of 2 and 10 kg/m^3 of sodium chloride. These results concur with the extensive agglomeration observed with increased ionic strength: the formation of larger agglomerates leads to a decrease in the surface contact between solid and liquid during filtration, i.e. the flow resistance by friction decreases. The structure of the cake formed by the agglomerated particles after the addition of salt is also more porous, as illustrated in Figure 36.
No significant difference in filtration properties was observed between the two additions of salt, which is also in agreement with the results of the particle size measurements: the agglomerates formed were found to be of similar size for additions between 2 and 10 kg/m^3. Furthermore, only a weak pressure dependency of the filter cake was found with no addition of salt, i.e. when particle agglomeration is hindered by the electrostatic repulsive forces. However, the more porous cake structure obtained at higher ionic strengths appears to be more compressible. A significantly higher dependency on pressure was observed after the addition of salt, especially in the early stage of the filtration process, which is possibly the result of the breaking up of a structure formed by larger and looser agglomerates.
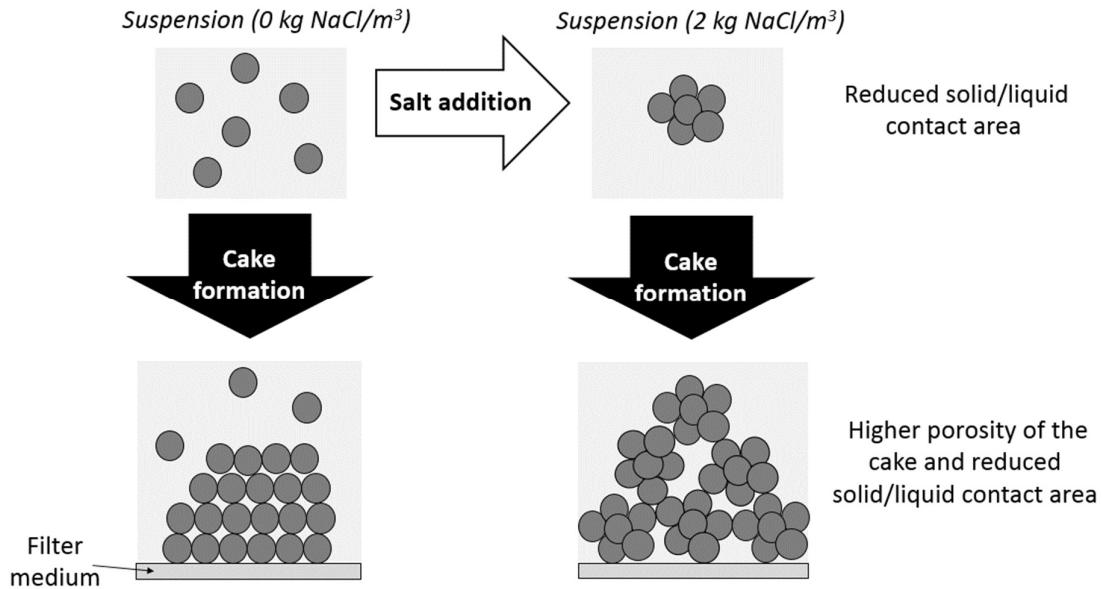
Figure 36. Hypothetical illustration of the effect the addition of salt (0 to 2 kg NaCl/m^3) may have on the agglomeration and filtration of titanium dioxide.

When the increase in ionic strength is sufficiently high, i.e. from 1.9 mol/L to 6.7 mol/L (Slurry 20'' vs 21), the addition of salt had a similar effect on the agglomeration and filtration of lignin to those observed for TiO$_2$: larger agglomerate sizes were measured (Figure 16 (a) and (b)) and lower filtration resistance and solidosity were obtained during filtration (Table 14).

For a lower range of ionic strength (i.e. between about 0.7 and 1.8 mol/L), however, the effect of salt addition differed in the case of lignin filtration. Even though the filtration resistance was also decreased at higher salt contents, the solidosity of the cake was shown to increase slightly when the ionic strength of the slurry was increased (Figure 27 (b) and Figure 30 (b)), i.e. a more compact structure is formed on average. Furthermore, the size of the lignin agglomerates was not found to increase between ionic strengths of 0.7 and 1.8 mol/L (see Section 7.1.2.3.2.). The different results obtained for the two materials with respect to the influence of salt additions on the filtration properties and sizes of the particles/agglomerates are gathered in Table 16 and discussed further below.

Table 16. The influence of ionic strength observed on the agglomeration and filtration properties of titanium dioxide and lignin. IS: ionic strength.

	Effect of:	**Effect on:**		
		Size of particles/agglomerates	α_{avg}	$\emptyset_{avg}$
Increase in ionic strength	Lignin (IS= 0.7 to 1.8 mol/L)	→	↘	↗
	Lignin (IS= 1.9 to 6.7 mol/L)	↗	↘	↘
	TiO$_2$ (0 to 2 kg NaCl/m^3)	↗	↘	↘

The differences in the agglomeration and related filtration properties observed between lignin and titanium dioxide are likely to be explained by the different structure, morphology, size of particles/agglomerate and inter-particle interactions of the two materials. Titanium dioxide is a

more crystalline material than lignin, with more rigid and significantly smaller primary particles and particles/agglomerates, see Section 7.2.1.

In the case of lignin, an increase in salt concentration may first lead to the particles and agglomerates that have already been formed becoming more compact in their internal structure, without their size being altered significantly. This, in turn, would also give the cake a denser and more solid structure, with a reduced contact area between the solid and liquid surfaces (see Section 7.1.3.2). Not only is the porosity within the agglomerates reduced but possibly also the distance between the agglomerates within the solid cake structure, as illustrated in Figure 37.

However, the denser lignin agglomerates may start to form larger clusters if a sufficient amount of salt is added (e.g. 6.7 mol/L in ionic strength). It is thus possible that a behaviour similar to that seen for TiO$_2$ (Figure 36) occurs: a more porous cake structure is formed, composed of large clusters of dense agglomerates.
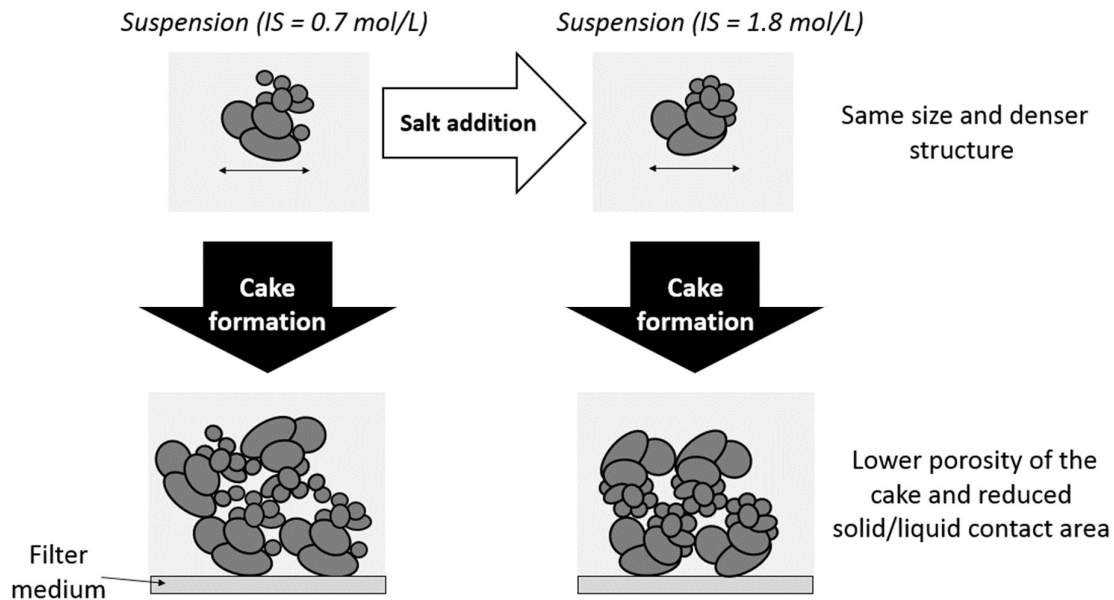

Figure 37. Hypothetical illustration of the possible effect the addition of salt at lower ionic strength (IS= 0.7 to 1.8 mol/L) may have on the agglomerates and filtration of lignin. IS: ionic strength.

7.2.4 Fitting the filtration models (Paper V)

The Kozeny-Carman equation, Happel's cell model and the porous sphere model were fitted to the local data obtained in order to evaluate their ability to describe the relationship between the local solidosity and the local filtration resistance of the filter cakes. The results from the fitting of the three models to the local data obtained on filtration of titanium dioxide at a sodium chloride addition of 10 kg/m^3 and of LignoBoost lignin (Slurry 1) are presented in Figure 38 (a) and (b), respectively. The resulting fitted parameters for the three different models obtained for LignoBoost lignin (Slurry 1) and for titanium dioxide at the three ionic strengths of the initial slurry studied are shown in Table 17.
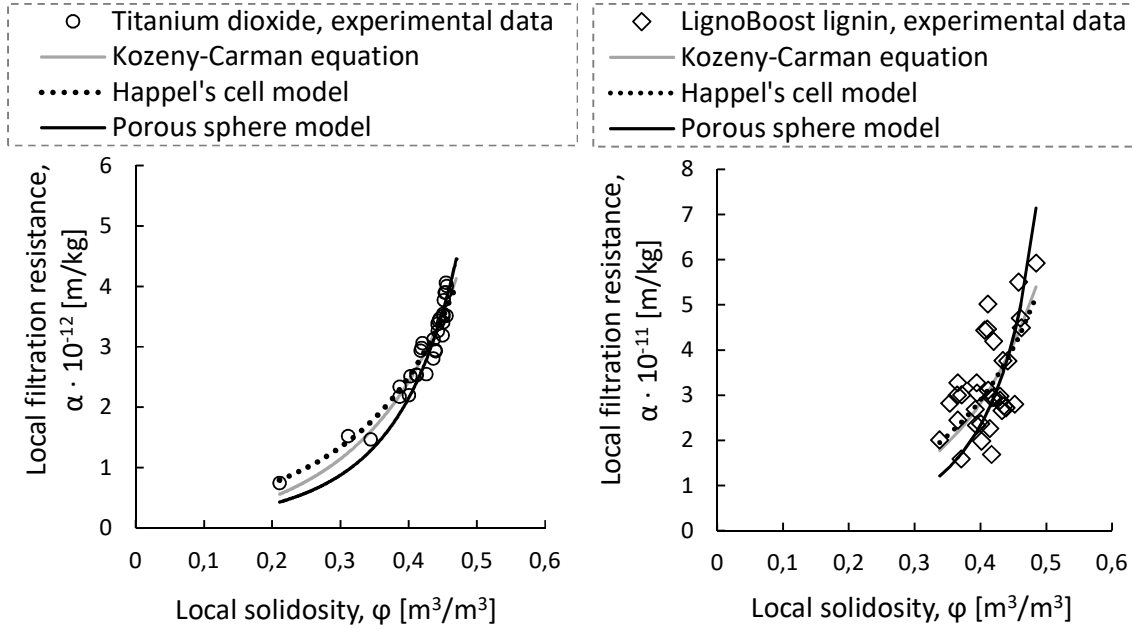
Figure 38: a (left) and b (right). Performance of the three filtration models fitted to experimental data obtained on filtration of (**a**) titanium dioxide with a sodium chloride addition of 10 kg/m^3 and (**b**) LignoBoost lignin (Slurry 1).

Table 17. Particle diameters obtained by fitting the filtration models to the local filtration properties of LignoBoost lignin (Slurry 1) and titanium dioxide with sodium chloride additions of 0, 2 and 10 kg/m^3.

	LignoBoost lignin [μm]	Titanium dioxide [μm]		
	(Slurry 1)	(0 kg$_{NaCl}$/m^3)	(2 kg$_{NaCl}$/m^3)	(10 kg$_{NaCl}$/m^3)
Kozeny-Carman	0.918	0.135	0.185	0.186
Happel′s cell model	0.936	0.134	0.187	0.189
Porous sphere model	0.593	0.269	0.355	0.353

All three filtration models could successfully describe the relationship between the local solidosity and the local filtration resistance that were determined experimentally.

In the case of titanium dioxide, the sizes of the particle diameters obtained from the model fittings for the Kozeny-Carman and Happel's cell models were in the range of those calculated from the B.E.T. measurements (i.e. about 0.14 μm): they were also in the range of the smallest particle size detected by laser diffraction. A slightly larger theoretical particle diameter was obtained when the porous sphere model was fitted to the local data.

Furthermore, an increase in the value of the fitted theoretical particle diameters was observed after the addition of salt in all cases. The extensive agglomeration that occurs at higher ionic strength leads, therefore, to an increase in the effective particle size that affects the flow resistance. The effective particle sizes obtained from these models do not, however, describe the complete actual formation of agglomerates. The filtration resistance is hence affected more directly by the particle surface area generated by the primary particles that compose the agglomerates than by the actual size of the (porous) agglomerates.

In the case of LignoBoost lignin, the fitted theoretical particle diameters obtained from the Kozeny-Carman and Happel's cell models were also in good agreement with the smallest

particle sizes detected using laser diffraction, i.e. 0.95 μm (Section 7.1.1.1). The porous sphere model, however, gave a particle size diameter smaller than what was measured using laser diffraction, but the value obtained was nevertheless larger than the particle size deduced from the B.E.T. surface area measurements (i.e. 0.28 μm for an air-dried sample). Moreover due to the uncertainty of the local data being relatively high in the LignoBoost lignin experiments, an investigation of the sensitivity of the models around the value of the fitted parameters d_p and $2a$ (describing the size of the solid particles/agglomerates) was conducted. The results obtained in the case of the porous sphere model and the Kozeny-Carman equation are presented in Figure 39 (a) and (b), respectively. The sensitivity of the models' fitting was found to be high, and the fitting diameters obtained can thus be considered relevant.
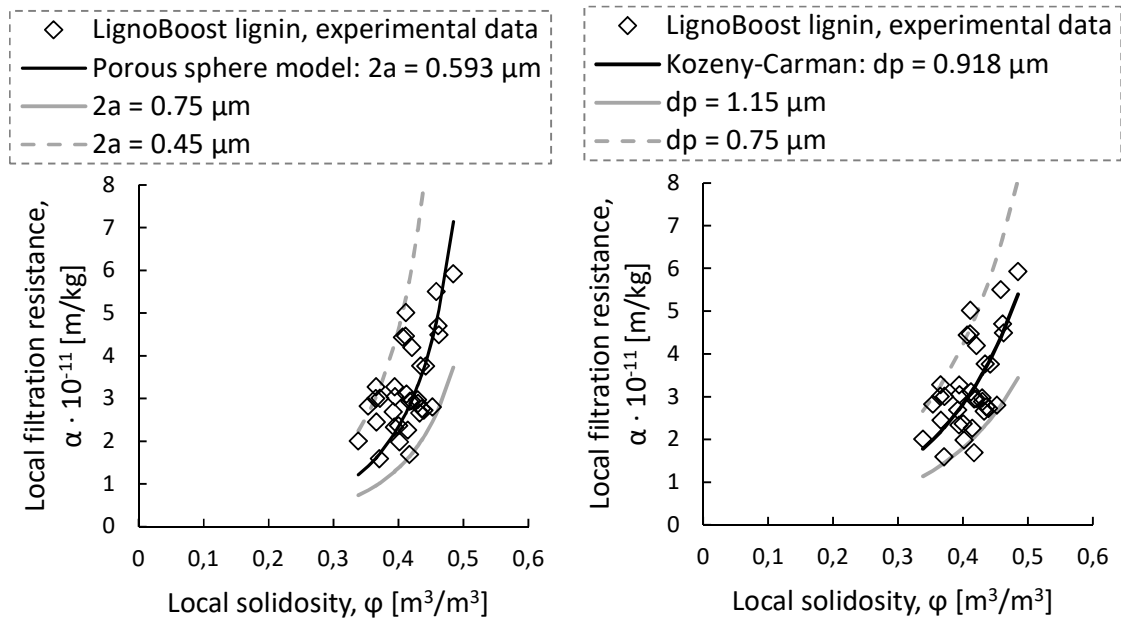

Figure 39: a (left) and b (right). Fitting performance when the fitting parameters of (a) the porous sphere model and (**b**) the Kozeny-Carman equation are varied.

8.   Concluding remarks

The main findings of this thesis are summarized in the first section and some potential industrial applications of the results are presented in the second.

8.1 Main findings

The LignoBoost lignin investigated was shown to be a relatively easy-to-filter material that formed weakly compressible filter cakes over the filtration pressure range studied (0.2 to 2.8 MPa) independently of the slurry concentration (8.8 to 21.6 wt%).

The addition of xylan was, however, found to increase the filtration resistance and the pressure dependency of the system significantly. Furthermore, this was independent of the preparation procedure employed: solid lignin and xylan (i) suspended together in acid water, (ii) dissolved together and then re-precipitated by a single main addition of acid, or (iii) dissolved together and then re-precipitated by a slow addition of acid over a 10 h time scale. Moreover, HPAEC and fluorescent microscopy analysis revealed that xylan, when precipitated together with lignin, was distributed evenly on the solid lignin that was forming the resulting filter cake.

These results strengthen the hypothesis that xylan is sorbed onto the surface of the lignin agglomerates for the model systems investigated. The sorbed xylan may then interact with lignin in such a way (via electrostatic and steric repulsive interactions) that the solid structure of the particle agglomerates becomes more open and porous locally. This would cause an increase in the contact area between the liquid and the solid during filtration, which could explain the significant increase in flow resistance observed.

Also, the effect of xylan on the filterability of lignin at lower ionic strengths (1.1 mol/L and lower) was found to be affected significantly by the pH of the suspension. The filtration resistance was considerably higher at pH 4 compared to pH 1-2.8 for a similar ionic strength. This is probably due to the content of unprotonated carboxylic acid groups, which are side groups on the xylan backbone, being greater at pH 4 than at pH 2.8 or lower, since the pKa of these acids groups is around 3.4. The surface charge of the xylan is thus significantly higher at pH 4 than at pH 2.8 or lower, which leads to greater electrostatic repulsive interactions, and thereby to the formation of an even more open local solid structure where xylan is sorbed onto the particle agglomerates of lignin. The filtration resistance is then increased as a result of the larger contact area that arises between the solids and the liquid during filtration.

The ionic strength was also found to have a significant influence on the filterability of the systems investigated. A decrease in filtration resistance was obtained at increased concentrations of salt in all of the cases studied: this was found valid with or without the addition of xylan and independent of the preparation procedure. The pressure dependency of the filtration resistance was also found to decrease as the ionic strength of the slurry increased. The formation of denser particles/agglomerates at increased ionic strength, i.e. when the solid surface charges are getting shielded and the electrostatic repulsive interactions between the solids particles are decreased, is the likely explanation for the results obtained.

Furthermore, the results of this work have confirmed the importance of the precipitation conditions used during the acidification stage with respect to the subsequent filtration of lignin. A temperature of 77 °C gave a lignin that was easier to filter (due to the larger size of the agglomerates formed) than temperatures of 65 °C or 45 °C. The onset of precipitation (chord lengths > 1 μm) was not found to be affected by the precipitation temperature investigated or the addition of xylan.

The precipitation of lignin was also found to be pH dependent in the neutral to acidic pH range in the cases of lower ionic strength (i.e. 1 M initial sodium ion concentration): both the size and amount of the particles formed increased when the pH was reduced between 7.9 and 3.9. This result indicates that, at lower ionic strength, the precipitation of lignin may also be influenced by the protonation of carboxylic groups.

Furthermore, fast precipitation led to a more heterogeneous formation of particles compared to slow precipitation: both smaller and larger sizes were obtained. This last result was shown to have an impact on filtration in the case of xylan being added to lignin, with a lower filtration time being required for the fast precipitation of the solids.

Finally, the local data obtained was used to evaluate the performance of several constitutive relationships which may be used in the modelling of the filtration process: i.e. Tiller and Leu, Kozeny-Carman, Happel's cell model and Deo's cell model with porous sphere. All could be fitted successfully to the local data. The average properties based on the parameters of the Tiller and Leu semi-empirical relationships, fitted to the local data, could also be used to accurately estimate the average experimental filtration properties obtained.

8.2 Industrial applicability

Relatively high filtration pressures and relatively small filter areas can be used industrially when the xylan content is low (i.e. in softwood lignin). Furthermore, the height of the filter cakes formed was not found to impact on the resulting structure and filterability of the solid cake. The heights measured were found to vary between 23 and 62 mm, along with the initial concentration of the slurry. These values are similar to the height range of cakes formed industrially.

The average filtration data obtained using the classical filtration equation can be used to design the filtration unit: a fairly high degree of accuracy was found between local and average measurements, especially at low residual contents of xylan (i.e. softwood lignin).

Xylan is likely to be one of the main reasons why the filtration resistance obtained for hardwood lignin is usually higher than that for softwood lignin. When the ionic strength is lowered (e.g. during the final filtration and washing stage of the LignoBoost process), a relatively small decrease in pH (from 4 to ≤ 2.8) may substantially facilitate the filtration of lignin when the content of residual xylan is high (i.e. in hardwood lignin).

Finally, the results confirmed that, during the acidification stage of the LignoBoost process, a controlled temperature and ionic strength are determinant for the efficiency of the filtration stages. A high ionic strength is required and a precipitation temperature close to 77 °C is preferred over the lower temperatures of 65 and 45 °C, for the investigated types of lignin.

9. Proposals for future work

Work on extending the understanding and knowledge on the filtration of Kraft lignin that is relevant for the LignoBoost process has been carried out in this thesis. Studies of the influence of several parameters, such as the content of beechwood xylan and ionic strength, were undertaken using model liquors based on a softwood lignin previously extracted using the LignoBoost process. Interesting work remains, however, so that the efficiency of the filtration stage of the LignoBoost process can be improved further. Some suggestions for such work are:

- Determining local filtration data while filtering lignin from industrial black liquor and/or other types of lignin.
- Further work on the influence of hemicelluloses, e.g. investigating whether or not their influence varies if they are linked covalently to lignin (lignin-carbohydrate complexes). Also, extend the study to different types of xylan and glucomannan to increase understanding of their respective influence.
- Developing knowledge of the mechanisms of particle formation during the precipitation stage of lignin: precipitation conditions were shown to have a great impact on the subsequent filtration of lignin. The influence of the precipitation temperature on the formation of particles is one notable domain requiring further investigation.
- Further studies using model liquors that include some residual constituents of black liquor that were not included in the liquors investigated here, and that might also have an impact on the filtration of lignin: metal ions, extractives, etc.
- Deepen knowledge of the impact of inter-particle interactions, such as electrostatic interactions, both in the suspension and in the filter cake formed, in order to develop improved models that describe the filtration process.

Acknowledgements

I would like to express my gratitude to a number of people who facilitated this work in different ways:

My main supervisor and examiner, Prof. **Hans Theliander**, for providing me with the opportunity of working within this interesting field of research. I am truly grateful for his precious support, rewarding guidance and all the interesting discussions we had throughout the duration of this work.

My co-supervisor, Dr. **Tuve Mattsson** is sincerely acknowledged for his continuous encouragement and support, and for his highly productive guidance.

My co-authors, Mr. **Tor Sewring** and Dr. **Jonas Wetterling** for their valuable contributions.

The talented Master students whom I supervised, Ms. **Lynn Schneider** and Ms. **Helen Schneider**, for the valuable contribution their thesis project made to my research.

Ms. **Annika Altskär** at Research Institute of Sweden (RISE) SP Food and Bioscience for her expertise in performing the confocal laser scanning fluorescence microscopy measurements.

Dr. **Cecilia Mattsson** for her expertise in determining the molecular weight of the components.

Mr. **Tommy Friberg**, Ms. **Ximena Rozo Sevilla** and Ms. **Lena Fogelquist** for their skilful advice with some of the experimental work and for ordering the experimental resources required.

Ms. **Eva Kristenson** and Ms. **Malin Larsson** for their prompt help with administrative tasks.

Ms. **Maureen Sondell** for her skill and efficiency in the linguistic revision of the articles and the thesis.

All my colleagues and friends at Chalmers, past and present, for creating a highly diverse, interesting and enriching working environment. Here, I would like to thank Mr. **Tor Sewring** again along with Mr. **Anders Åkesjö** for all the interesting and fun discussions we shared while working and/or having lunch together. I would like to acknowledge Mr. **Tallal Belkheri** for his support and for allowing me to practice French with him at work! Ms. **Laura Collura** and Dr. **Marco Maschietti** are warmly thanked for their friendliness and for being the best guides I could wish for during a trip to their beautiful country Italy. I am sincerely grateful to Dr. **Erik Karlsson** for his support and kindness: thank you for your powerful good vibes!

All my **friends** in France, Sweden and elsewhere: thanks for everything. ☺

My dear and beloved **family**: words are not enough to express my gratitude towards you. ☺

Nomenclature

A	filtration area [m^2]
a	radius of the inner cell sphere [m]
b	cell radius [m]
c	mass of solids per unit of filtrate volume [kg/m^3]
$D_{(x)}$	diameter for which x% of the particles by number are smaller than the value stated [μm]
d_γ	average path of the γ-radiation [m]
f_s	liquid drag force on solid particles [N]
IS	ionic strength [mol/L]
K	local permeability [m^2]
k	Kozeny-Carman constant [-]
k_i	permeability of the inner sphere [m^2]
L	height of the filter cake formed [m]
n	parameter [-]
P_a	parameter [Pa]
P_c	pressure drop over the filter cake [Pa]
p_l	local liquid pressure [Pa]
P_m	pressure drop over the filter media [Pa]
P_{piston}	applied piston pressure [Pa]
p_s	local solid pressure [Pa]
P_a	Tiller and Leu equations parameter [Pa]
ΔP	pressure drop over the filter cell [Pa]
R_m	resistance of the filter medium [m^{-1}]
S_p	specific surface area [m^{-1}]
T	temperature [°C]
t	time [s]
V	volume of filtrate [m^3]
V_{solid}	volume of non-dissolved solid in the cake [m^3]
V_{total}	total volume of the cake [m^3]
v	superficial liquid velocity [m/s]
v_s	superficial solid velocity [m/s]
z	distance from the filter medium [m]

Greek letters

α	local specific filtration resistance [m/kg]
α_0	parameter [m/kg]
α_{av}	average specific filtration resistance [m/kg]
β	parameter [-]

$\overline{\Delta_{rel}\alpha}$	Averaged relative experimental uncertainty in local filtration resistance [%]
$\lvert\Delta\phi\rvert$	absolute deviation in local solidosity [m^3/m^3]
$\Delta_{rel}\phi$	relative experimental uncertainty in local solidosity [%]
ε	local porosity of the filter cake [m^3/m^3]
ε_{av}	average porosity of the filter cake [m^3/m^3]
η_γ	number of counts [-]
$\eta_{\gamma,0}$	number of counts for the empty filter cell [-]
μ	viscosity of the fluid [Pa·s]
$\mu_{\gamma,l}$	attenuation coefficient for the liquid phase [m^{-1}]
$\mu_{\gamma,s}$	attenuation coefficient for the solid phase [m^{-1}]
$\mu_{\gamma,TiO2}$	attenuation coefficient of titanium dioxide [m^{-1}]
$\mu_{\gamma,water}$	attenuation coefficient of water [m^{-1}]
ρ_s	solid density [kg/m^3]
$\emptyset_{av}$	average solidosity [m^3/m^3]
ϕ	local solidosity [m^3/m^3]
ϕ_0	parameter [m^3/m^3]
ϕ_i	solidosity of the inner sphere [m^3/m^3]

Abbreviations

B.E.T.	Brunauer–Emmett–Teller
CLD	Chord Length Distribution
C-P	Compression- Permeability
FBRM	Focus Beam Reflectance Measurement
GPC	Gel Permeation Chromatography
HPAEC	High Performance Anion Exchange Chromatography
L	Lignin
LCC	Lignin – Carbohydrate Complexes
MeGlcA	4-O-MethylGlucuronic Acid
prec.	precipitation
PSD	Particle Size Distribution
RBBR	Remazol Brilliant Blue R
S	extra salt added
X	Xylan

References

Alder, E. (1977). Lignin chemistry- past, present and future. Wood Science and Technology, 11, 169-218.

Aminzadeh, S., Lauberts, M., Dobele, G., Ponomarenko, J., Mattsson, T., Sevstyanova, O. and Lindström, M.E. (2017). Membrane filtration of lignoboost kraft lignin: poperties of the low molecular weight fraction. 19th ISWFPC, Porto Seguro, Bahia, Brazil, 246-250.

Arkell, A., Olsson, J. and Wallberg, O. (2014). Process performance in lignin separation from softwood black liquor by membrane filtration. Chemical Engineering Research and Design, 92, 1792-1800.

Bai, R. and Tien, C. (2005). Further work on cake filtration analysis. Chemical Engineering Science, 60, 301-313.

Baker, D.A., Gallego, N.C and Baker, F.S. (2011). On the characterization and spinning of an organic-purified lignin towards the manufacture of low-cost carbon fiber. Journal of Applied Polymer Science, 124 (1), 227-234.

Bergström, L. (1992). Sedimentation of Flocculated Alumina Suspensions: g-Ray measurements and comparison with model predictions. Journal of the Chemical Society, Faraday Transactions, 88, 3201-3211.

Bertin, E. P. (1975). Principles and practice of X-ray spectrometric analysis. Plenum Press, New York, USA.

Brinkman, H. (1947). A calculation of the viscous force exerted by a flowing fluid on a dense swarm of particles. Applied Scientific Research, 1, 27-34.

Brodin, I., Ernstsson, M., Geerstedt, G. and Sjöholm, E. (2012). Oxidative stabilisation of kraft lignin for carbon fibre production. Holzforschnung, 62 (2), 141-147.

Buchert, J., Teleman, A., Harjunpaa, V., Tenkanen, M., Viikari, L., Vuorinen, T. (1995). Effect of cooking and bleaching on the structure of xylan in conventional pine kraft pulp. Tappi Journal, 78(11), 125-130.

Celzard, A., Fierro, V., Amaral-Labat, G., Pizzi, A., Fredon, E. and Mareche, J-F. (2008). Carbon materials derived from lignin. Nordic Wood Biorefinery Conference (NWBC), Proceedings, March 11-13, Stockholm, Sweden.

Chase, G.G. and Willis, M.S. (1992). Compressive cake filtration. Chemical Engineering Science, 47, 1373-1381.

Cherubini, F. and Strømman, A.H. (2011). Principles of Biorefining. Biofuels, Academic Press. Amsterdam, 3-24.

Clavijo, L., Cabrera, M. N., Kuitunen, S., Liukko, S., Rauhala, T. and Vuorinen, T. (2012). Changes in a eucalyptus kraft pulp during a mild acid treatment at high temperature. Papel, 73(4), 59-64.

Connors, W.J., Sarkanen, S. and McCarthy, J.L. (1980). Gel chromatography and association complexes of lignin. . Holzforschung, 34, 80.

Darcy, H. P. G. (1856). Les Fontaines Publiques de la Ville de Dijon. Victor Dalamont, Paris, France.

Dell, C.C. and Sinha, J. (1964). The mechanism of removal of water from flocculated clay sediments. Transactions of the British Ceramic Society, 63, 603-614.

Deo, S. (2009). Stokes Flow Past a Swarm of Deformed Porous Spheroidal Particles with Happel Boundary Condition. Journal of Porous Media, 12 (4), 347-359.

Dirckx, C.J., Clark, S.A., Hall, L.D., Antalek, B., Tooma, J., Hewitt, J.M. and Kawaoka, K. (2000). Magnetic resonance imaging of the filtration process. AIChE Journal, 46, 6-14.

Ek, M., Gellerstedt, G. and Henriksson, G. (2009). Wood chemistry and Wood Biotechnology. De Gruyter Ed. Textbook, Chap. 5, 111.

Fathi-Najafi, M. and Theliander, H. (1995). Determination of local filtration properties at constant pressure filtration. Sep. Tech., 5,165-178.

Froass, P.M., Ragauskas, A.J. and Jiang, J., E. (1998). NMR studies Part 3: analysis of lignins from modern kraft pulping technologies. Holzforschung, 52, 385-390.

Fu, L.F. and Dempsey, B.A. (1998). Modeling the effect of particle size and charge on the structure of the filter cake in ultrafiltration. Journal of Membrane Science, 149, 221-240.

Gellerstedt, G. and Lindfors, E.-L. (1984). Structural changes in lignin during kraft pulping. Holzforschnung, 38, 151-158.

Gellerstedt, G. (2009). Chemistry of chemical pulping. In: Ek, M., Gellerstedt, G and Henriksson, G. (eds) The Pulp and Paper Chemistry and Technology, Volume 2 Pulping Chemistry and Technoloy. Berlin, Germany: Walter De Gruyter.

Gellerstedt, G. and Henriksson, G. (2009). Hemicelluloses and pectins, in: M. Ek, G. Gellerstedt, G. Henriksson (Eds.), Pulp and Paper Chemistry and Technology 1, Wood Chemistry and Wood Biotechnology, Walter De Gruyter, Stockholm, 101–120.

Gellerstedt, G. (2004). Chemistry of pulping. Chap. 20 of: Cellul. Technol. Stockholm: Fiber and Polymer Technology, KTH.

Gierer, J. (1970). The reactions of lignin during pulping. A description and comparison of conventional pulping processes. Svensk Papperstidning, 73, 571-596.

Goring, D. A. I. (1962). The physical chemistry of lignin. Pure Appl. Chem., 5, 1-2.

Gosselink, R.J.A. (2011). Lignin as a renewable aromatic resource for the chemical industry. Ph.D. thesis (Online), 20-25. Wageningen University. The Netherlands.

Green, J., Pearl, I., Hardacker, K., Andrews, B. and Haigh, F. (1977). The peeling reaction in alkaline pulping. Tappi 60 (10), 120 - 125.

Grace, H. P. (1953). The resistance and compressibility of filter cakes. Chemical Engineering Progress, 49 (6), 303-318.

Happel, J. (1958). Viscous Flow in Multiparticle Systems: Slow Motion of Fluids Relative to Beds of Spherical Particles. AIChE Journal, 4 (2), 197-201.

Henriksson, G. (2009). Lignin. In: Ek, M., Gellerstedt, G. and Henriksson, G. (Eds.). Pulp and paper chemistry and technology. Volume 1, Wood chemistry and wood biotechnology. Walter de Gruyter, Berlin, Germany.

Henriksson, G., Li, G., Zhang, L. and Lindström, M.E. (2010). Lignin Utilization. In: Thermochemical Conversion of Biomass to Liquid Fuels and Chemicals, Ed. M. Crocker, Royal Society of Chemistry, 223-262.

Hermia, J. (1988). Consideration upon the use of constant pressure cake filtration law. Particle Technology in Relation to Filtration Separation. Antwerp, Belgium, 1-9.

Higson, A. (2011). Lignin. Factsheet: Overview of the current and potential market for lignin based materials. www.nnfcc.co.uk.

Hilpmann, G., Becher, N., Pahner, F.-A., Kusema, B., Maeki-Arvela, P., Lange, R., Murzin, D. Yu. and Salmi, T. (2016). Acid hydrolysis of xylan. Catalysis Today, 259 (Part 2), 376-380.

Holladay, J.E., Bozell, J.J., White, J.F. and Johnson, D. (2007). Top value added chemicals from biomass. Volume II – results of screening for potential candidates from biorefinery lignin. Pacific Northwest National Laboratory and the National Renewable Energy Laboratory. Prepared for the US Department of Energy under contract number DE-ACOS-76RL01830.

Horsfield, M.A., Fordham, E.J. and Hall, L.D. (1989). ^{1}HNMR imaging studies of filtration in colloidal suspensions. Journal of Magnetic Resonance, 81, 593-596.

Hutto, F. B. (1957). Distribution of porosity in filter cakes. Chemical Engineering Progress, 53, 328-32.

Jönsson, A. S. and Wallberg, O. (2009). Cost estimates of kraft lignin recovery by ultrafiltration. Desalination, 237(1-3), 254–267.

Johansson, C. and Theliander, H. (2003). Measuring concentration and pressure profiles in dead-end filtration. Filtration, 3, 114-120.

Johansson, C. (2005). Pressure and solidosity profiles in cake filtration. An experimental study of filtration properties of lignin from bioethanol production and model materials. Ph.D. thesis, 35. Chalmers University of Technology, Gothenborg, Sweden.

Kadla, J.F., Kubo, S., Venditti, R.A, Gilbert, R.D., Compere, A.L. and Griffith, W. (2002). Lignin-based carbon fibers for composite fiber applications. Carbon, 40 (15), 2913-2920.

Kannangara, M., Marinova, M., Fradette, L. and Paris, J. (2016). Effect of mixing hydrodynamics on the particle and filtration properties of precipitated lignin. Chemical Engineering Research and Design, 105, 94-106.

King, C. J. (1980). Separation Processes. Mc-Graw-Hill, New-York, USA. 2nd edition.

Kobayashi, K., Hakoda, M., Hosoda, Y., Iwata, M., Yukawa, H. (1979). Electroosmotic flow through particle beds and electroosmotic pressure distribution. Journal of Chemical Engineering of Japan, 12, 492-494.

Koenders, M. A. and Wakeman, R. J. (1996). The initial stages of compact formation from suspension by filtration. Chemical Engineering Science, 51 (16), 3897-3908.

Koenders, M. A. and Wakeman, R. J. (1997). Filter cake formation from structured suspensions. Chemical Engineering Research Design, 75 (A3), 309-320.

Koenders, M. A., Reymann, S. and Wakeman, R. J. (2000). The intermediate stage of the dead-end filtration process. Chemical Engineering Science, 55, 3715-3728.

Kopinga, K. and Pel, L. (1994). One-dimensional scanning of moisture in porous materials with NMR. Review of Scientific Instruments, 65, 3673-3691.

Kozeny, J. (1927). Über Kapillare Leitung des Wassers im Boden. Sitzungsberichte der Akademia der Wissenschaften in Wien, Mathematisch-Naturwissenschaftliche, 136, IIa, 271-306.

La Heij, E.J., Kerkhof, P.J.A.M., Kopinga, K. and Pel, L. (1996). Determining porosity profiles during filtration and expression of sewage sludge by NMR imaging. AIChE Journal, 42, 953-959.

Laine, J., Liivgren,L., Stenius, P. and Sjaberg, S. (1994). Potentiometric titration of unbleached kraft cellulose fibre surfaces. Colloids Surfaces, A: Physicochemical and Engineering Aspects, 88(2-3), 277-87.

Landman, K. A., White, L., R., and Eberl, M. (1995). Pressure filtration of flocculated suspensions. AIChE Journal, 41(7), 1687-1700.

Larue, O., Vorobiev, E., Vu, C. and Durand, B. (2003). Electrocoagulation and coagulation by iron of latex particles in aqueous suspensions. Separation and Purification Technology, 31, 177-192.

Lerche, D. and Sobisch, T. (2007). Consolidation of concentrated dispersions of nano-and microparticles determined by analytical centrifugation. Powder Technology, 174, 46.

Leu, W.-F. (1981). Cake filtration. PhD thesis, University of Houston, Department of Chemical Engineering, Texas, USA.

Leubner, I. H. (2000). Particle nucleation and growth models. Curr. Opin. Colloid Interface Sci., 5(1-2), 151–159.

Lindström, T. (1979). The colloidal behaviour of kraft lignin. Part I. Association and gelation of kraft lignin in aqueous solutions. Colloid and Polymer Science, 257, 277-285.

Lindström, T. and Westman, L. (1980). The colloidal behaviour of kraft lignin. Part III. Swelling behaviour and mechanical properties of kraft lignin gels. Colloid and Polymer Science, 258, 390-397.

Ljungberg. (2008). The Ljungberg Textbook. Wood Chemistry.

Loginov, M., Lebovka, N. and Vorobiev, E. (2014). Filterability of mineral suspensions predicted with the analytical photocentrifuge: method of multistage centrifugation. Filtration, 14 (2), 109-120.

Loufti, H., Blackwell, B. and Uloth, V. (1991). Lignin recovery from kraft black liquor: preliminary process design. Tappi J., 74(1), 203-210.

Macdonald, C. (2013). Betting on Biochemicals. Pulp and Paper Canada, 12.

Marton, J. (1964). On the structure of kraft lignin. Tappi, 47, 713-719.

Mattsson, T., Sedin, M. and Theliander, H. (2011). Zeta-potential and local filtration properties: Constitutive relationships for TiO_2 from experimental filtration measurements. Chemical Engineering Science, 66, 4573-4581.

Mattsson, T., Sedin, M. and Theliander, H. (2012). Filtration properties and skin formation of micro-crystalline cellulose. Separation and Purification Technology, 96, 139-146.

McNaughton, J.G., Yean, W.Q and Goring, D.A.I. (1967). Macromolecular properties of kraft lignins from spruce made soluble by a continuous flow process. Tappi, 50, 548-553.

Meeten, G.H. (1993). A dissection method for analysing filter cakes. Chemical Engineering Science, 48, 2391-2398.

Nelson, W. (1970). Confidence intervals for the ratio of two poisson means and poisson predictor intervals. IEEE Transactions of reliability, R-19(2), 42-49.

Norgren, M., and Lindström, B. (2000). Dissociation of phenolic groups in kraft lignin at elevated temperatures. Holzforschung, 54(5).

Norgren, M., Edlund, H., Wågberg, L., Lindström, B. and Annergren, G. (2001). Aggregation of kraft lignin derivatives under conditions relevant to the process, part I: phase behaviour. Colloids Surfaces A Physicochem. Eng. Asp. 194(1-3), 85–96.

Norgren, M., Edlund, H. and Wågberg, L. (2002). Aggregation of lignin derivatives under alkaline conditions. Kinetics and aggregate structure. Langmuir, 18(7), 2859–2865.

Öhman, F. and Theliander, H. (2006): Washing lignin precipitated from kraft black liquor. Paperi J.Puu, 88(55), 287-292.

Öhman, F., Wallmo, H. and Theliander, H. (2007a). A novel method for washing lignin precipitated from kraft black liquor: Laboratory trials. Nordic Pulp and Paper Research Journal, 22(1), 9-16.

Öhman, F. and Theliander, H. (2007b). Filtration properties of lignin precipitated from black liquor. Tappi Journal, 6(7), 3-9.

Öhman, F., Wallmo,H. and Theliander, H. (2007c). Precipitation and filtration of lignin from black liquor of different origin. Nordic Pulp & Paper Research Journal, 22(2), 188-193.

Okamura, S. and Shirato, M. (1955). Liquid Pressure Distribution within Cakes in the Constant Pressure Filtration. Chemical Engineering, 19, 104-110.

Pye, E. K. (2008). Industrial Lignin Production and Applications. Biorefineries-Industrial Processes and Products. Wiley-VCH Verlag GmbH.

Ragauskas, A. J., Williams, C. K., Davison, B. H., Britovsek, G., Cairney, J., Eckert, C. A., Frederick, W. J., Jr., Hallett, J. P., Leak, D. J. and Liotta, C. L. (2006). The path forward for biofuels and biomaterials. Science (Washington, DC, USA), 311(5760), 484-489.

Rudatin, S., Sen, Yasar L. and Woerner Douglas, L. (1989). Association of kraft lignin in aqueous solution. Lignin: Properties and Materials. American Chemical Society.

Ruth, B., F. (1935). Studies in filtration iii. Derivation of general filtration equations. Industrial and Engineering Chemistry, 27, 707-723.

Ruth, B., F. (1946). Correlating filtration theory with industrial practice. Industrial and Engineering Chemistry, 38, 564-571.

Saveyn, H., Curvers, D., Pel, L., De Bndt, P and Van der Meeren, P. (2006). In situ determination of solidosity profiles during activated sludge electrodewatering. Water Research, 40, 2135-2142.

Shen, C., Russel, W.B. and Auzerais, F.M. (1994). Colloidal gel filtration: Experiment and theory. AIChE Journal, 40, 1876-1891.

Shirato, M., Sambuichi, M., Kato, H. and Aragaki, T. (1969). Internal flow mechanism in filter cakes. AIChE Journal 15, 405-409.

Shirato, M., Aragaki, T., Ichimura, K. and Ootsuji, N. (1971). Porosity variation in filter cake under constant-pressure filtration. Journal of Chemical Engineering of Japan, 4(2), 60-65.

Sixta, H. (2006). Handbook of pulp. Vol.1 Wiley-VCH, 9.

Sjöström, E. (1993). Wood Chemistry: Fundamentals and Applications, Gulf Professional Publishing. (Online Textbook).

Sorensen, P. B., Mouldrup, P. and Hansen, J. A. A. (1996). Filtration and expression of compressible cakes. Chemical Engineering Science, 51, 967-979.

Stickland, A.D. and Buscall, R. (2009). Whither compressional rheology? Journal of Non-Newtonian Fluid Mechanics, 157, 151-157.

Teoh, S.K., Tan, R. B. H. and Tien C. (2002). Correlation of C–P cell and filtration test data using a new test cell. Separation and Purification Technology, 29, 131–139.

Theander, O., and Westerlund, E. A. (1986). Studies on dietary fiber. 3. Improved procedures for analysis of dietary fiber. Journal of Agricultural and Food Chemistry, 34, 330-336.

Theliander, H. (1990). On the filtration properties of lime mud. Nordic Pulp and Paper Resources J., 5 (2), 74-82.

Tien, C. and Bai, R. (2003). An assessment of the conventional cake filtration theory. Chemical Engineering Science, 58, 1323 – 1336.

Tiller, F.M. and Hrong, L.L. (1983). Hydraulic deliquoring of filter cakes-1. Reverse flow in filter presses, AIChE J., 29(2), 297-305.

Tiller, F.M. and Shirato, M. (1964). The role of porosity in filtration: VI. New definition of filtration resistance. AIChE Journal, 10 (1), 61-67.

Tiller, F.M, Haynes, S. and Lu, W. M. (1972). The role of porosity in filtration VII: Effect of side-wall friction in compression permeability cells. AIChE Journal, 18(1), 13-20.

Tiller, F.M., Hsyung, N.B and Cong, D.Z. (1995). Role of porosity in filtration: XII. Filtration with Sedimentation. AIChE Journal, 41, 1153-1164.

Tiller, F.M. and Leu, W.F. (1980). Basic data fitting in filtration. Journal of the Chinese Institute of Chemical Engineers 11, 61-70.

Tiller, F.M. (1955). The role of porosity. Part II: Analytical equations for constant rate filtration. Chemical Engineering Progress, 51, 282-290.

Toledano, A., García, A., Mondragon, I. and Labidi, J. (2010). Lignin separation and fractionation by ultrafiltration. Separation and Purification Technology, 71, 38-43.

Tomani, P. (2010). The LignoBoost process. Cellulose Chemistry and Technology, 44(1-3), 53-58.

Trajano, H.L., Pattathil, S., Tomkins, B. A., Tschaplinski, T. J., Hahn, M. G., Van Berkel, G. J., Wyman, C. E. (2015). Acid hydrolysis of xylan. Bioresource Technology, 179, 202-210.

Uloth, V.C. and Wearing, J.T. (1989a). Kraft lignin recovery: acid precipitation versus ultrafiltration. Part I: Laboratory test results. Pulp and Paper Canada, 90, 67-71.

Uloth, V.C. and Wearing, J.T. (1989b). Kraft lignin recovery: acid precipitation versus ultrafiltration. Part II: Technology and economics. Pulp and Paper Canada, 90, 34-37.

Wakeman, R.J. (1978). A numerical integration of the differential equations describing the formation of and flow in compressible filter cakes. Transactions of the Institution of Chemical Engineers, 56, 258-265.

Wakeman, R.J. (1981). The formation and properties of apparently incompressible filter cakes under vaccum on downward facing surfaces. Transactions of the Institution of Chemical Engineers, 56, 258-265.

Wakeman, R.J., Thuraisingham, S.T. and Tarleton, E.S. (1989). Colloid science in solid/liquid separation technology: is it important? Filtration and Separation, 26, 277-283.

Wallberg, O. and Jönsson, A.S. (2006). Separation of lignin in kraft cooking liquor from a continuous digester by ultrafiltration at temperatures above 100°C. Desalination, 195, 187-200.

Wallmo, H., Richards, T. and Theliander, H. (2007). Lignin precipitation from Kraft black liquors: kinetics and carbon dioxide absorption. Paperi ja Puu, 89(7-8), 436-442.

Wallmo, H., Theliander, H., Jönsson, A.S., Wallberg, O. and Lindgren,K. (2009). The influence of hemicelluloses during the precipitation of lignin in kraft black liquor. Nordic Pulp and Paper Research Journal, 24, 165-171.

Watanabe, T. (2003). Analysis of native bonds between lignin and carbohydrate by specific chemical reactions. Textbook (Online).

Yim, S.S. and Song, Y.M. (2008). Porosity distribution in highly compressible cake: Experimental and theoretical verification of the dense skin. Korean Journal of Chemical Engineering, 25, 1524-1531.

Yllner, S. and Enström, B. (1956). Studies of the absorption of xylan on cellulose fibers during the sulphate cook. Part 1. Sven. Papperstidning 59 (6), 229.

Ziesig, R., Tomani, P. and Theliander H. (2014a). Production of a pure lignin product, part 1: distribution and removal of inorganics in Eucalyptus globulus kraft lignin. Tappi Journal, 13(3), 65-72, 8.

Ziesig, R., Tomani, P. and Theliander H. (2014b). Production of a pure lignin product, part 2: separation of lignin from membrane filtration permeates of black liquor. Cellulose Chemistry and Technology, 48(9-10), 805-811.

Ziesig, R., Tomani, P., Sedin, M. and Theliander H. (2015). Production of a pure lignin product, part 3: distribution and removal of inorganics from softwood lignin. Nordic Pulp and Paper Research Journal, 30(2), 199-206.

Zhao, J., Wang, C.H., Lee, D.J. and Tien, C. (2003) Cake consolidation in a compression–permeability cell: effect of side-wall friction. Journal of Colloid and Interface Science, 262, 60–72.

Zhu, W., Westman, G. and Theliander, H. (2014). Investigation and Characterization of Lignin Precipitation in the LignoBoost Process. Journal of Wood Chemistry and Technology, 34(2), 77-97.

Zhu, W., Westman, G. and Theliander, H. (2015a). The molecular properties and carbohydrate content of lignins precipitated from black liquor. Holzforschung. 69(2), 143-152.

Zhu, W. (2015b). Precipitation of Kraft Lignin. Yield and Equilibrium. PhD Thesis. Chalmers University of Technology, Department of Chemistry and Chemical Engineering, Gothenburg, Sweden.